

NATIONAL AERONAUTICS AND SPACE ADMINISTRATION

Technical Report 32-1062

*Trajectory Analysis of an
Earth - Venus - Mercury Mission
in 1973*

F. M. Sturms, Jr.

GPO PRICE \$ _____

CFSTI PRICE(S) \$ _____

Hard copy (HC) 9.00

Microfiche (MF) 65

ff 653 July 65

N67 17827

(ACCESSION NUMBER)

62
(PAGES)

PR-81636
(NASA CR OR TMX OR AD NUMBER)

(THRU)

1
(CODE)

30
(CATEGORY)

JET PROPULSION LABORATORY
CALIFORNIA INSTITUTE OF TECHNOLOGY
PASADENA, CALIFORNIA

January 1, 1967


NATIONAL AERONAUTICS AND SPACE ADMINISTRATION

Technical Report 32-1062

*Trajectory Analysis of an
Earth – Venus – Mercury Mission
in 1973*

F. M. Sturms, Jr.

Approved by:

A handwritten signature in black ink, appearing to read "T. W. Hamilton", is written over a horizontal line.

T. W. Hamilton, Manager
Systems Analysis Section

JET PROPULSION LABORATORY
CALIFORNIA INSTITUTE OF TECHNOLOGY
PASADENA, CALIFORNIA

January 1, 1967

Technical Report 32-1062

**Copyright © 1967
Jet Propulsion Laboratory
*California Institute of Technology***

**Prepared Under Contract No. NAS 7-100
National Aeronautics & Space Administration**

Acknowledgment

The author expresses his appreciation to Elliott Cutting for his work on the guidance analysis for the 1970 mission, which was fully incorporated in the 1973 study, as well as for his many helpful comments and suggestions. Thanks are extended to Alva Joseph and Ronald Richard for their work in developing the conic computer program, SPARC. Thanks are also extended to Helen Ling and the Systems Analysis Computing Services Group, for 1620 programming and analysis, and for plotting many of the original graphs for this report.

Contents

I. Introduction	1
A. Principle of Venus Swingby	1
B. Mission Opportunities in the 1970's	2
II. Conic Trajectory Analysis	2
A. Conic Computer Program	2
B. Region of Possible Trajectories	2
C. Launch Periods	5
D. Plots of Conic Trajectory Parameters	7
III. Integrated Trajectory Analysis	21
A. Targeting of Integrated Trajectories	22
B. Comparison of Conic and Integrated Trajectories	22
C. Plots of Integrated Trajectory Parameters	22
IV. Near-Planet Geometry	34
V. Guidance Analysis	35
A. Mapping Equations	44
B. Injection Covariance Matrix	46
C. Obtaining Mapping Matrices	46
D. Conic Error Analysis	48
E. Results	50
Nomenclature	51
References	52

Tables

1. Launch period vs energy for variable Venus arrival date	5
2. Launch period vs energy for fixed Venus arrival date	5
3. Launch window parameters	21
4. Comparison of conic and integrated trajectories	23
5. Injection covariance matrix for October 26, 1973 launch date	46

Contents (contd)

Tables (contd)

6. Mapping matrices for the October 26, 1973 launch date	47
7. Covariance matrices of target errors for October 26, 1973 launch date	48
8. Covariance matrices of midcourse corrections for October 26, 1973 launch date	48
9. Summary of target errors	49
10. Summary of midcourse corrections	50

Figures

1. Velocity changes during Venus flyby	2
2. Region of positive altitudes for 1973 opportunity	4
3. Altitude of closest approach at Venus	4
4. Launch energy	5
5. Declination of launch asymptote	6
6. Venus arrival speed	6
7. Impact parameter for Venus aiming point	7
8. Angle between \mathbf{T} axis and Venus impact parameter vector	7
9. Celestial latitude of Venus arrival asymptote	8
10. Celestial longitude of Venus arrival asymptote	8
11. Celestial latitude of Venus departure asymptote	9
12. Celestial longitude of Venus departure asymptote	9
13. Deflection angle of Venus hyperbola	9
14. Angle between arrival asymptote and Venus-Earth vector (ζ_E)	10
15. Angle between \mathbf{T} axis and Earth-Venus projection (η_E)	10
16. Angle between arrival asymptote and Venus-Sun vector (ζ_s)	11
17. Angle between \mathbf{T} axis and Sun-Venus projection (η_s)	11
18. Angle between arrival asymptote and Venus-Canopus vector (ζ_c)	12
19. Angle between \mathbf{T} axis and Canopus-Venus projection (η_c)	12
20. Mercury arrival speed	13
21. Total time of flight to Mercury	13
22. Communication distance at Mercury encounter	13
23. Celestial latitude of Mercury arrival asymptote	14

Contents (contd)

Figures (contd)

24. Celestial longitude of Mercury arrival asymptote	14
25. Angle between arrival asymptote and Mercury–Earth vector (ζ_E)	15
26. Angle between T axis and Earth–Mercury projection (η_E)	15
27. Angle between arrival asymptote and Mercury–Sun vector (ζ_S)	16
28. Angle between T axis and Sun–Mercury projection (η_S)	16
29. Angle between arrival asymptote and Mercury–Canopus vector (ζ_C)	17
30. Angle between T axis and Canopus–Mercury projection (η_C)	17
31. Definition of aiming zone parameters	18
32. Venus occultation zones for October 21 launch	18
33. Venus occultation zones for October 26 launch	18
34. Venus occultation zones for October 31 launch	19
35. Venus occultation zones for November 5 launch	19
36. Venus occultation zones for November 10 launch	19
37. Mercury occultation zones for October 21 launch	19
38. Mercury occultation zones for October 26 launch	20
39. Mercury occultation zones for October 31 launch	20
40. Mercury occultation zones for November 5 launch	20
41. Mercury occultation zones for November 10 launch	20
42. Projection of trajectory on ecliptic plane for October 21, 1973 launch	22
43. Projection of trajectory on ecliptic plane for October 26, 1973 launch	22
44. Projection of trajectory on ecliptic plane for October 31, 1973 launch	24
45. Projection of trajectory on ecliptic plane for November 5, 1973 launch	24
46. Projection of trajectory on ecliptic plane for November 10, 1973 launch	24
47. Geocentric range vs time from launch for five launch dates	25
48. Geocentric range-rate vs time from launch for five launch dates	26
49. Heliocentric range vs time from launch for five launch dates	27
50. Celestial latitude vs time from launch for five launch dates	28
51. Celestial longitude vs time from launch for five launch dates	29
52. Sun–Earth–probe angle vs time from launch for five launch dates	30
53. Earth–probe–Sun angle (Earth cone angle) vs time from launch for five launch dates	31

Contents (contd)

Figures (contd)

54. Clock angle of Earth (with respect to Canopus) vs time from launch for five launch dates	32
55. Canopus-probe-Sun angle (Canopus cone angle) vs time from launch for five launch dates	33
56. Cone angle of Venus vs time from closest approach for five launch dates	34
57. Clock angle of Venus vs time from closest approach for five launch dates	34
58. Radius from Venus vs time from closest approach for five launch dates	34
59. Velocity with respect to Venus vs time from closest approach for five launch dates	35
60. Percent illumination vs time from closest approach for five launch dates	35
61. Angular semi-diameter of Venus vs time from closest approach for five launch dates	35
62. Near-Venus geometry for October 21, 1973 launch	36
63. Near-Venus geometry for October 26, 1973 launch	37
64. Near-Venus geometry for October 31, 1973 launch	37
65. Near-Venus geometry for November 5, 1973 launch	38
66. Near-Venus geometry for November 10, 1973 launch	38
67. Cone angle of Mercury vs time from closest approach for five launch dates for occultation flyby	39
68. Clock angle of Mercury vs time from closest approach for five launch dates for occultation flyby	39
69. Radius from Mercury vs time from closest approach for five launch dates for occultation flyby	39
70. Velocity with respect to Mercury vs time from closest approach for five launch dates for occultation flyby	39
71. Percent illumination vs time from closest approach for five launch dates for occultation flyby	40
72. Angular semi-diameter of Mercury vs time from closest approach for five launch dates for occultation flyby	40
73. Near-Mercury geometry for October 21, 1973 launch	41
74. Near-Mercury geometry for October 26, 1973 launch	42
75. Near-Mercury geometry for October 31, 1973 launch	42

Contents (contd)

Figures (contd)

76. Near-Mercury geometry for November 5, 1973 launch	43
77. Near-Mercury geometry for November 10, 1973 launch	43
78. Cone angle of Mercury vs time from closest approach for five launch dates for Sun-side flyby	44
79. Clock angle of Mercury vs time from closest approach for five launch dates for Sun-side flyby	44
80. Percent of illumination vs time from closest approach for five launch dates for Sun-side flyby	44
81. Near-Mercury geometry for five launch dates for Sun-side flyby	45

Abstract

The report gives the results of a preliminary study of trajectory and guidance considerations for an Earth-Venus-Mercury mission in 1973. The mission utilizes a trajectory having a close encounter with Venus en route to Mercury in order to reduce launch energy requirements. Conic trajectory data are presented for the region of possible trajectories having launch energies (C_3) less than $21 \text{ km}^2/\text{sec}^2$. Integrated trajectory data and near-planet geometry are presented for selected mission designs. Based on a maximum C_3 of $19.5 \text{ km}^2/\text{sec}^2$ and a constant Venus arrival date of February 5, 1974, the resulting launch period is 23 days long, extending from October 20 to November 11, 1973. The total flight times range from 131 to 165 days, with Mercury encounter near the end of March 1974. The mission can be accomplished with Earth-based radio tracking and three midcourse corrections at times about 6 days after injection, 6 days before Venus encounter, and 8 days after Venus encounter. Statistics are presented for the three midcourse corrections and associated target errors. A total midcourse velocity capability of about 120 m/sec is required. The final rms miss at Mercury ranges from 1400 to 2900 km.

Trajectory Analysis of an Earth-Venus-Mercury Mission in 1973

I. Introduction

In Ref. 1, Minovitch showed that indirect missions to Mercury that have a close encounter with Venus en route require considerably less launch energy than does a direct mission. The launch energy saving is achieved by the gravitational perturbation of Venus, which removes energy from the heliocentric trajectory.

A. Principle of Venus Swingby

The method by which energy is removed during the close encounter with Venus is illustrated in Fig. 1. During the time the spacecraft is near Venus, the motion with respect to Venus closely approximates a hyperbola. The heliocentric velocity of the spacecraft is the vector sum of the orbital velocity of Venus, \bar{V}_φ , and the velocity of the spacecraft with respect to Venus (on the hyperbola). The spacecraft arrives at Venus along an asymptote approaching from a direction opposite the Sun and with asymptotic velocity, \bar{V}_{h1} . The heliocentric arrival velocity, \bar{V}_1 , is computed from

$$\bar{V}_1 = \bar{V}_\varphi + \bar{V}_{h1}$$

and is shown by vectors in Fig. 1. Now the spacecraft departs Venus in a direction determined by the bending caused by the gravitational attraction of Venus' mass. The asymptotic departure speed on the hyperbola is equal to the arrival speed. For the heliocentric departure velocity,

$$\bar{V}_2 = \bar{V}_\varphi + \bar{V}_{h2}$$

This vector sum is also shown on Fig. 1. During the relatively short time that the spacecraft is near Venus, the orbital velocity of Venus is approximately constant.

It can be seen readily from the vector sums of Fig. 1 that the deflection of the hyperbolic velocity resulting from Venus' gravity causes the heliocentric velocity, and hence the heliocentric energy, to decrease. This decrease in energy lowers the perihelion and allows the spacecraft to reach the orbit of Mercury. An academic point should be made here, that the energy removed from the spacecraft is added to Venus. However, because of the extreme difference in mass, the change in the velocity of Venus is completely negligible.

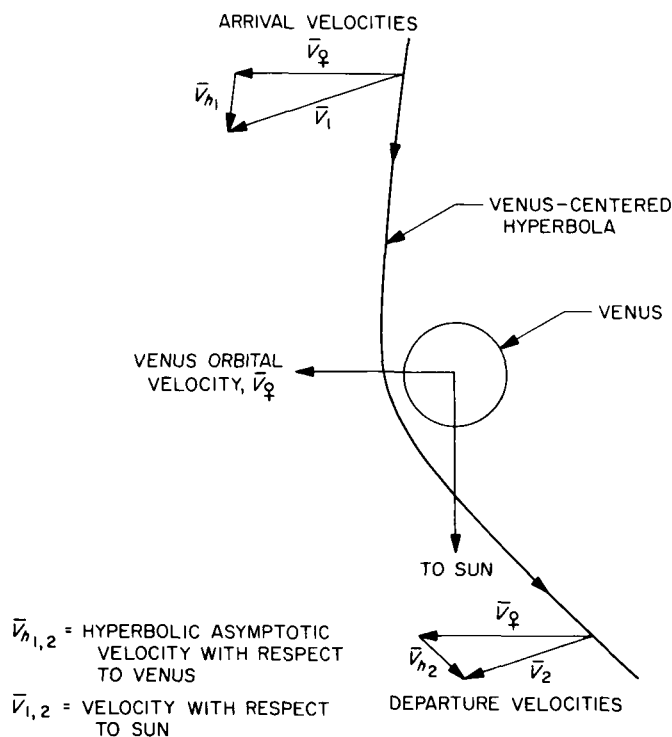


Fig. 1. Velocity changes during Venus flyby

B. Mission Opportunities in the 1970's

A detailed trajectory-and-guidance analysis by Sturms and Cutting (Ref. 2) of an Earth-Venus-Mercury mission in 1970 demonstrated that this mission is feasible with Earth-based radio guidance and an Atlas-Centaur boost vehicle. The interest aroused by this study resulted in a survey to find other mission opportunities in the decade of the 1970's. The results of that survey are presented in Ref. 3.

Of the six Venus opportunities in the 1970's, two (1970 and 1973) result in favorable trajectories to Mercury; two (1972 and 1975) result in unfavorable trajectories to Mercury because of very low altitudes at Venus closest approach; and two (1977 and 1978) result in no trajectories to Mercury within the constraints of the survey.

The 1973 mission was selected for a spacecraft design study at JPL. This report gives the results of trajectory and guidance analyses for the 1973 mission, and is similar in scope to that in Ref. 2 for the 1970 mission.

Section II gives the results of a parameter study of trajectories for the 1973 opportunity, using conic approximations. From these data, three design launch periods are selected for further study. In Section III, results from

five precision-integrated trajectories are given. These five trajectories cover two of the selected launch periods. In Section IV, data are presented on the near-planet geometry for the flybys of Venus and Mercury. Two aiming points are investigated for the Mercury flyby, one for Earth occultation and one for a Sun-side flyby. The guidance analysis is presented in Section V. Data are presented on the statistics of the miss at each planet and the required velocity correction capability for three mid-course maneuvers.

II. Conic Trajectory Analysis

A. Conic Computer Program

The first step in the trajectory analysis is the generation of large amounts of data concerning trajectories throughout the launch opportunity, based on conic trajectory approximations. A conic computer program has been developed at JPL for investigating multiple-planet and other advanced missions. This program, called the Space Research Conic (SPARC) Program, is documented in Ref. 4.

Multiple-planet trajectories for the subject mission are computed by finding heliocentric Earth-Venus and Venus-Mercury conic trajectory legs, such that the arrival and departure speeds on the Venus hyperbolic asymptotes are equal. The SPARC program is operated by inputting the Earth-departure and Venus-arrival dates. These inputs define the Earth-Venus leg and the Venus arrival velocity. The program then initiates a search for the proper Venus-Mercury flight time that will result in a departure speed equal to the Venus arrival speed from the first leg. The computer program may obtain planetary positions and velocities from analytic mean elements or from planetary ephemeris tapes. For this study, the faster option of mean elements was chosen.

The heliocentric trajectory legs define the approach and departure asymptotes and speeds at Venus, which in turn, define the Venus-centered hyperbolic trajectory. In addition, the launch site and launch azimuth constraints, along with the Earth departure asymptote, define the near-Earth escape hyperbola. The SPARC printout includes many useful parameters for preliminary mission design.

B. Region of Possible Trajectories

Computer runs were made on SPARC at 1-day increments in launch date and Venus arrival date. Those

combinations of launch date and Venus arrival date that satisfy all constraints define the region of possible trajectories.

For any given date at Venus, there is a minimum energy for the Venus-Mercury leg. All launch-date flight-time combinations on the Earth-Venus leg that result in arrival energies less than this minimum for continuing to Mercury are outside the region of possible mission trajectories. This requirement for energy matching at Venus on the two legs of the trajectory is the *first* of three constraints that define the region of possible trajectories.

The *second* constraint requires that the point of closest approach at Venus be above the surface. After the energy matching has been obtained, the arrival and departure asymptotes define a Venus-centered hyperbola. The periapsis radius of this hyperbola must be greater than the radius of Venus, which in this study, is taken as 6200 km.

The *third* constraint requires that the launch energy at Earth (C_3) be less than some selected maximum. The maximum value of C_3 chosen for this study was $21 \text{ km}^2/\text{sec}^2$. This value was selected as being an approximate upper bound for which the multiple-planet mission can be performed with a sizable payload on the Atlas-Centaur and is, therefore, more attractive than a direct Earth-Mercury mission. The value is also usually the maximum C_3 found on Earth-Venus contour plots in publications (e.g., Ref. 5).

To summarize, the constraints are the following:

- (1) Energy match possible.
- (2) Venus altitude positive.
- (3) Launch energy less than $21 \text{ km}^2/\text{sec}^2$.

These three constraints, when plotted on a grid of launch date vs Venus arrival date, result in a closed boundary defining the region of possible trajectories.

Because of the launch energy constraint, the Earth-Venus-Mercury trajectories will coincide with Earth-Venus opportunities in 1973 for which there are two closed regions inside which C_3 is less than $21 \text{ km}^2/\text{sec}^2$. The two regions are known as Type I and Type II trajectories. Type I trajectories have heliocentric transfer angles less than 180° ; Type II trajectories have transfer angles greater than 180° .

For each date at Venus, there are, similarly, both Type I and Type II Venus-Mercury trajectories, each having a separate and distinct minimum energy. The energy match constraint must, therefore, be investigated separately for Type I and Type II Venus-Mercury legs.

For a given type Venus-Mercury leg for which an energy match is possible, two solutions—denoted as Class I and Class II—will be found (see Ref. 5). The Class I solution has a shorter flight time than does Class II. The altitude constraint must be investigated separately for Class I and Class II trajectories. There are, then, eight possible solutions which may satisfy all three constraints, consisting of all combinations of:

- (1) Type I and Type II Earth-Venus legs.
- (2) Type I and Type II Venus-Mercury legs.
- (3) Class I and Class II Venus-Mercury legs.

The computer runs showed that positive altitudes of closest approach at Venus were possible only for energy matches between Type I Earth-Venus legs and Type I Venus-Mercury legs. Positive altitudes were obtained for both Class I and Class II Venus-Mercury solutions. Figure 2 shows the boundaries of the region of possible trajectories on a launch date-Venus arrival date grid. The upper bound is the energy match limit, above which the arrival velocity at Venus is too low to continue to Mercury on a Type I trajectory. The lower bound for both Class I and Class II is the locus of zero altitude, below which the altitude of closest approach is negative. The limiting launch energy bound of $C_3 = 21 \text{ km}^2/\text{sec}^2$ is also shown.

The range of Venus arrival dates is February 2 to 7, 1974. These six arrival dates are convenient parameters for plotting conic trajectory parameters, shown in the following manner: The abscissa shows launch date, the ordinate shows the range of the trajectory parameter being plotted, and the parameter is shown for each of the six Venus arrival dates from February 2 to 7, 1974.

Figure 3 shows the altitude of closest approach at Venus, plotted in the above manner. From Figs. 2 and 3, it is seen that the region of Class II trajectories is small and that the altitudes are smaller than the corresponding Class I trajectory. Since the Class I trajectories also have shorter flight times, the Class II's are of little interest and, therefore, are not shown on subsequent figures.

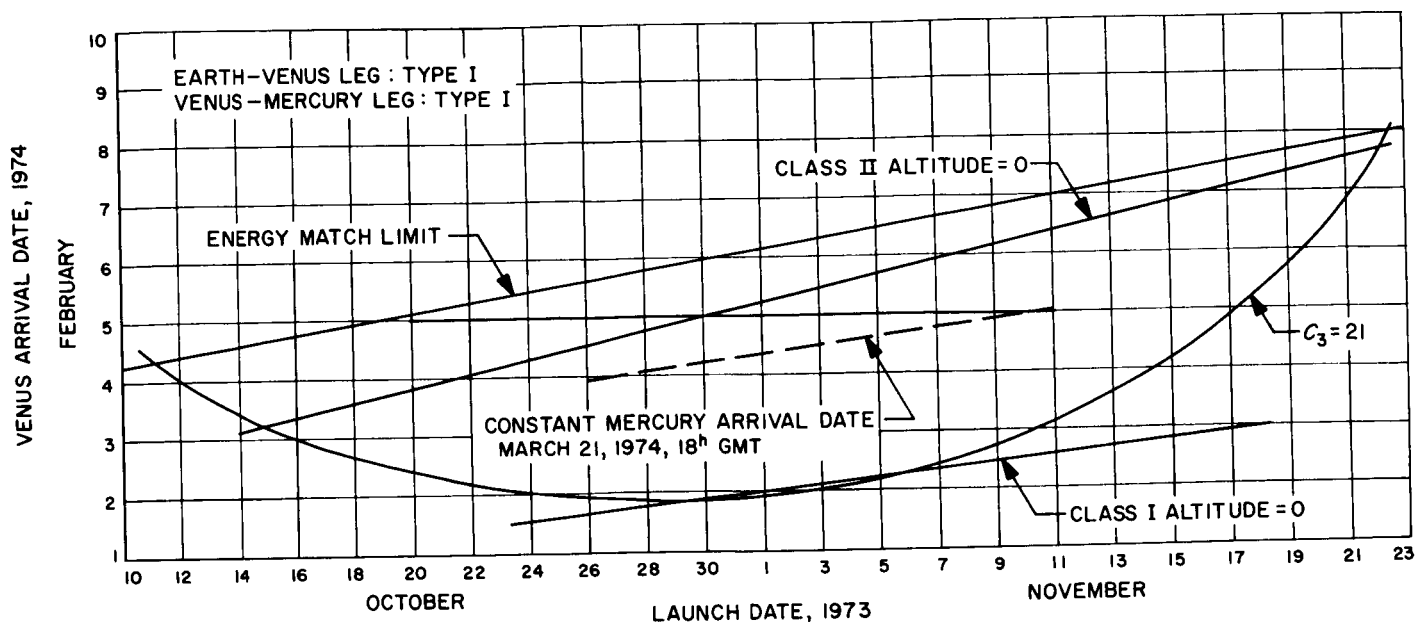


Fig. 2. Region of positive altitudes for 1973 opportunity

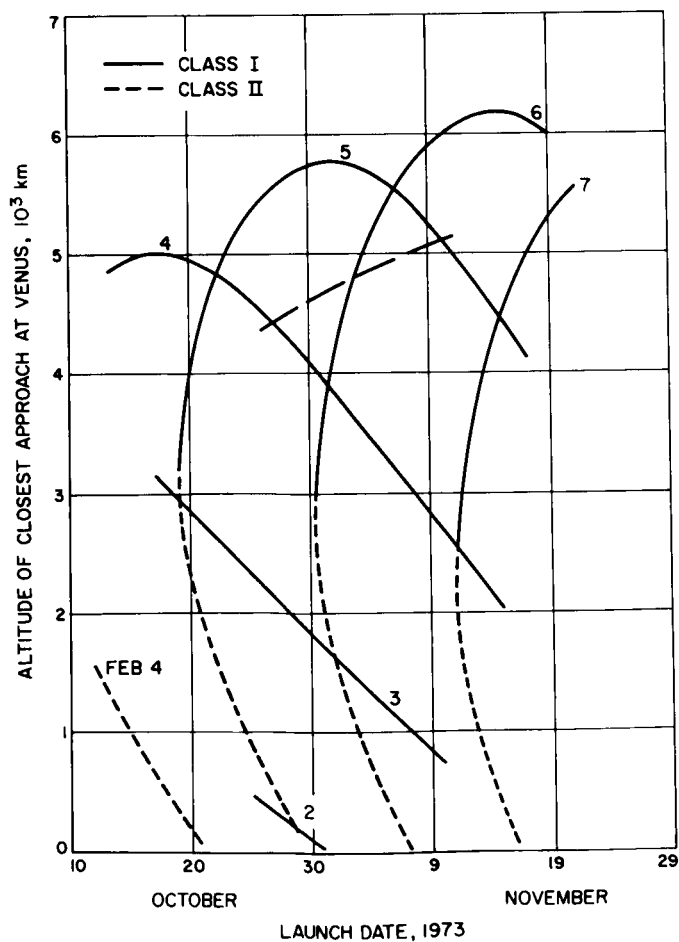


Fig. 3. Altitude of closest approach at Venus

C. Launch Periods

The available launch period depends on several constraints, the most important of which is the limit on launch energy. Figure 4 shows plots of launch energy for the 1973 mission. From this plot, the launch period for a given limit on C_3 can be determined. Tables 1 and 2 list the available launch days for selected values of launch energy. In Table 1, the arrival date at Venus is allowed to vary during the launch period; the result is a longer launch period than if the arrival date were constrained to be constant. The constant arrival date constraint is applied in Table 2. The minimum launch energy is about $18.15 \text{ km}^2/\text{sec}^2$.

To provide a basis for obtaining precision integrated trajectories and for performing guidance analysis, a mis-

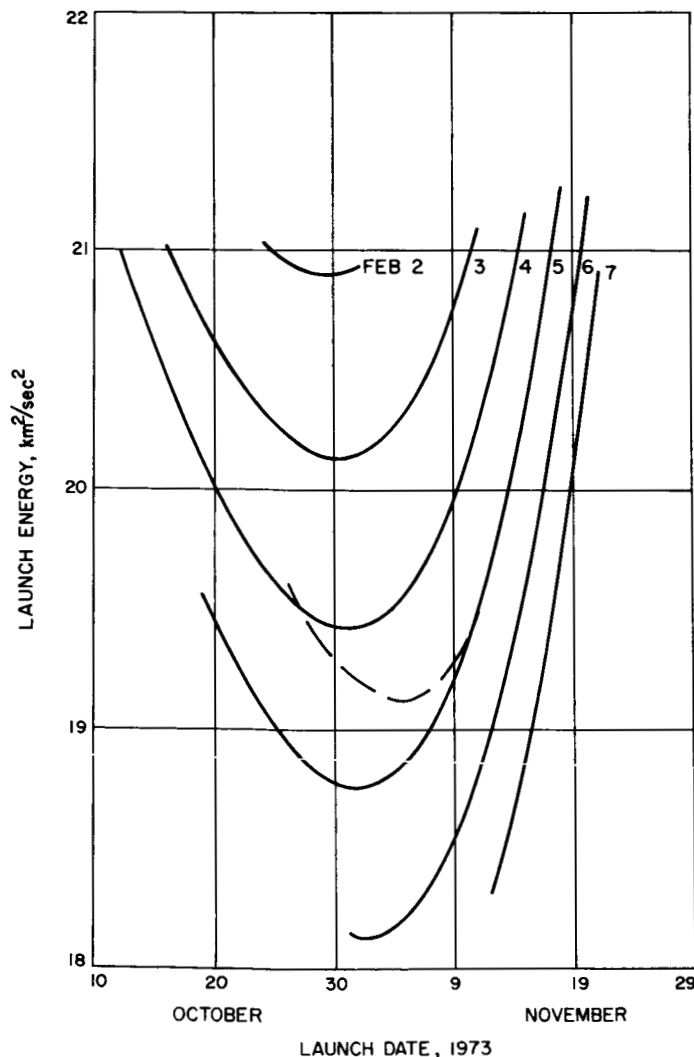


Fig. 4. Launch energy

sion design has been selected that adopts a Venus arrival date of February 5, 1974. For this arrival date, two launch periods are considered, based on launch energy limits of 19.0 and $19.5 \text{ km}^2/\text{sec}^2$. From Table 2, these

Table 1. Launch period vs energy for variable Venus arrival date

Maximum launch energy, km^2/sec^2	Range of launch dates, 1973	Launch period, days
21.0	Oct. 12 to Nov. 21	41
20.5	Oct. 16 to Nov. 20	36
20.0	Oct. 19 to Nov. 18	31
19.5	Oct. 20 to Nov. 17	29
19.0	Oct. 25 to Nov. 15	22
18.5	Oct. 31 to Nov. 8, Nov. 12-13	11
18.15	Nov. 1 to Nov. 2	2

Table 2. Launch period vs energy for fixed Venus arrival date

Maximum launch energy, km^2/sec^2	Venus arrival date, 1974	Range of launch dates, 1973	Launch period, days
21.0	Feb. 3	Oct. 17 to Nov. 10	25
	4	12 to 14	34
	5	20 to 17	29
20.5	Feb. 3	Oct. 22 to Nov. 6	16
	4	16 to 12	28
	5	20 to 15	27
20.0	Feb. 4	Oct. 20 to Nov. 9	21
	5	20 to 13	25
19.5	Feb. 5	Oct. 20 to Nov. 11	23
	6	31 to 14	15
19.0	Feb. 5	Oct. 25 to Nov. 7	14
	6	31 to 12	13
18.5	Feb. 6	Oct. 31 to Nov. 8	9
18.15	Feb. 6	Nov. 1 to Nov. 2	2

energy limits result in launch periods of 14 and 23 days, respectively. Since the longer launch period is merely an extension on both ends of the shorter period, the analysis can be combined.

The longer launch period ($C_3 = 19.5 \text{ km}^2/\text{sec}^2$) is from October 20 to November 11, 1973, and the shorter period ($C_3 = 19.0 \text{ km}^2/\text{sec}^2$) from October 25 to November 7. The corresponding ranges of Mercury arrival dates are April 2 to March 21, 1974, and March 29 to March 23, 1974, respectively.

Using the same payload curve as in Ref. 2 (which gave 1300 lb for $C_3 = 14 \text{ km}^2/\text{sec}^2$), the Atlas-Centaur booster can inject 1020 lb to a C_3 of $19.0 \text{ km}^2/\text{sec}^2$ and 990 lb to a C_3 of $19.5 \text{ km}^2/\text{sec}^2$. Improvements in the Atlas-Centaur vehicle will undoubtedly raise these figures somewhat.

Five launch dates have been selected for detailed analysis. They give points near the beginning, middle, and end of the two launch periods. The five dates are: October 21, October 26, October 31, November 5, and

November 10, 1973. Integrated trajectories and guidance sensitivities are obtained for these launch dates.

Analysis of near-Mercury geometry revealed that a constant Mercury arrival date of about March 21, 1974, would be useful. Consequently, a third launch period has been defined for a maximum C_3 of $19.5 \text{ km}^2/\text{sec}^2$, extending from October 27 to November 11, 1973, with Mercury arrival at 18^h GMT on March 21, 1974, at which time Mercury is in the Goldstone view period.

The three launch periods defined are shown on the graphs of conic trajectory parameters. The first two, of course, overlap and are simply portions of the February 5 arrival-date curve on the graphs. The constant Mercury-arrival-date launch period is shown as a dashed line.

Trajectories in the third and second launch periods coincide for a launch date of about November 10. Hence, although integrated trajectories and guidance sensitivities are not obtained for the entire constant Mercury-arrival-date launch period, the November 10/February 5

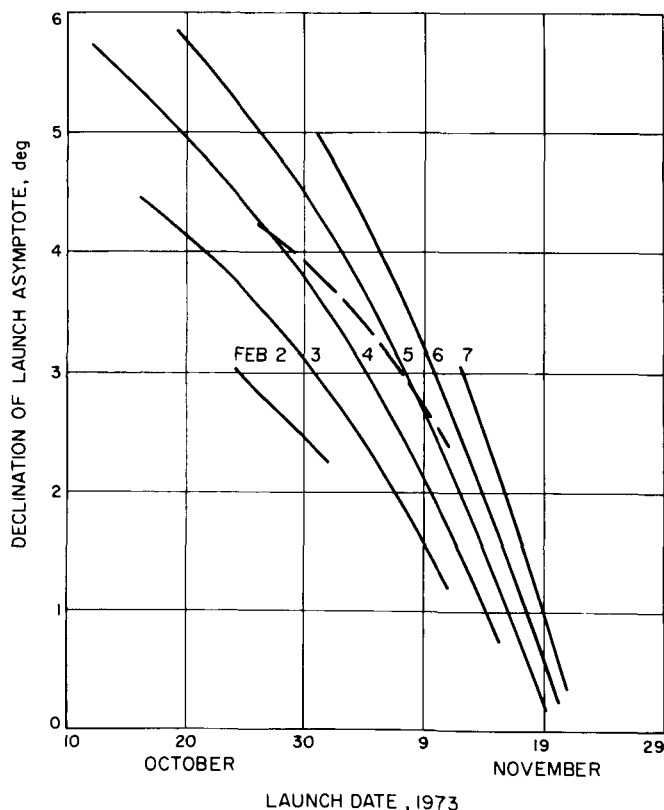


Fig. 5. Declination of launch asymptote

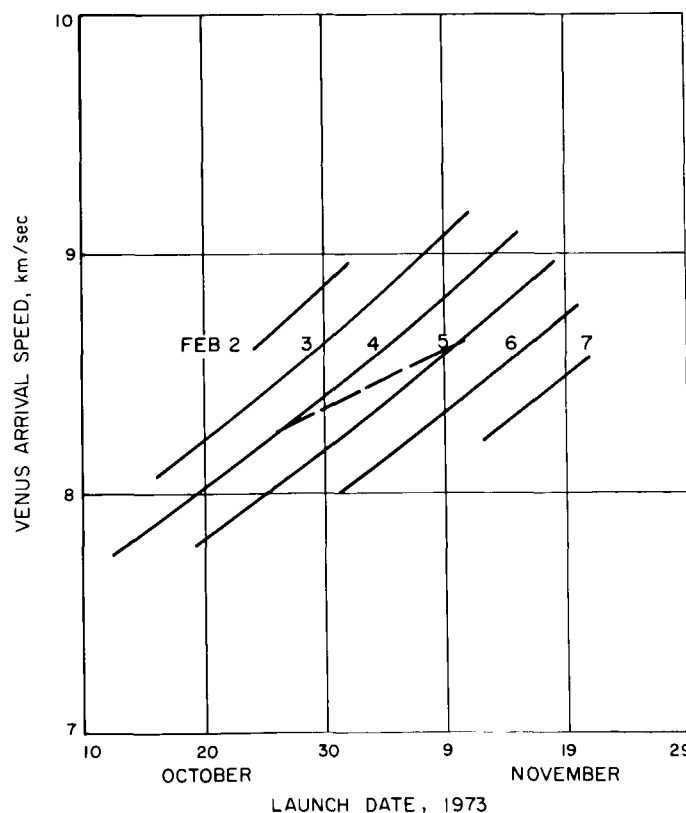


Fig. 6. Venus arrival speed

information for the constant Venus-arrival-date launch period is approximately correct for a typical case.

D. Plots of Conic Trajectory Parameters

Figures 3 to 30 show various trajectory parameters, plotted from the SPARC computer runs, vs launch date for each of the six Venus arrival dates. Most of the important design parameters are included. No attempt will be made here to discuss each of the figures; only the more general conclusions will be discussed.

Many of the parameters require an understanding of the **RST** coordinate system (Ref. 6). In this system, centered at the target planet, \hat{S} is a unit vector in the direction of the incoming hyperbolic asymptote (see Fig. 31).

A unit vector, \hat{T} , is then defined perpendicular to \hat{S} and parallel to the ecliptic. Finally, \hat{R} completes the right-hand system, **RST**. The ambiguity in the direction of \hat{T} is resolved by defining

$$\hat{T} = \frac{\hat{S} \times \hat{K}}{|\hat{S} \times \hat{K}|}$$

where \hat{K} is a unit vector toward the north ecliptic pole. The \hat{R} vector then points toward the south ecliptic hemisphere.

A view along the incoming asymptote looks normal to the R-T plane, which is sometimes called the *B* plane, since the impact parameter vector, \bar{B} —extending out

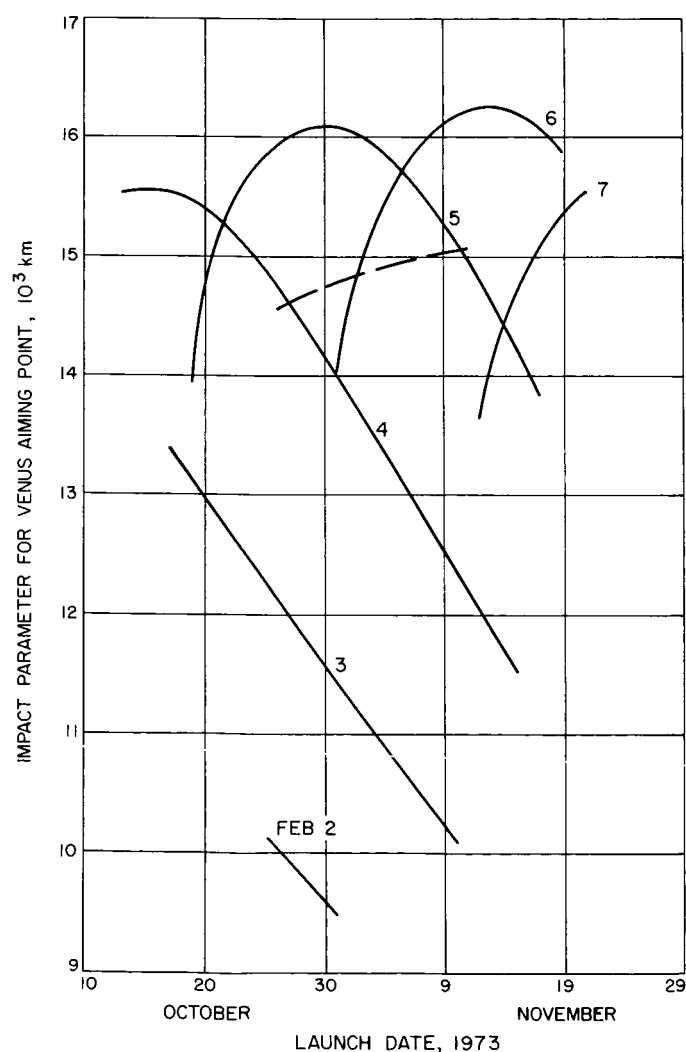


Fig. 7. Impact parameter for Venus aiming point

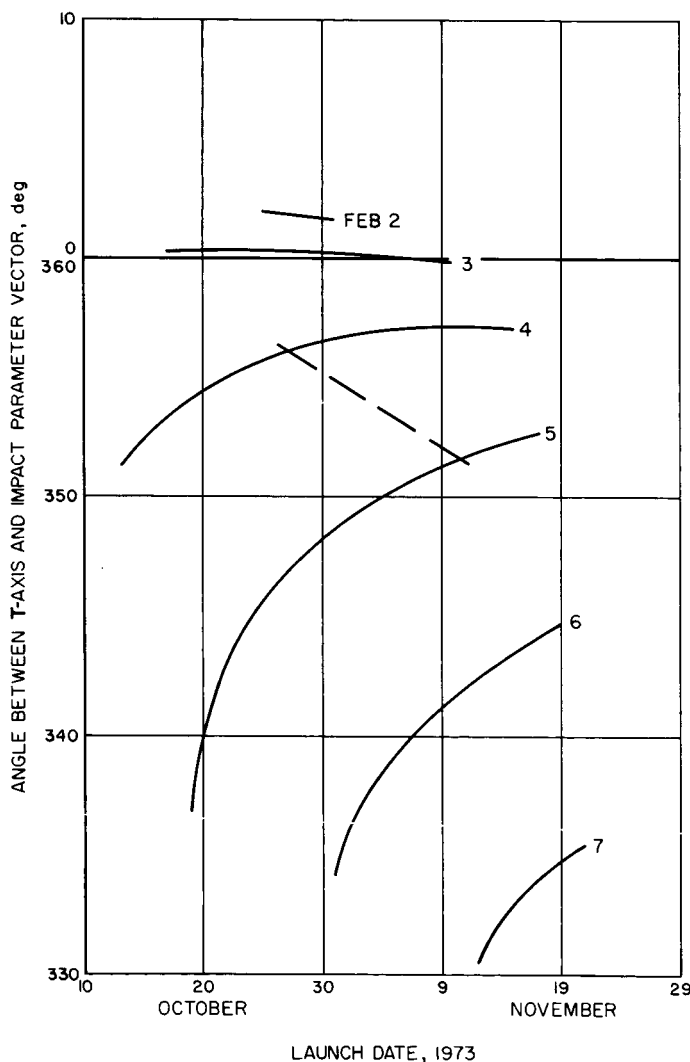


Fig. 8. Angle between T axis and Venus impact parameter vector

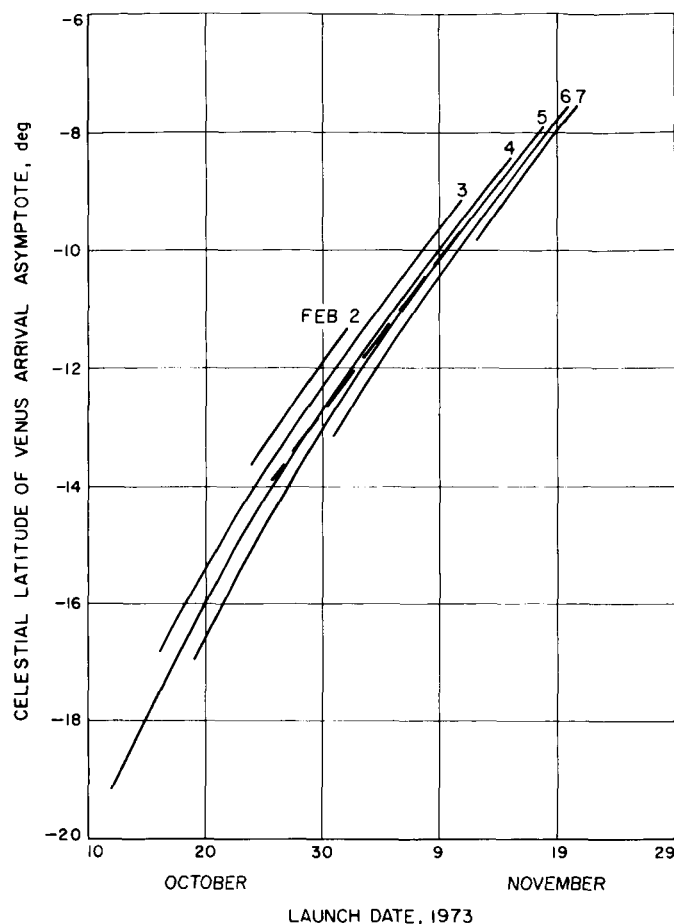


Fig. 9. Celestial latitude of Venus arrival asymptote

from the center of the planet, perpendicular to the incoming asymptote—lies in this plane. The point in the R - T plane, at the tip of the \mathbf{B} vector, where the asymptote pierces the plane, is called the *aiming point*. It is used for differential correction of end conditions and is denoted commonly by the components of the \mathbf{B} vector on the T and R axes— $\mathbf{B} \cdot \mathbf{T}$ and $\mathbf{B} \cdot \mathbf{R}$, respectively.

The directions to important reference bodies are measured by spherical coordinates in the \mathbf{RST} coordinate system. The polar angle, ζ (e.g., Fig. 13), is measured from $\hat{\mathbf{S}}$ to the target-body vector; and a second angle, η (e.g., Fig. 14), is measured in the R - T plane from $\hat{\mathbf{T}}$ to the projection of the body-target vector. The sense of the vector for η is reversed from that of ζ so that η denotes the location of the occultation centerline—that is, the location of aiming points that result in the spacecraft's passing behind the planet, as seen from the reference body.

Figures 32 to 36 show plots in the Venus B -plane of occultation zones for the Earth, Sun, and Canopus for

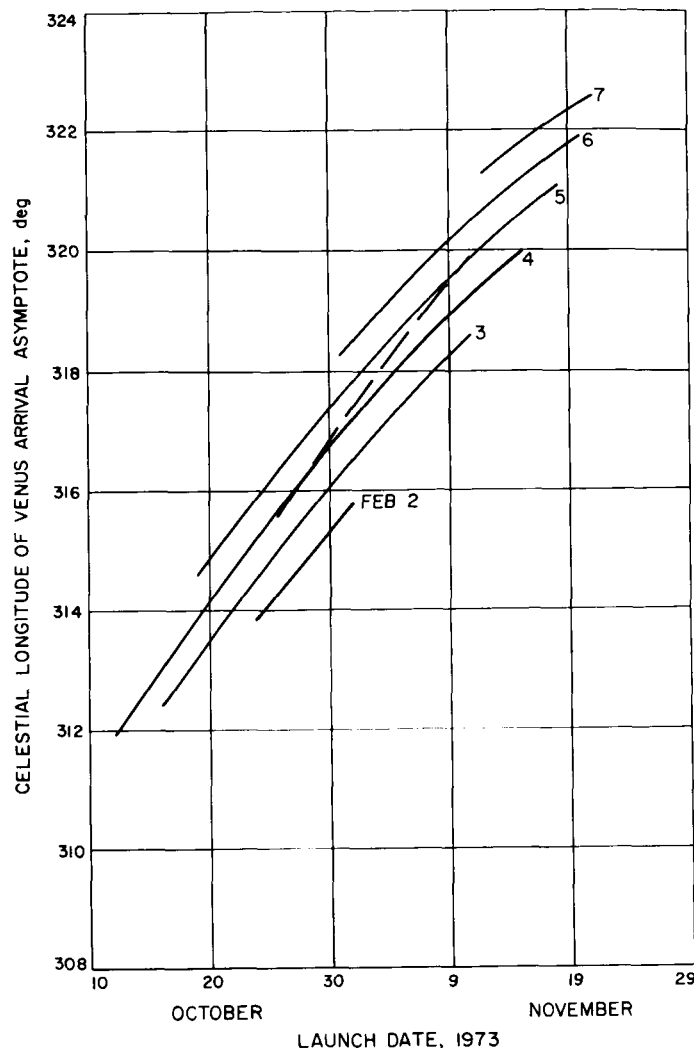


Fig. 10. Celestial longitude of Venus arrival asymptote

each of the five launch dates. Also shown are the required Venus aiming points that result in Earth occultation.

Figures 37 to 41 show corresponding plots for the Mercury encounter. The Mercury aiming point may be selected freely to meet science requirements, within constraints of planetary quarantine and science instrument ranges.

From the quantity ζ_* at Venus (Fig. 16) it is seen that the arrival at Venus is from the dark side and departure is on the sunlit side. Closest approach at Venus is, therefore, near the terminator. Similarly, from Fig. 27, the arrival at Mercury is from a direction nearly over the terminator. If an Earth occultation experiment is performed at Mercury, the aiming point will cause closest approach to be over the southern hemisphere of the dark side.

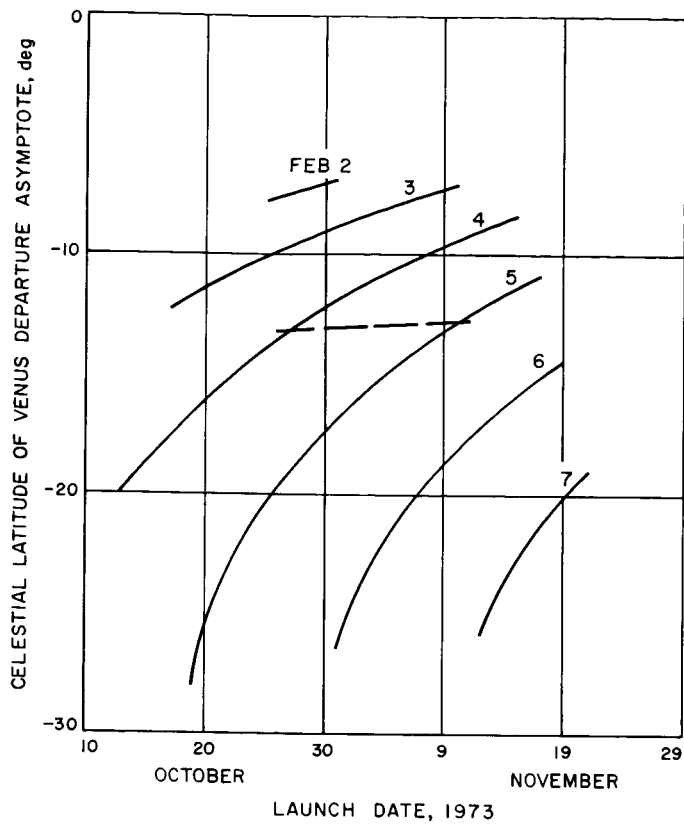


Fig. 11. Celestial latitude of Venus departure asymptote

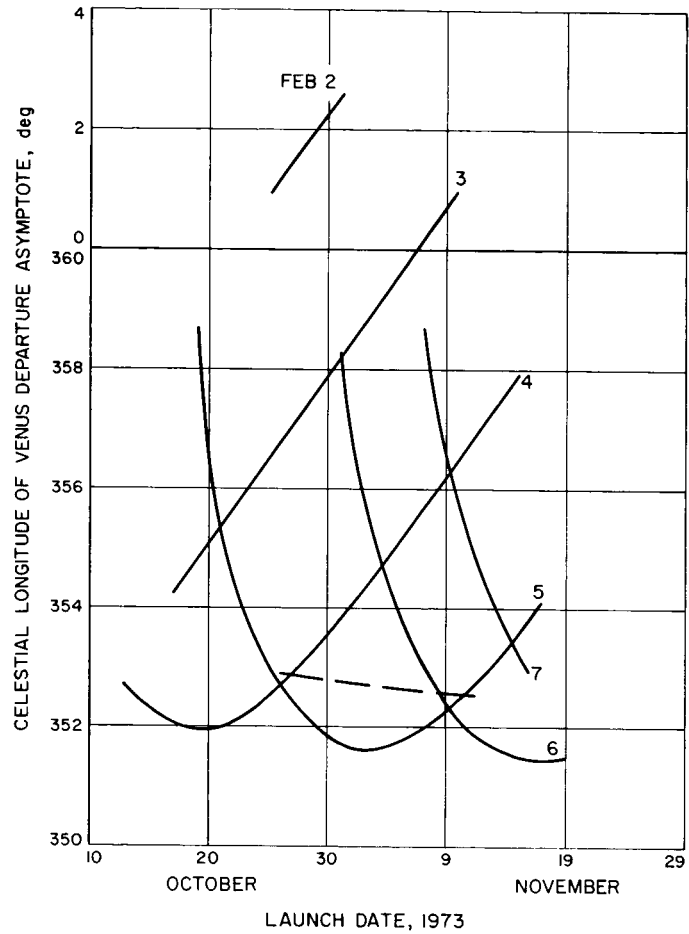
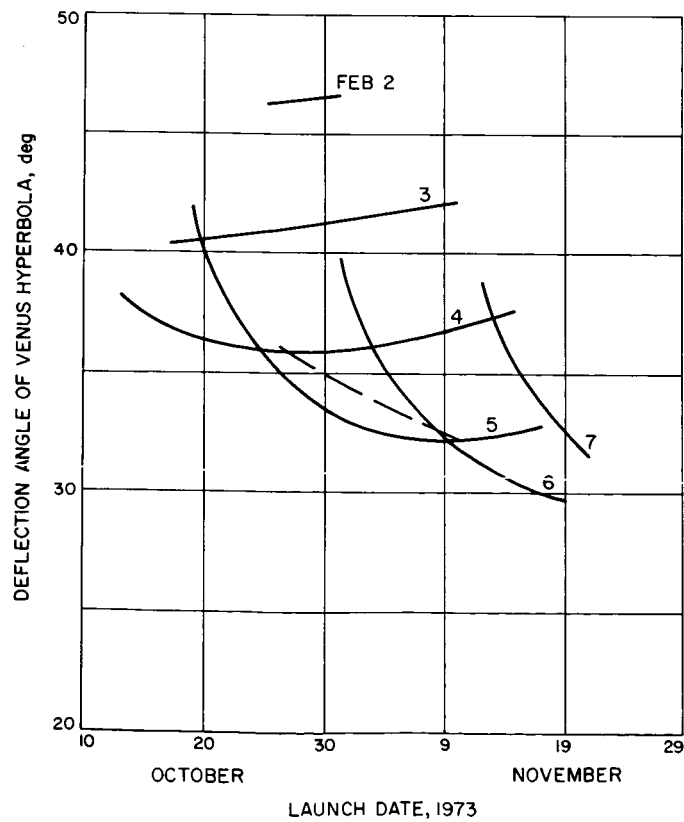


Fig. 12. Celestial longitude of Venus departure asymptote

Fig. 13. Deflection angle of Venus hyperbola

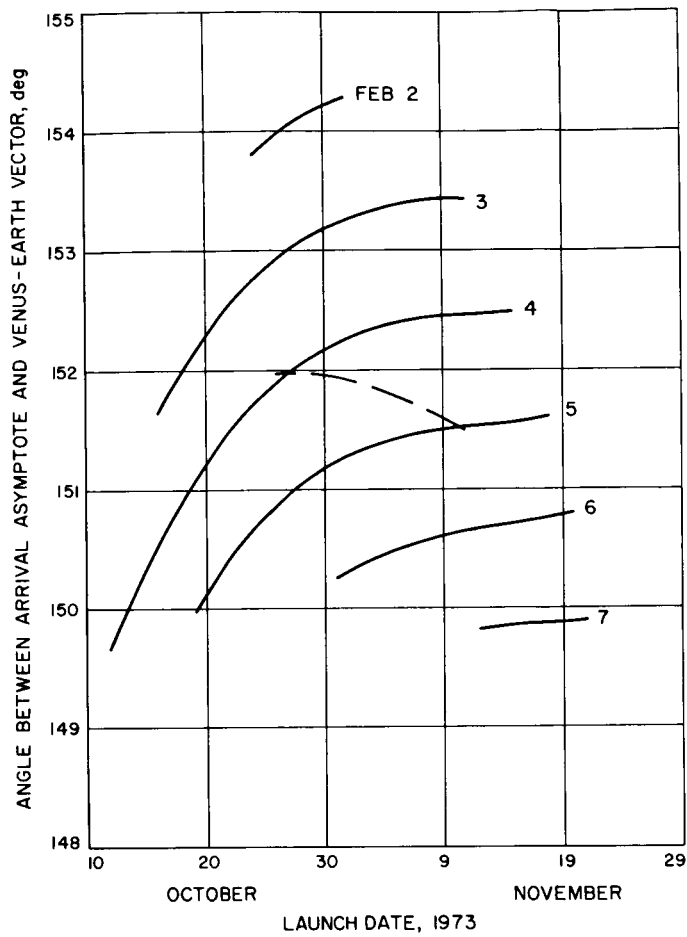


Fig. 14. Angle between arrival asymptote and Venus-Earth vector (ζ_E)

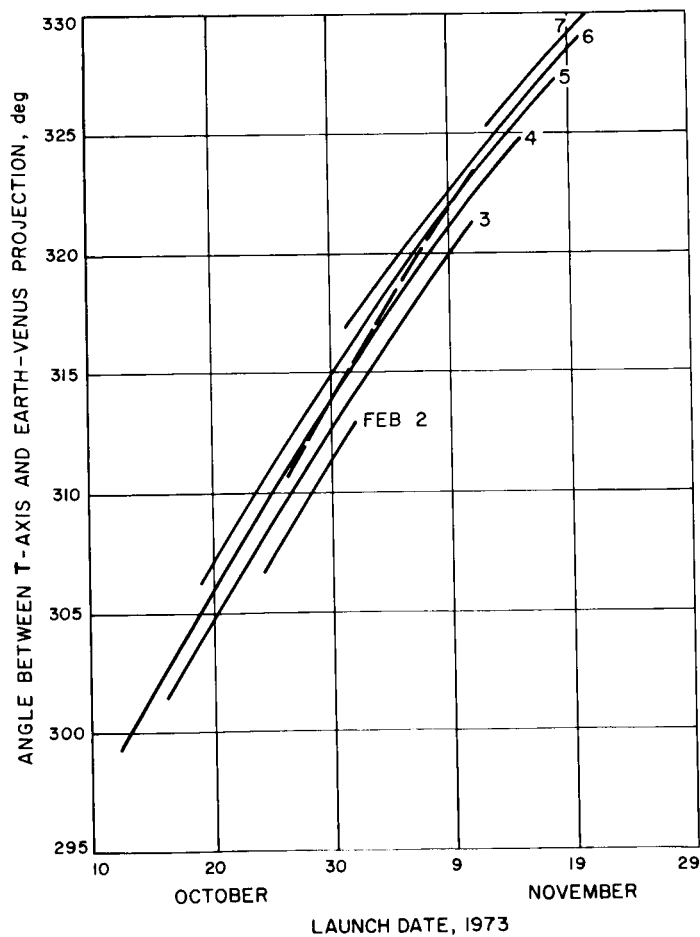
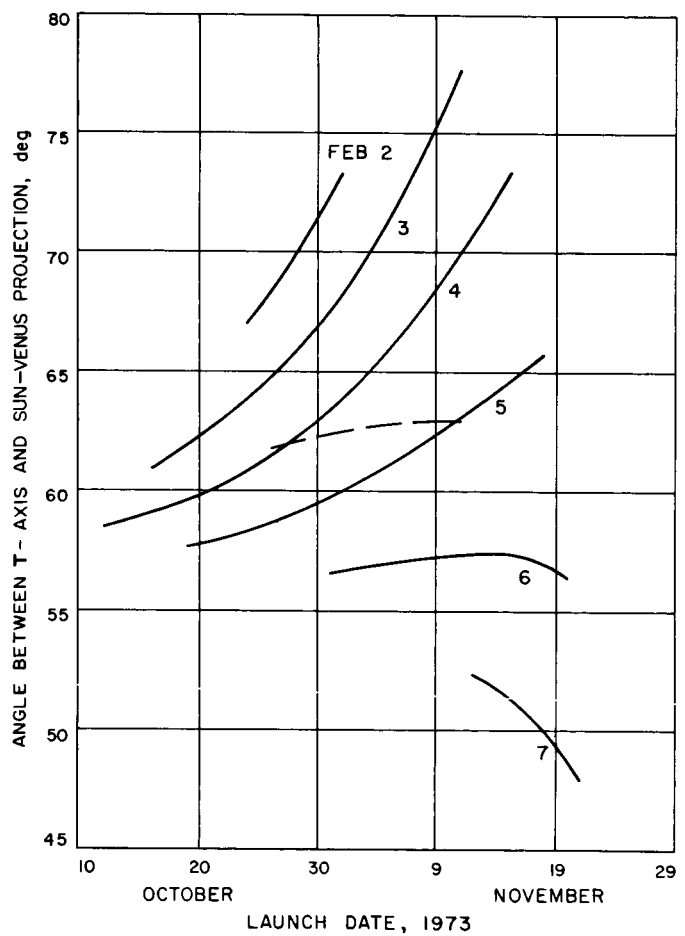
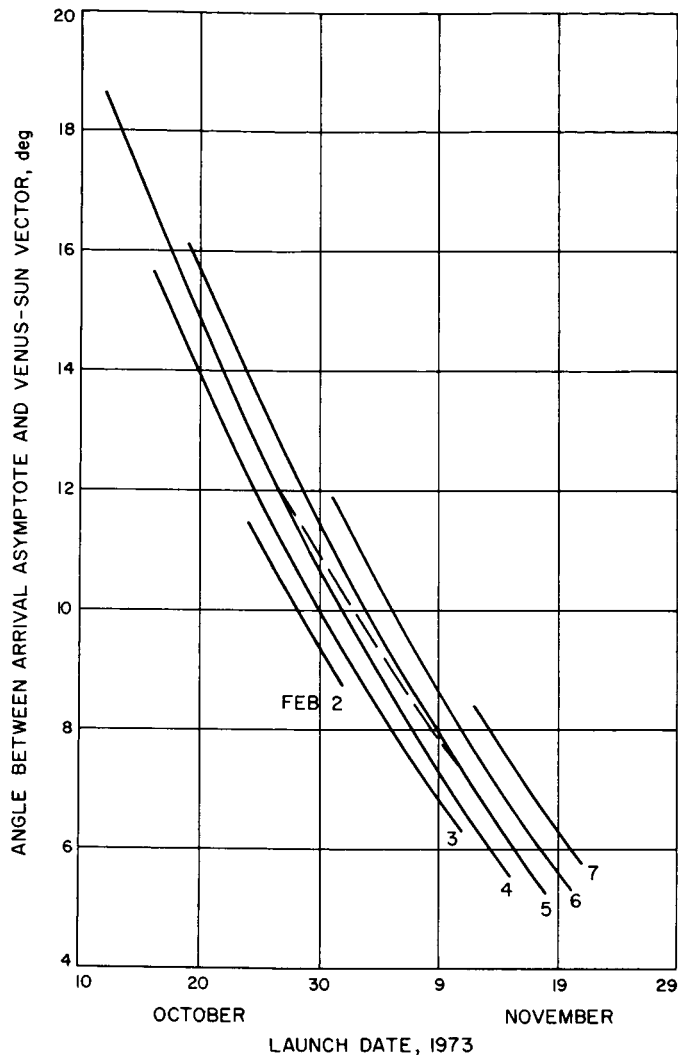


Fig. 15. Angle between T axis and Earth-Venus projection (η_E)



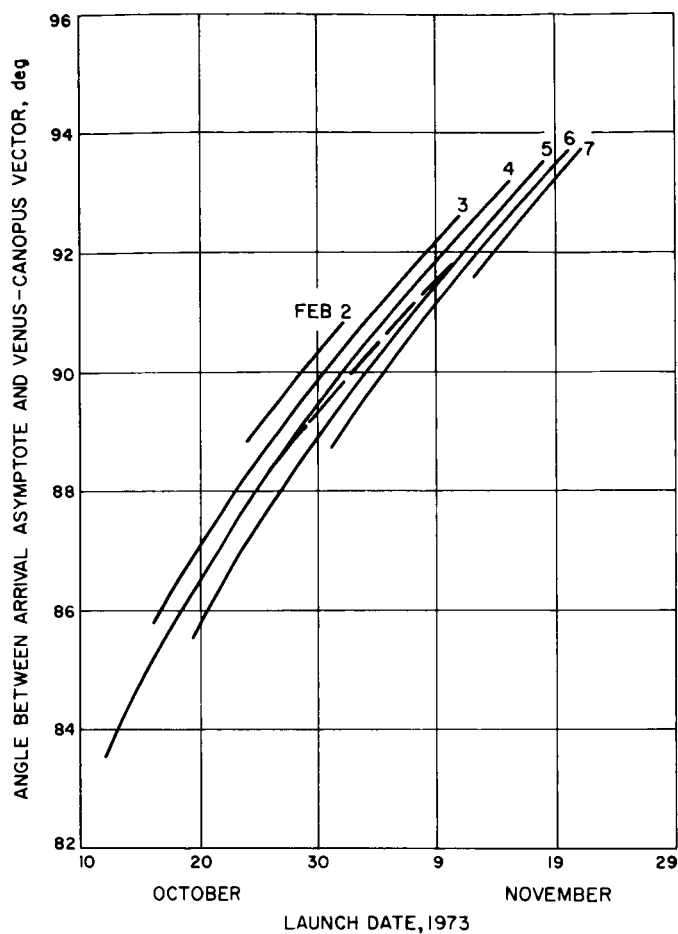


Fig. 18. Angle between arrival asymptote and Venus-Canopus vector (ζ_c)

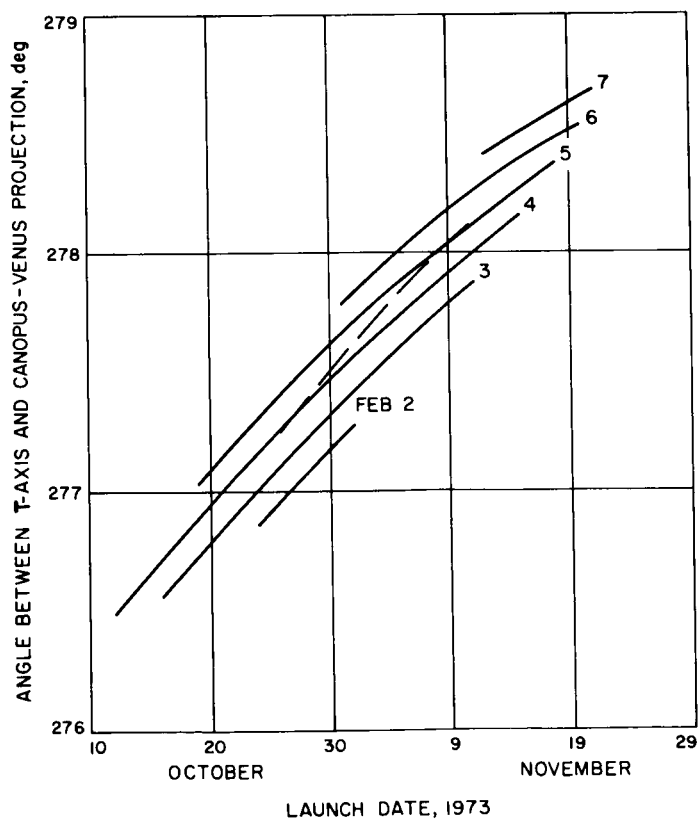


Fig. 19. Angle between T axis and Canopus-Venus projection (η_c)

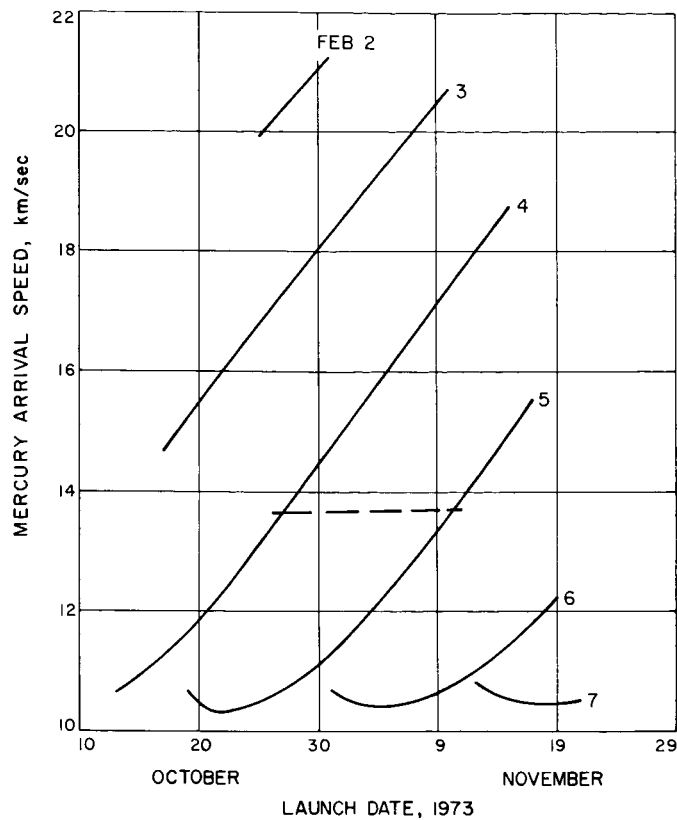


Fig. 20. Mercury arrival speed

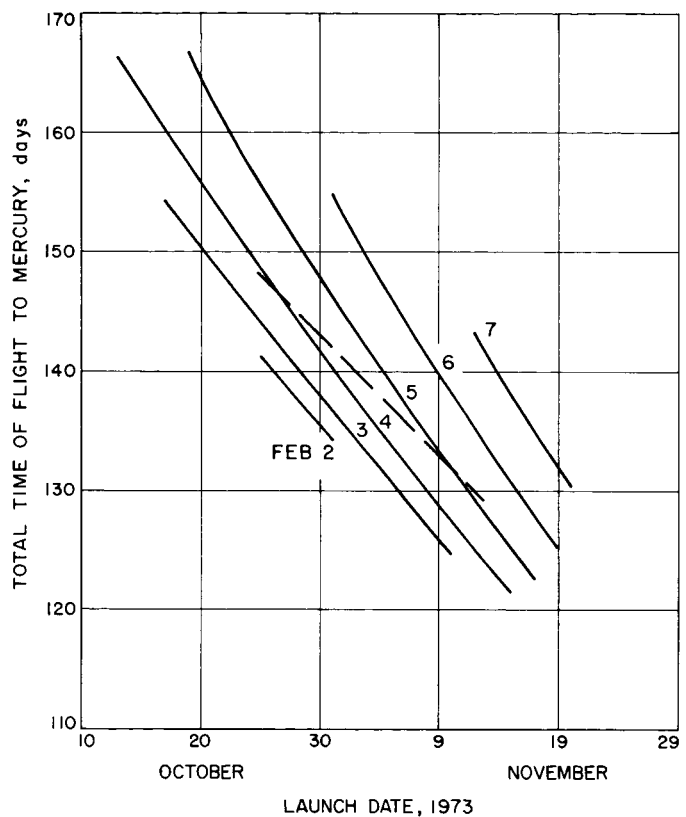


Fig. 21. Total time of flight to Mercury

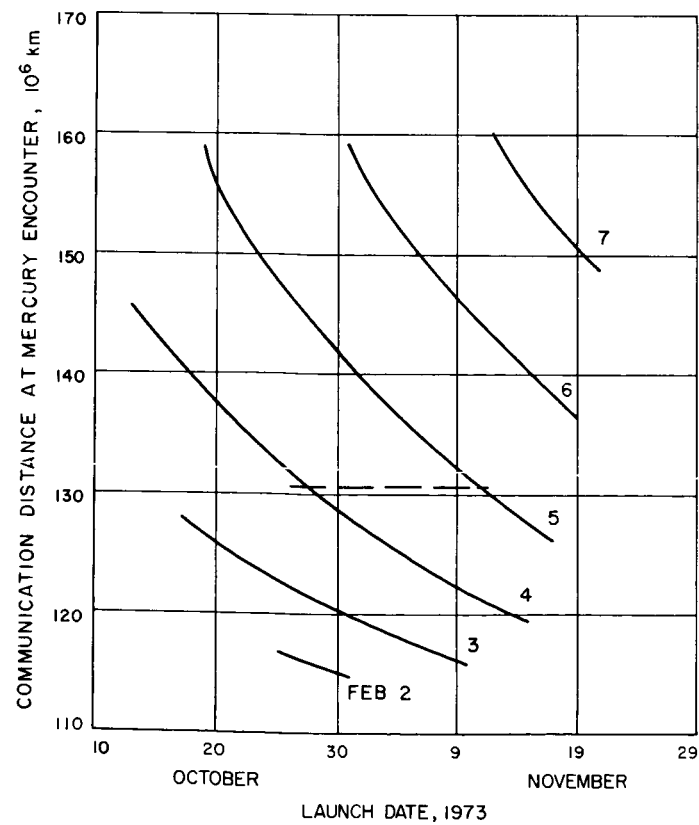


Fig. 22. Communication distance at Mercury encounter

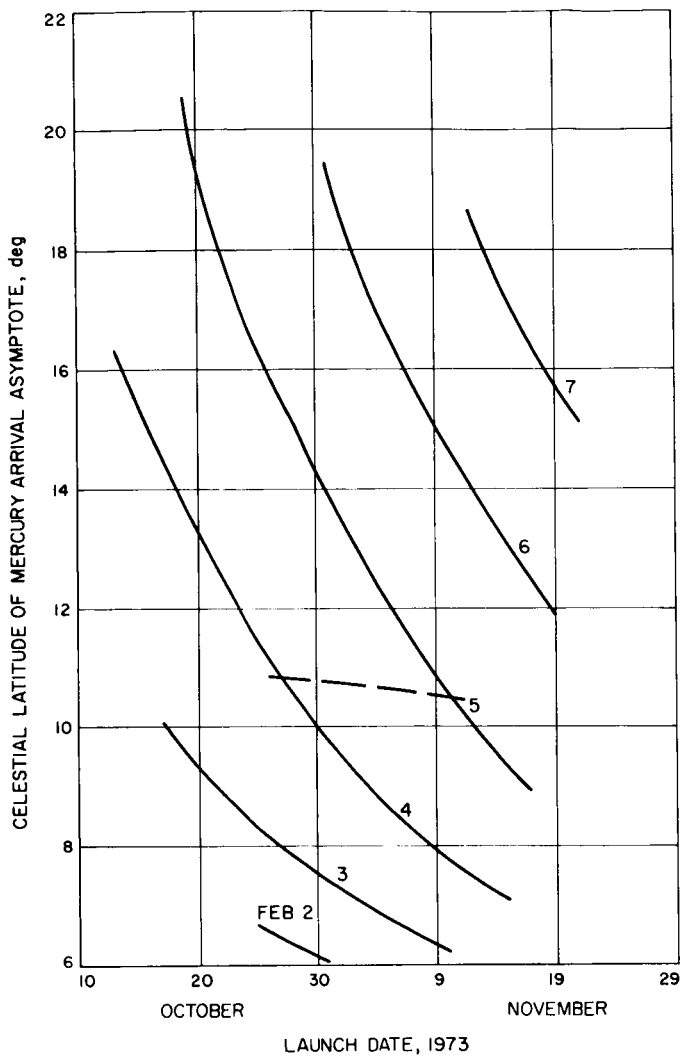


Fig. 23. Celestial latitude of Mercury arrival asymptote

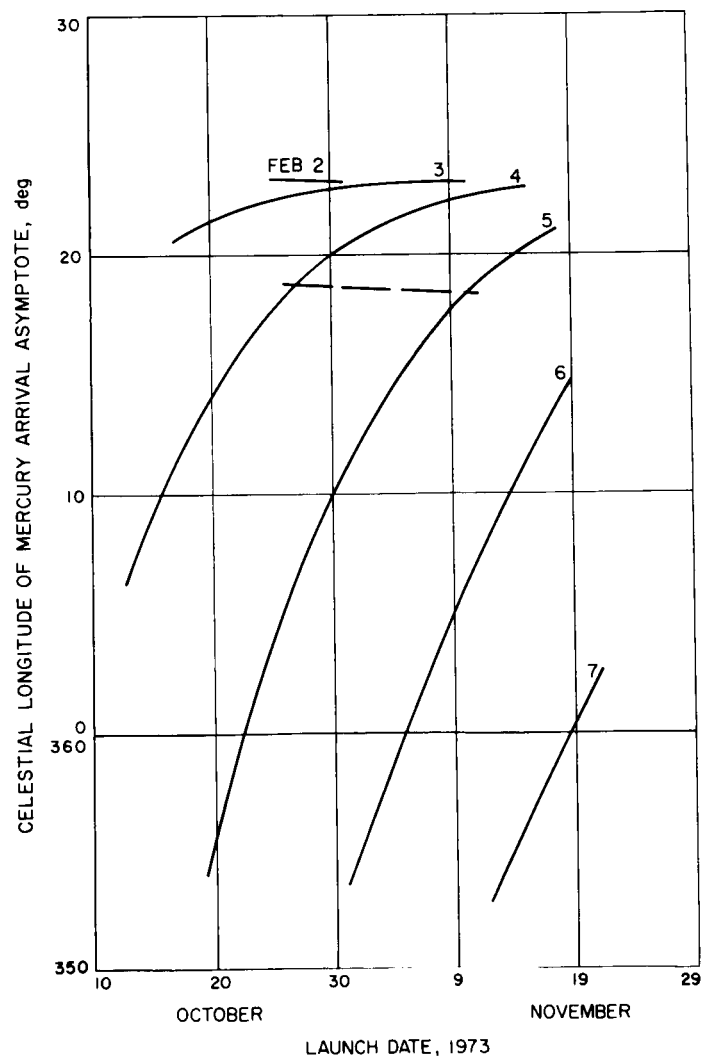


Fig. 24. Celestial longitude of Mercury arrival asymptote

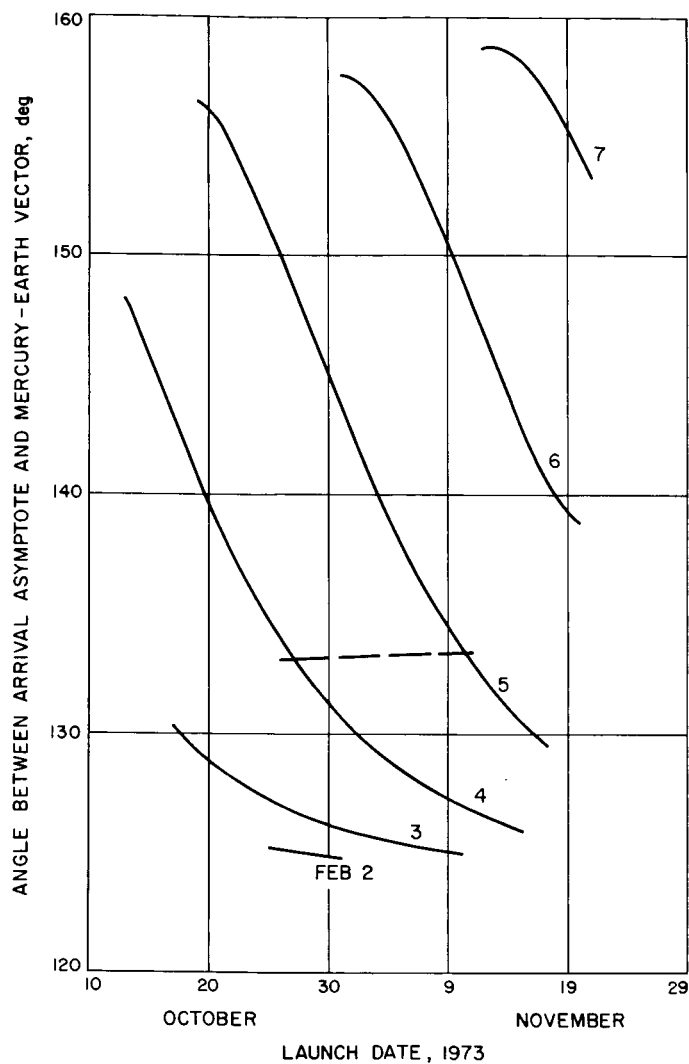


Fig. 25. Angle between arrival asymptote and Mercury-Earth vector (ζ_E)

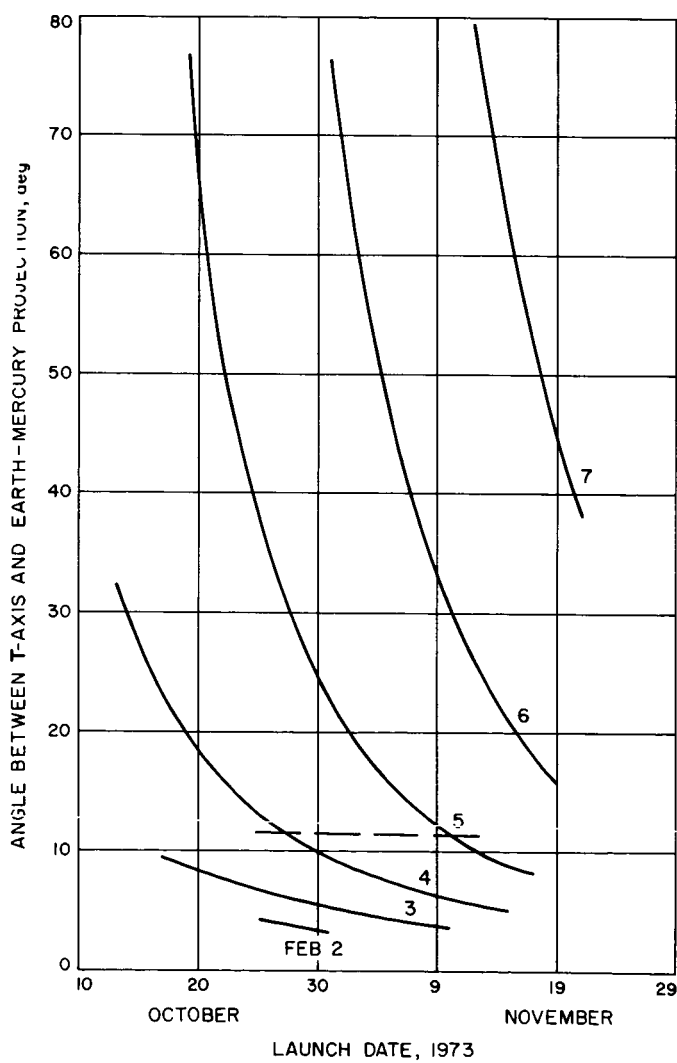


Fig. 26. Angle between T axis and Earth-Mercury projection (η_E)

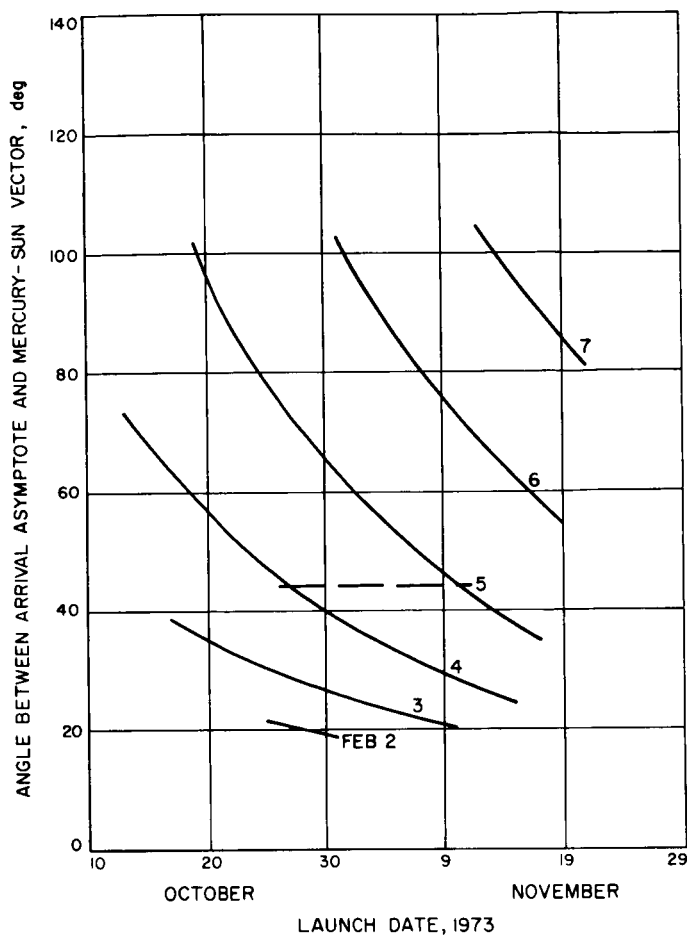


Fig. 27. Angle between arrival asymptote and Mercury-Sun vector (ζ_s)

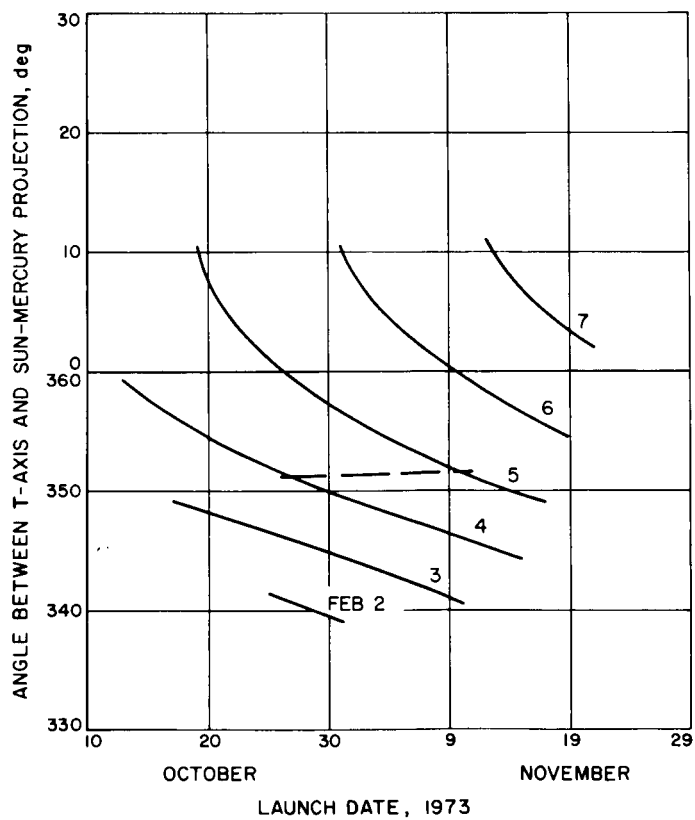


Fig. 28. Angle between T axis and Sun-Mercury projection (η_s)

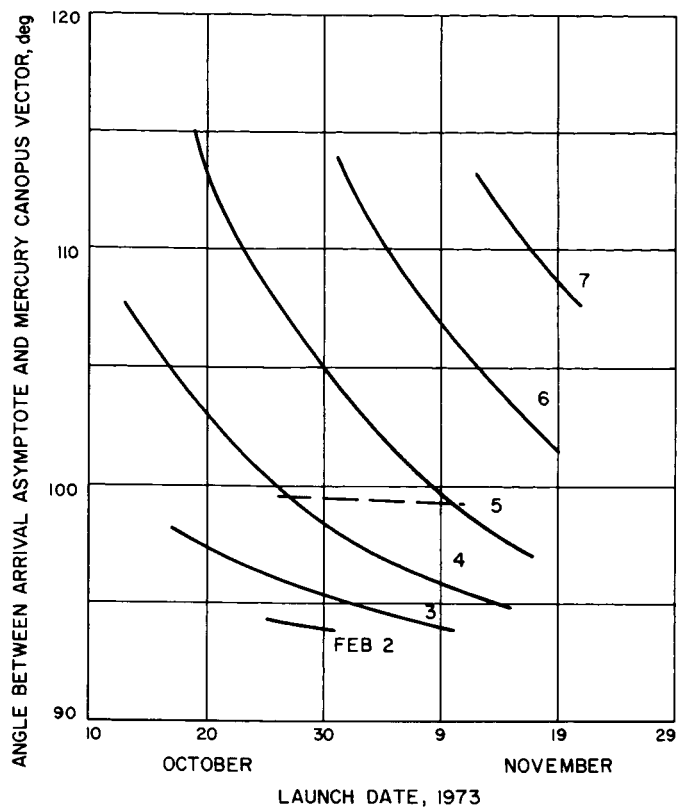


Fig. 29. Angle between arrival asymptote and Mercury-Canopus vector (ζ_c)

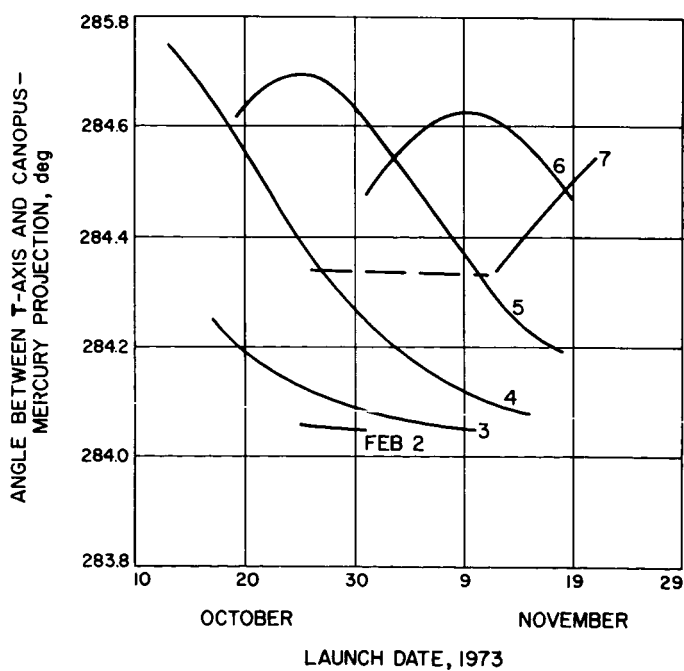


Fig. 30. Angle between T axis and Canopus-Mercury projection (η_c)

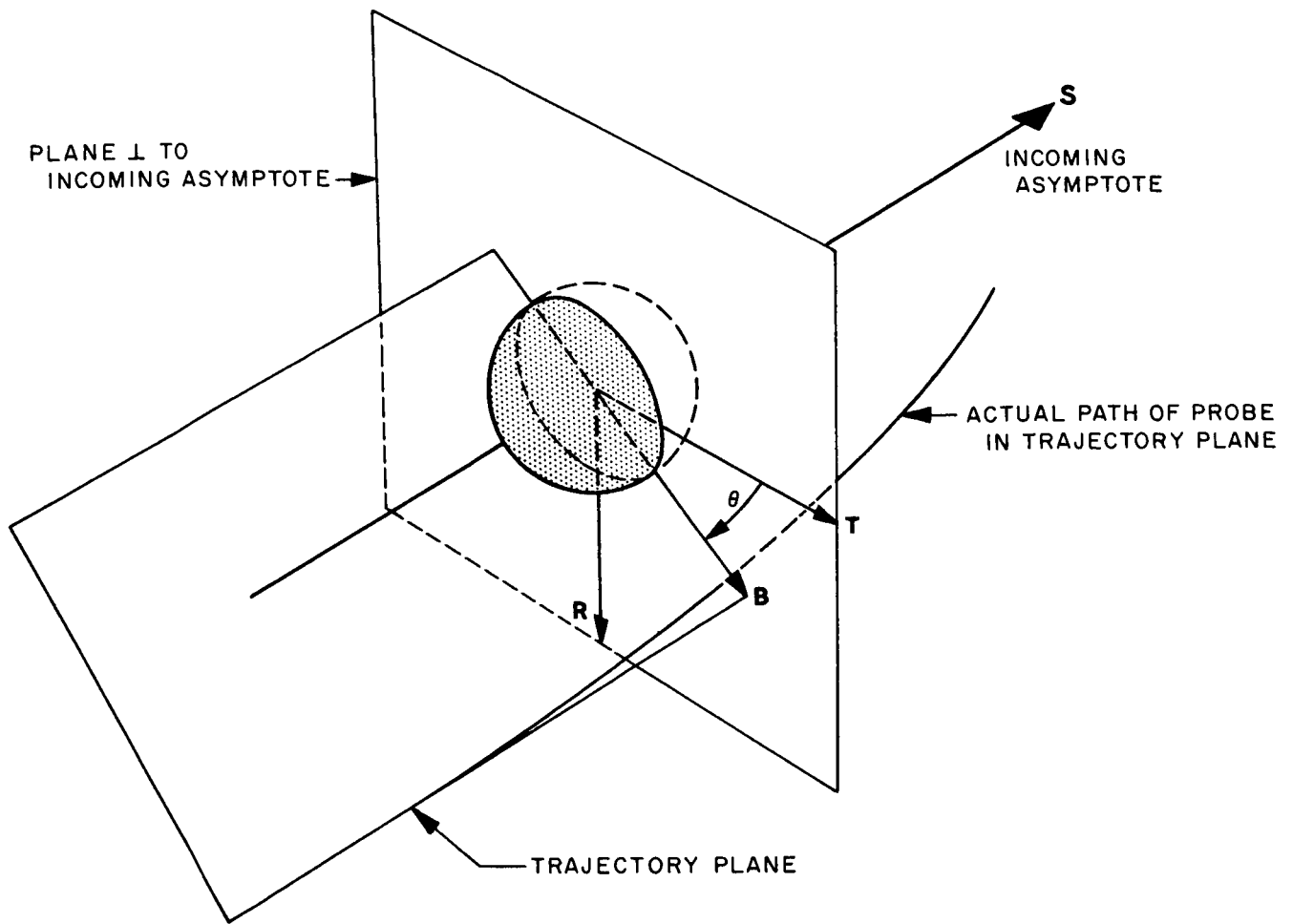


Fig. 31. Definition of aiming zone parameters

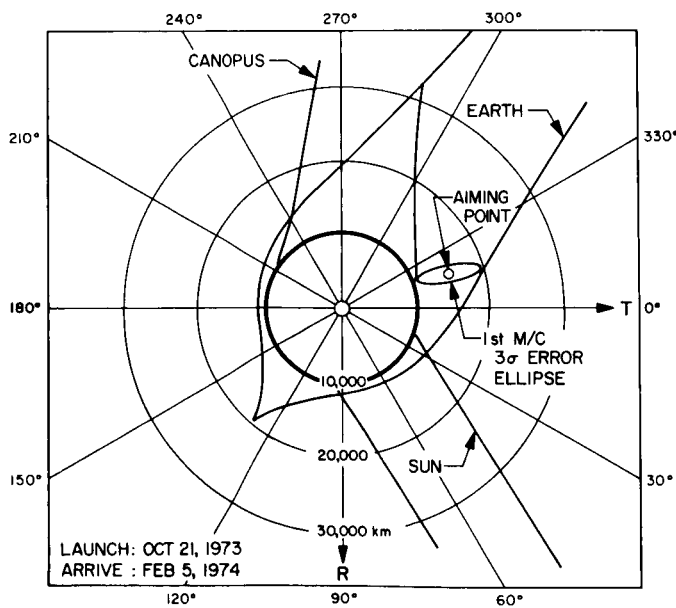


Fig. 32. Venus occultation zones for October 21 launch

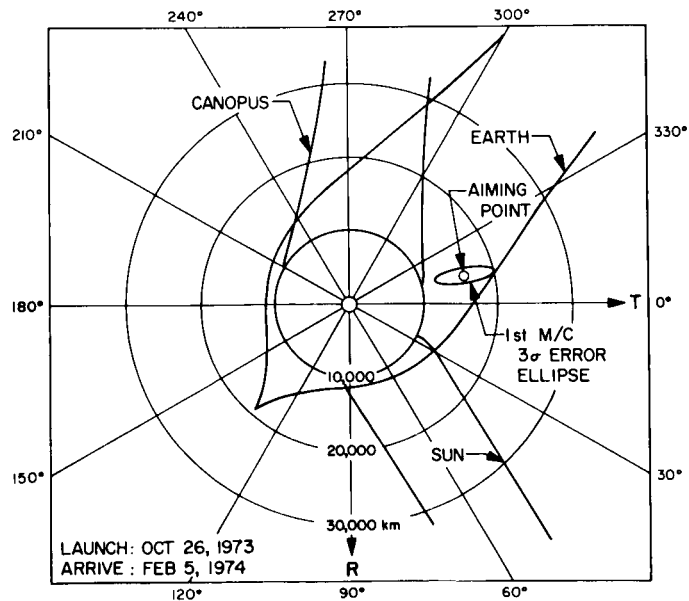


Fig. 33. Venus occultation zones for October 26 launch

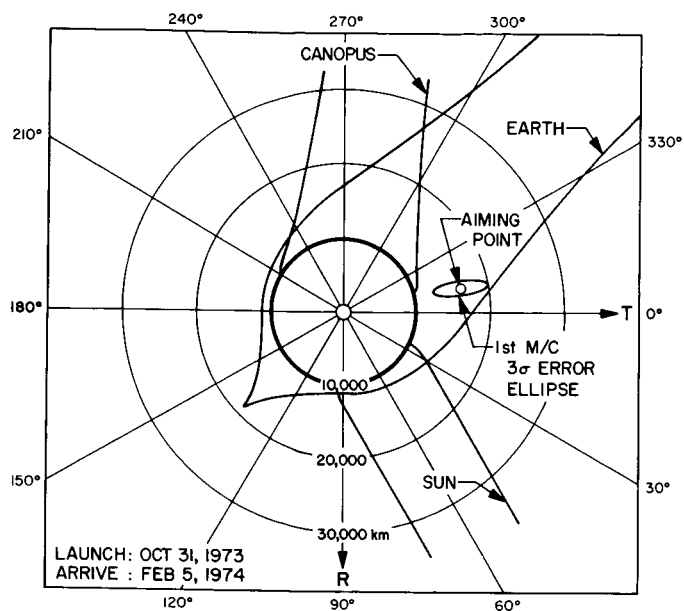


Fig. 34. Venus occultation zones for October 31 launch

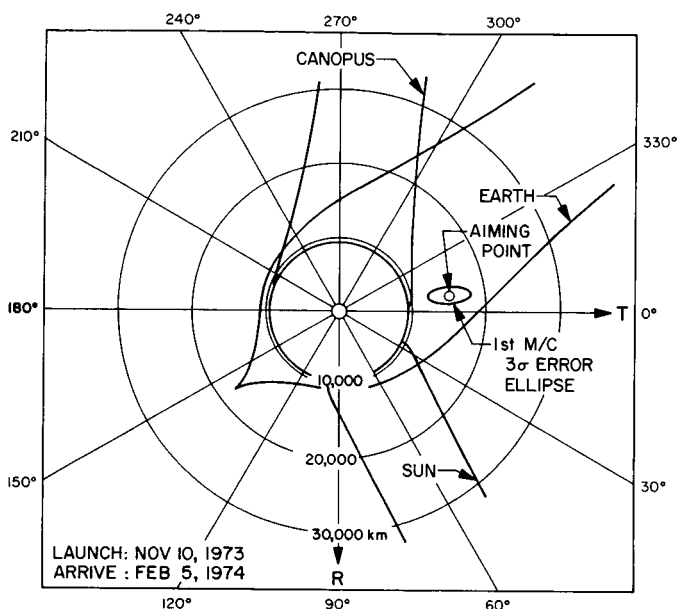


Fig. 36. Venus occultation zones for November 10 launch

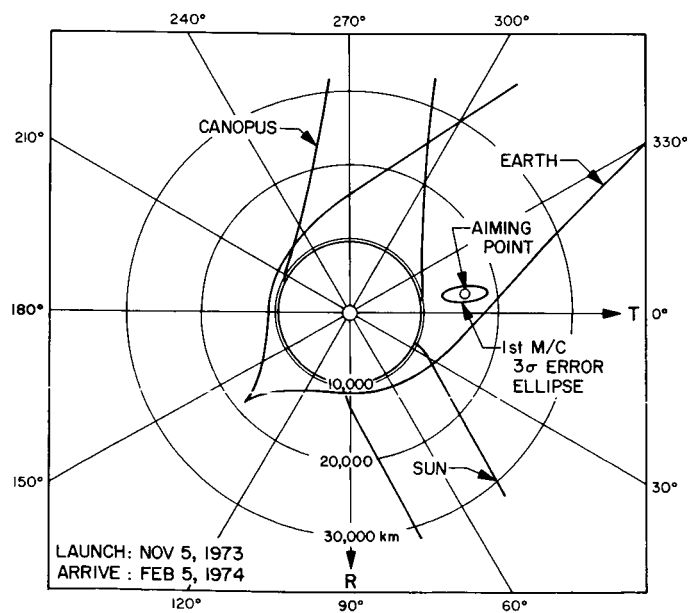


Fig. 35. Venus occultation zones for November 5 launch

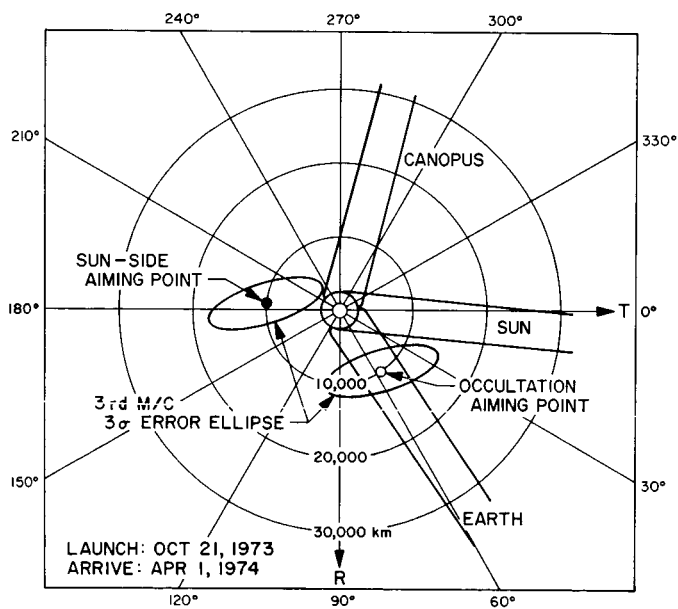


Fig. 37. Mercury occultation zones for October 21 launch

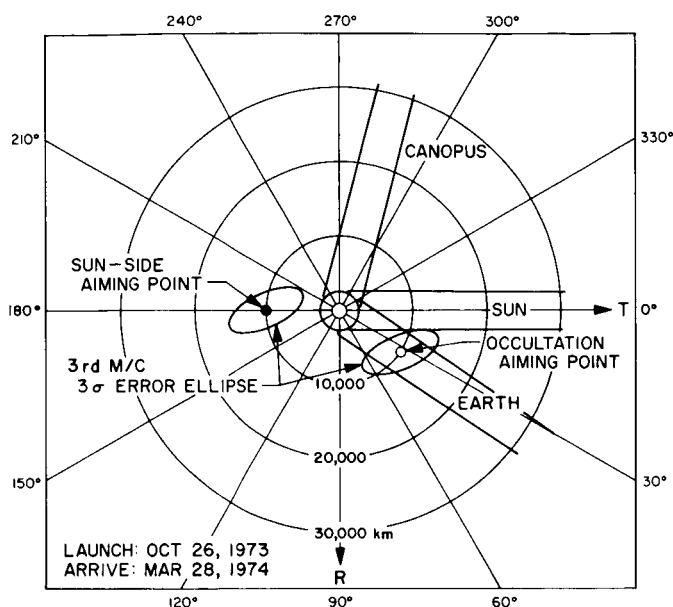


Fig. 38. Mercury occultation zones for October 26 launch

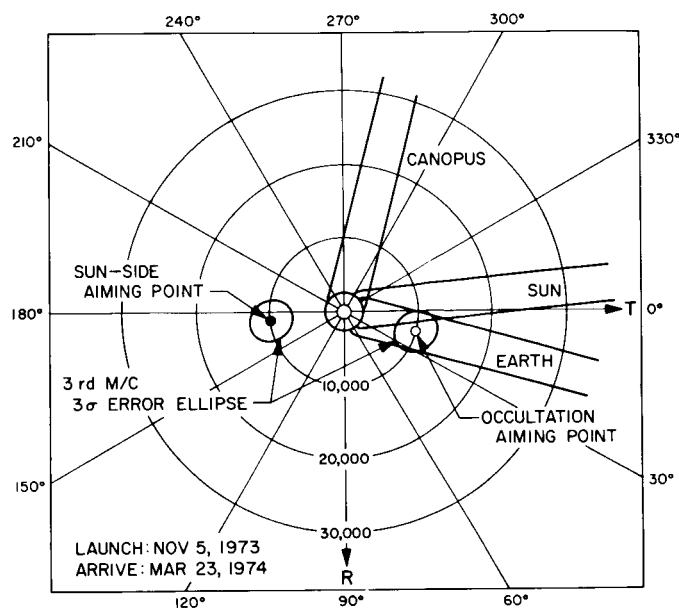


Fig. 40. Mercury occultation zones for November 5 launch

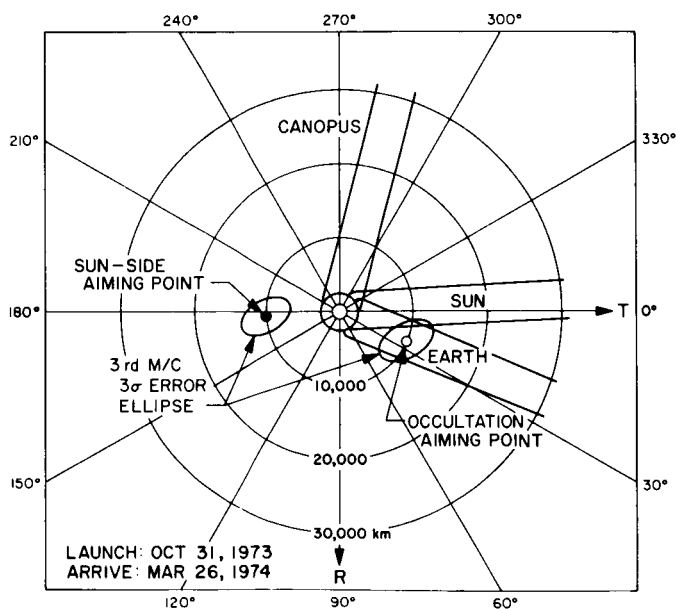


Fig. 39. Mercury occultation zones for October 31 launch

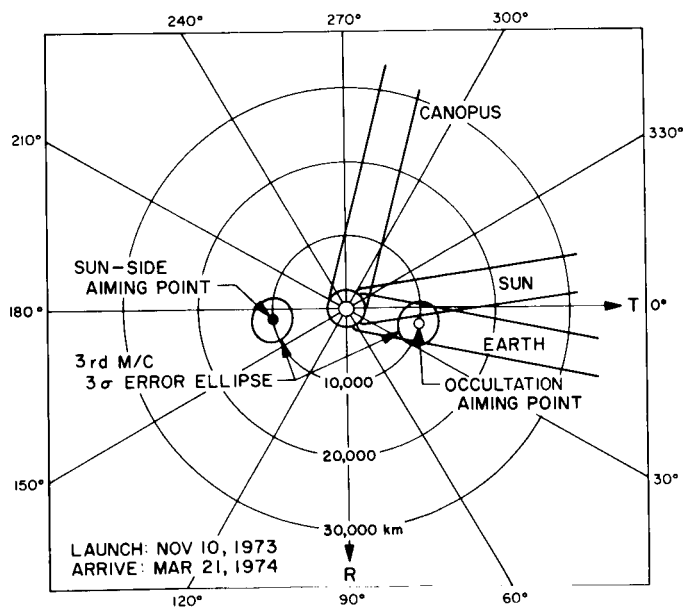


Fig. 41. Mercury occultation zones for November 10 launch

In comparison with the 1970 mission (see Ref. 2), the 1973 mission has the following characteristics:

- (1) Higher launch energies.
- (2) Larger altitudes at closest approach to Venus.
- (3) Higher Venus arrival speeds.
- (4) Smaller deflection angle at Venus.
- (5) Smaller total flight times.
- (6) Smaller communication distance at Mercury encounter.

As in the 1970 mission, the aiming points for the 1973 mission also result in the spacecraft's passing behind Venus as seen from the Earth, providing opportunity for an occultation experiment. Arrival speeds at Mercury can be obtained for 1973 that are slightly lower than for the selected 1970 mission design.

From Fig. 4, it is seen that the declination of the launch asymptote is near zero. This condition results in relatively long parking-orbit coast times and transfer-orbit injection points that are relatively far east.

The SPARC program prints a number of launch-window parameters, some of which are listed in Table 3

for each of the five sample launch dates. Eight assumptions are required for these data:

- (1) Parking orbit altitude, 90 nmi.
- (2) Launch azimuth sector, 90 to 114 deg.
- (3) Parking orbit ascent time, 570 sec.
- (4) Parking orbit ascent angle, 20 deg.
- (5) Final injection burn time, 105 sec.
- (6) Final injection angle, 8.5 deg.
- (7) Injection true anomaly, 4 deg.
- (8) Perigee radius of hyperbola, 6545 km.

These numbers are typical for Atlas-Centaur boost profiles.

III. Integrated Trajectory Analysis

To obtain detailed data along the trajectory and to check the accuracy of the conic trajectories, integrated trajectories were obtained for five launch dates at 5-day intervals over the launch period. For a constant Venus arrival date of February 5, 1974, the launch period for $C_3 = 19.5 \text{ km}^2/\text{sec}^2$ is 23 days, extending from October 20 to November 11, 1973. A shorter launch period (14 days), for $C_3 = 19.0 \text{ km}^2/\text{sec}^2$, extending from October 25 to

Table 3. Launch-window parameters

Launch date, 1973	Launch time, GMT	Launch azimuth, deg	Coast time, sec	Injection latitude, deg	Injection longitude, deg	Injection time, GMT
Oct. 21	05 49 54	90.	1728.	-23.31	52.55	06 29 57
	07 29 55	102.	1407.	-24.85	28.29	08 04 37
	08 53 40	114.	1150.	-28.78	6.68	09 24 05
Oct. 26	05 35 34	90.	1704.	-22.83	50.93	06 15 13
	07 15 10	102.	1384.	-24.34	26.75	07 49 30
	08 38 04	114.	1130.	-28.23	5.32	09 08 08
Oct. 31	05 19 52	90.	1680.	-22.34	49.33	05 59 07
	06 59 00	102.	1362.	-23.83	25.25	07 32 56
	08 20 54	114.	1110.	-27.68	4.03	08 50 39
Nov. 5	05 03 04	90.	1655.	-21.81	47.71	05 41 54
	06 41 38	102.	1339.	-23.30	23.75	07 15 12
	08 02 22	114.	1091.	-27.12	2.77	08 31 48
Nov. 10	04 45 27	90.	1630.	-21.26	46.06	05 23 52
	06 23 21	102.	1316.	-22.74	22.24	06 56 32
	07 42 42	114.	1072.	-26.56	1.55	08 11 50

November 7, 1973, is covered by the middle three of the five launch dates.

A. Targeting of Integrated Trajectories

Integrated trajectories were obtained by a differential correction process on the aiming point parameters, $\mathbf{B} \cdot \mathbf{T}$ and $\mathbf{B} \cdot \mathbf{R}$. The process is the same as that used in Ref. 2, except that the construction of the matrix of partial derivatives from differences of perturbed runs is done automatically by a double search routine using a 7094 program SEARCH (Ref. 7) to drive the single precision trajectory program, SPACE (Ref. 8). An outline of the process is:

- (1) Initialize with conic values of injection conditions and $\mathbf{B} \cdot \mathbf{T}$, $\mathbf{B} \cdot \mathbf{R}$ at Venus.
- (2) Search over Earth-Venus leg, varying injection velocity and flight path angle to obtain desired $\mathbf{B} \cdot \mathbf{T}$ and $\mathbf{B} \cdot \mathbf{R}$ at Venus.
- (3) Continue converged case to Mercury and note resulting $\mathbf{B} \cdot \mathbf{T}$ and $\mathbf{B} \cdot \mathbf{R}$.
- (4) Perturb Venus aiming point and repeat steps 2 and 3.
- (5) From results of step 4, construct partials of $\mathbf{B} \cdot \mathbf{T}$, $\mathbf{B} \cdot \mathbf{R}$ at Mercury with respect to $\mathbf{B} \cdot \mathbf{T}$, $\mathbf{B} \cdot \mathbf{R}$ at Venus.
- (6) Compute and apply differential corrections to $\mathbf{B} \cdot \mathbf{T}$, $\mathbf{B} \cdot \mathbf{R}$ at Venus.
- (7) Repeat steps 2, 3, and 6 until convergence at Mercury is obtained.

The number of iterations in step 7 was either 2 or 3. The average running time was 45 min. The long running time is almost entirely due to the number of iterations required on the Earth-Venus leg (step 2). A large number of these was required because of the tight convergence criteria on $\mathbf{B} \cdot \mathbf{T}$ and $\mathbf{B} \cdot \mathbf{R}$ at Venus (± 2 km). The convergence criteria at Mercury was ± 1000 km.

B. Comparison of Conic and Integrated Trajectories

The excellent agreement between the final integrated trajectory parameters and those obtained from the conic analysis is shown in Table 4. The conic values from SPARC and the integrated values from SPACE are compared for a number of parameters for each launch date.

C. Plots of Integrated Trajectory Parameters

There are 14 plots from fine prints of the converged integrated runs. The first five (Figs. 42 to 46) are plan views of the five integrated trajectories projected onto

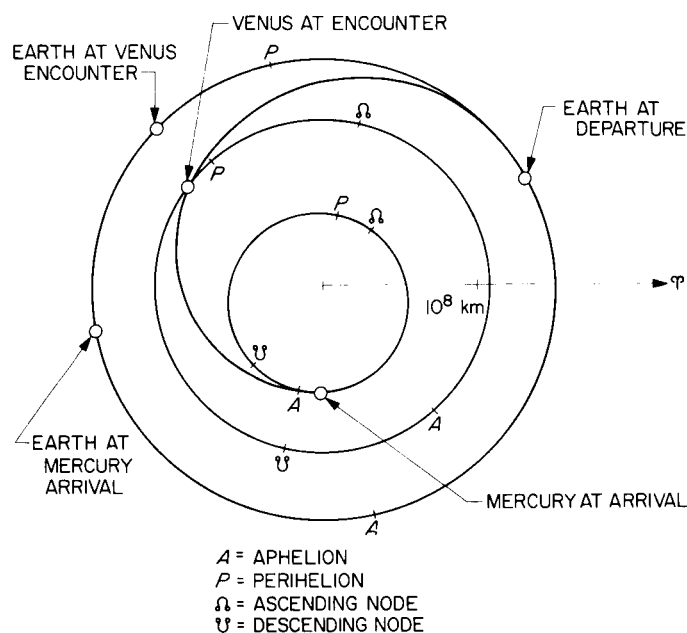


Fig. 42. Projection of trajectory on ecliptic plane for October 21, 1973 launch

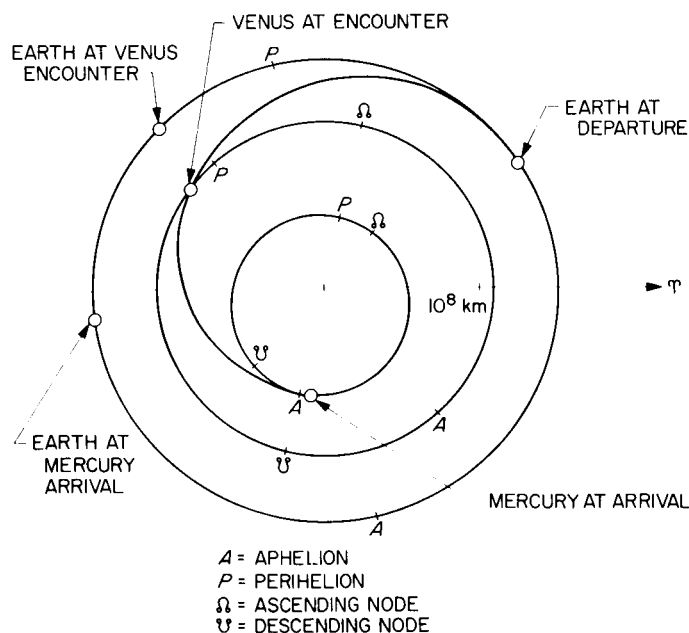


Fig. 43. Projection of trajectory on ecliptic plane for October 26, 1973 launch

Table 4. Comparison of conic and integrated trajectories

Launch	Oct. 21, 1973		Oct. 26, 1973		Oct. 31, 1973		Nov. 5, 1973		Nov. 10, 1973	
	SPARC ^a	SPACE ^b	SPARC	SPACE	SPARC	SPACE	SPARC	SPACE	SPARC	SPACE
t_{inj} , GMT	06 29 57	06 29 57	06 15 13	06 15 13	05 59 07	05 59 07	05 41 54	05 41 54	05 23 52	05 23 52
V_{inj} , km/sec	11.873	11.874	11.856	11.860	11.849	11.852	11.854	11.853	11.874	11.870
γ_{inj} , deg	2.27	2.34	2.27	2.24	2.27	2.12	2.27	2.23	2.27	2.32
C_r , km ² /sec ²	19.3417	19.3598	18.9385	19.0148	18.7623	18.8325	18.8733	18.8638	19.3620	19.2542
ϕ_i , deg	5.6313	5.5708	5.0175	5.0041	4.3164	4.4063	3.4788	3.5128	2.4693	2.4767
θ_i , deg	317.0327	316.9038	317.2053	317.1657	316.8604	317.0220	315.9898	316.0659	314.6131	314.6271
V_{h_2} , km/sec	7.8544	7.8495	8.0329	8.0169	8.2211	8.2111	8.4179	8.4299	8.6230	8.6295
β_2 , deg	-16.1590	-16.1881	-14.3672	-14.4199	-12.7496	-12.7839	-11.2716	-11.2698	-9.9043	-9.9100
λ_2 , deg	315.1311	315.1495	316.4166	316.4648	317.6136	317.6442	318.7143	318.6891	319.7085	319.7003
$E-V T_r$, days	107. (106.73) ^c	106.70	102. (101.74)	101.76	97. (96.75)	96.75	92. (91.76)	91.67	87. (86.78)	86.71
h_{ca} , km	4531.93	4680.30	5481.01	5510.71	5796.52	5847.40	5637.68	5541.45	5171.54	5048.44
Date Venus Encounter	2/5/74 0 ^h	2/4/74 23 20 12	2/5/74 0 ^h	2/5/74 00 35 36	2/5/74 0 ^h	2/4/74 23 57 15	2/5/74 0 ^h	2/4/74 21 44 48	2/5/74 0 ^h	2/4/74 22 20 22
$B \cdot T_2$, km	14356.	14553.	15467.	15491.	15777.	15841.	15562.	15473.	14957.	14847.
$B \cdot R_2$, km	-4699.	-4613.	-3846.	-3939.	-3209.	-3202.	-2667.	-2399.	-2224.	-2054.
β_3 , deg	-23.8116	-23.4802	-19.7185	-19.9353	-16.9268	-16.9151	-14.7006	-14.2153	-12.8717	-12.5721
λ_3 , deg	355.3457	355.0324	352.7188	352.8069	351.7676	351.7598	351.7801	351.9432	352.4610	352.6919
V_{h_1} , km/sec	10.3924	10.3741	10.5883	10.5608	11.2869	11.2903	12.3469	12.6860	13.6346	13.9054
β_1 , deg	18.4206	18.2182	15.9789	16.0615	13.9567	13.9144	12.1372	11.7061	10.5819	10.3111
λ_1 , deg	358.2096	358.8076	5.0715	4.6475	10.7319	10.7910	15.1519	16.1674	18.2647	18.7578
$V-M T_r$, days	55.2348	54.9443	51.9277	52.0706	49.2729	49.2280	46.9316	46.4157	44.8850	44.5597
Total T_r , days ^d	161.96	161.64	153.67	153.83	146.02	145.98	138.69	138.09	131.66	131.27
Date Mercury Encounter	4/1/74 05 38 02	3/31/74 22 00 00	3/28/74 22 15 51	3/29/74 02 17 20	3/26/74 06 33 02	3/26/74 05 25 38	3/23/74 22 21 27	3/23/74 07 43 28	3/21/74 21 14 26	3/21/74 11 46 23
$B \cdot T_1$, km	5600.	6351.	8300.	7319.	9200.	8660.	9600.	10381.	9800.	10015.
$B \cdot R_1$, km	8300.	8099.	5600.	5751.	3900.	3979.	2800.	2849.	2100.	1984.

^aThe Mercury aiming point values shown in the SPARC column are the target values of the integrated searches, chosen to result in Earth occultation.

^bThe values in the SPACE columns are those of the final, converged trajectory.

^cMeasured from injection that is not actually zero hour, as assumed in the heliocentric part of the conic runs.

^dTotal flight time is measured from the injection epoch.

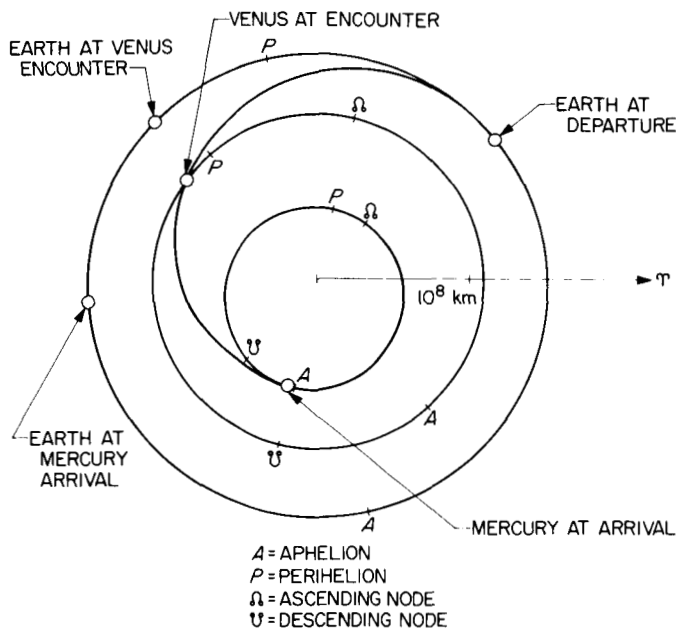


Fig. 44. Projection of trajectory on ecliptic plane for October 31, 1973 launch

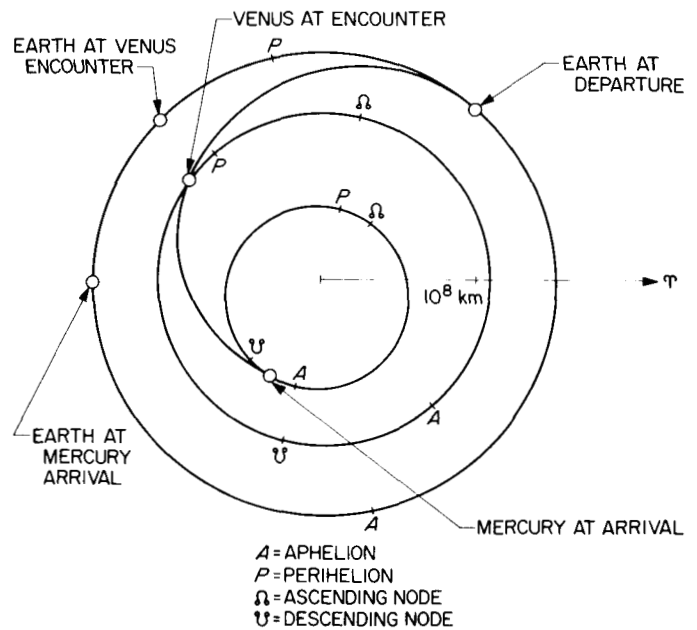


Fig. 46. Projection of trajectory on ecliptic plane for November 10, 1973 launch

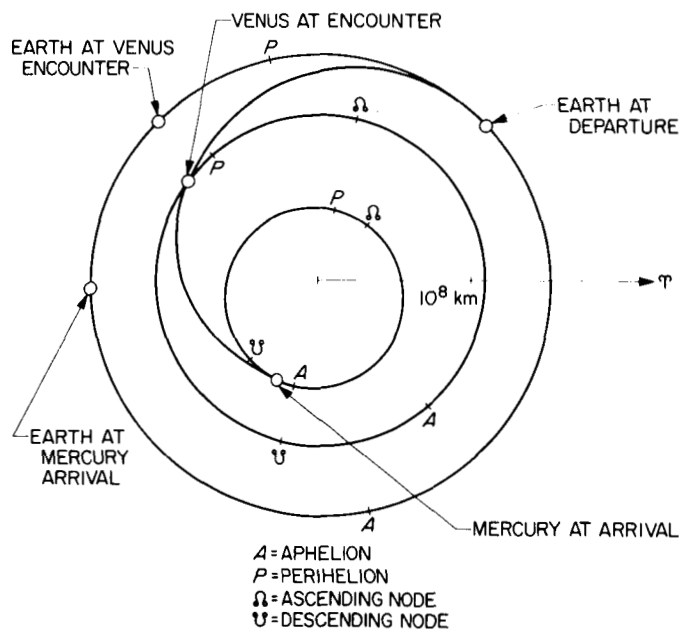


Fig. 45. Projection of trajectory on ecliptic plane for November 5, 1973 launch

the ecliptic plane. Note that Mercury encounter occurs near aphelion of Mercury's fairly eccentric orbit. The angular separation of the Sun and Mercury as seen from the Earth is near its maximum value for this condition.

This is important for minimizing solar noise in telemetry and tracking data.

Figures 47 to 55 show important parameters plotted vs time from launch, extending about 100 days past Mercury encounter.

Parameters that are important with regard to tracking data and communication power are geocentric radius and range-rate, which are shown vs time from launch in Figs. 47 and 48, respectively. The Sun-centered coordinates, radius, celestial latitude, and celestial longitude, are shown in Figs. 49 to 51. The heliocentric radius is important in the design of temperature control and solar panels, if they are used.

Figures 52 to 55 present important angles that are used for design of spacecraft antennas and attitude sensors. The Sun-Earth-probe angle approaches very near zero about 200 days after launch. This means that tracking stations would be pointing their antennas almost directly at the Sun, which might cause temporary communications difficulty.

The spacecraft roll axis is pointed toward the Sun if solar panels are used. The direction of the Earth in spacecraft coordinates is, therefore, defined by the Earth-probe-Sun angle (called the *cone angle* of the Earth,

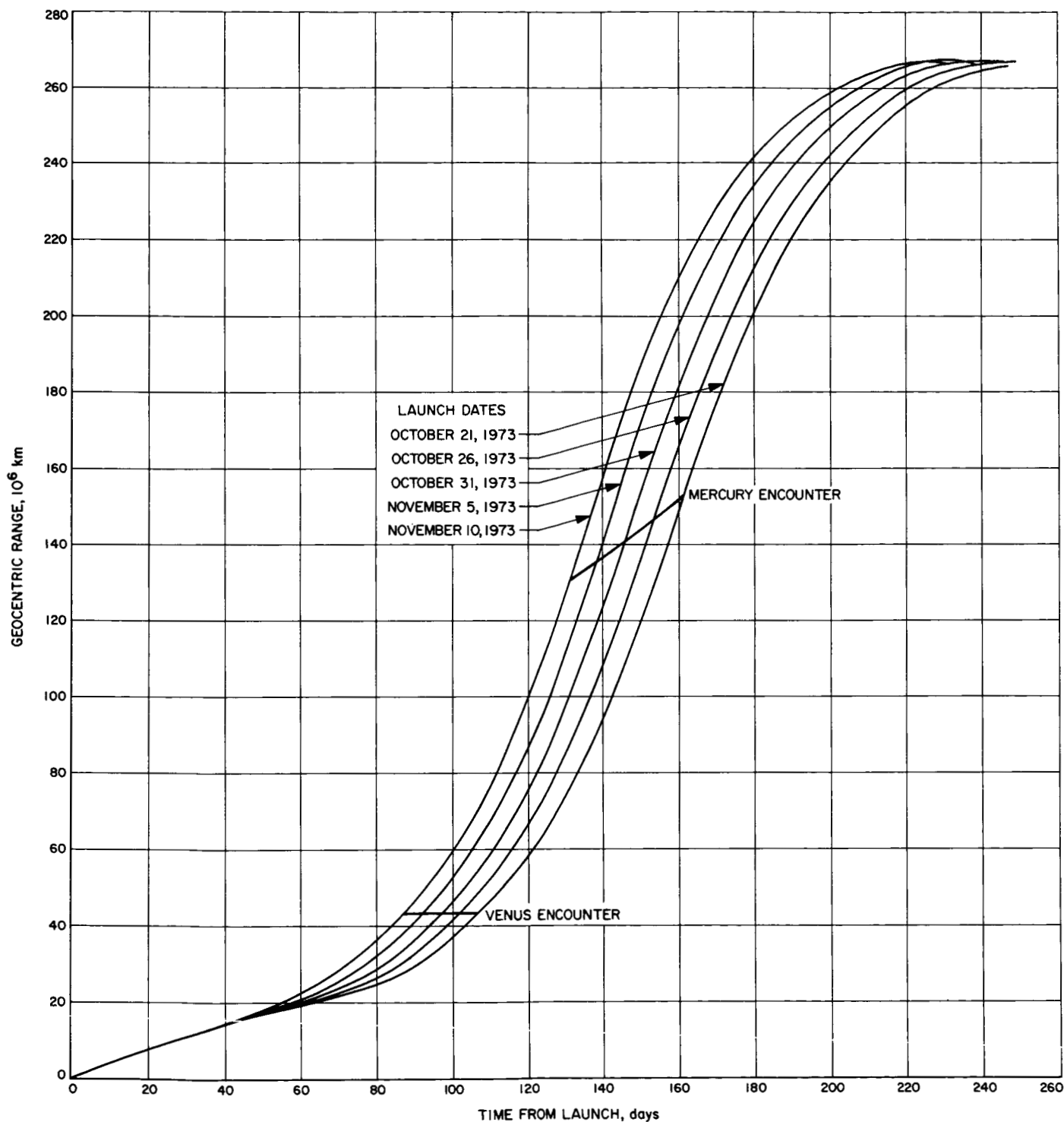


Fig. 47. Geocentric range vs time from launch for five launch dates

because it is the angle of the Earth from the roll axis), and the *clock* angle of the Earth (defined as the angle from the projection of the probe-Canopus vector, measured in a plane perpendicular to the probe-Sun

vector, or roll-axis). These two angles are shown in Figs. 53 and 54. Since they undergo large variations, a fixed high-gain antenna (such as was possible on the *Mariner* Mars mission in 1964) cannot be used.

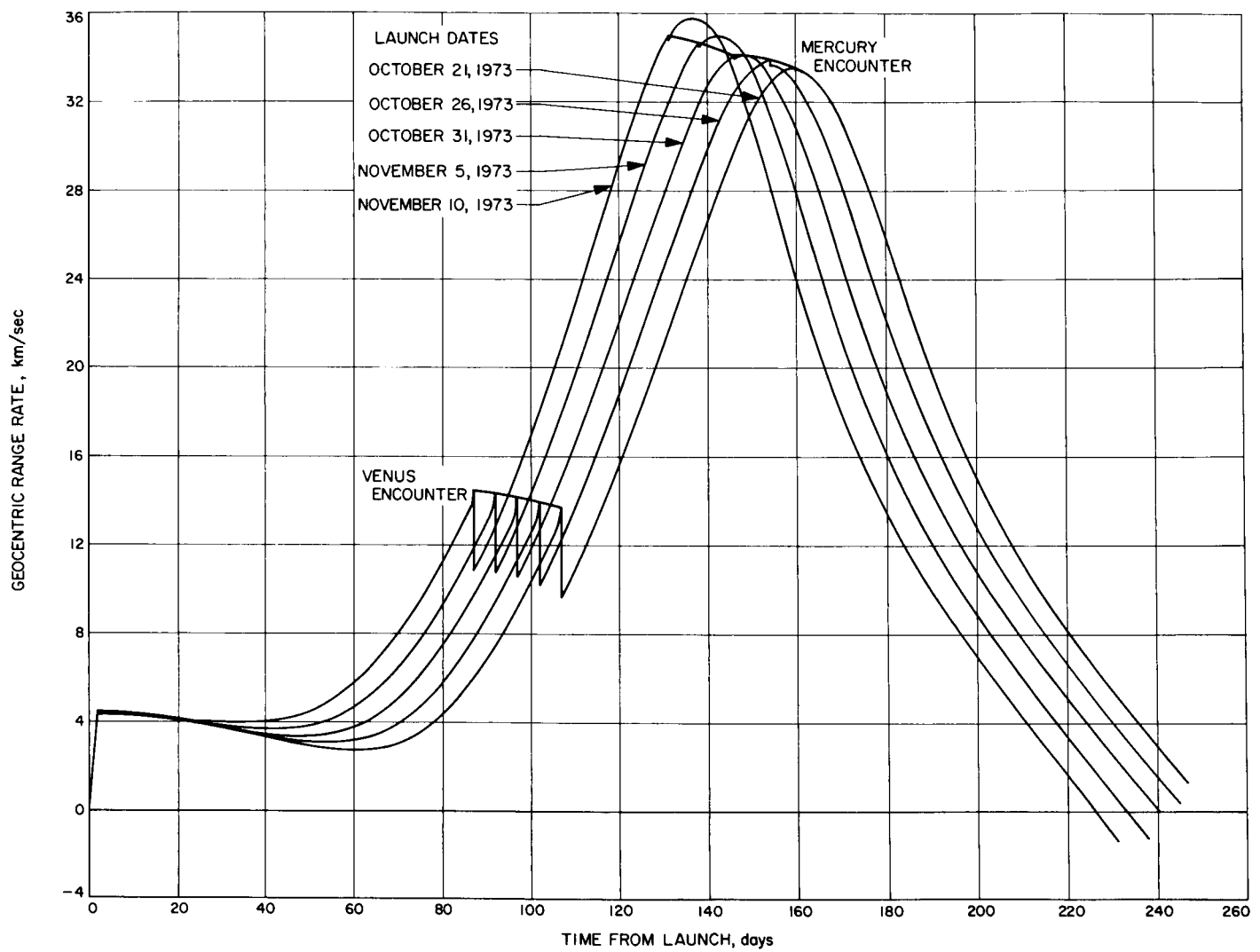


Fig. 48. Geocentric range-rate vs time from launch for five launch dates

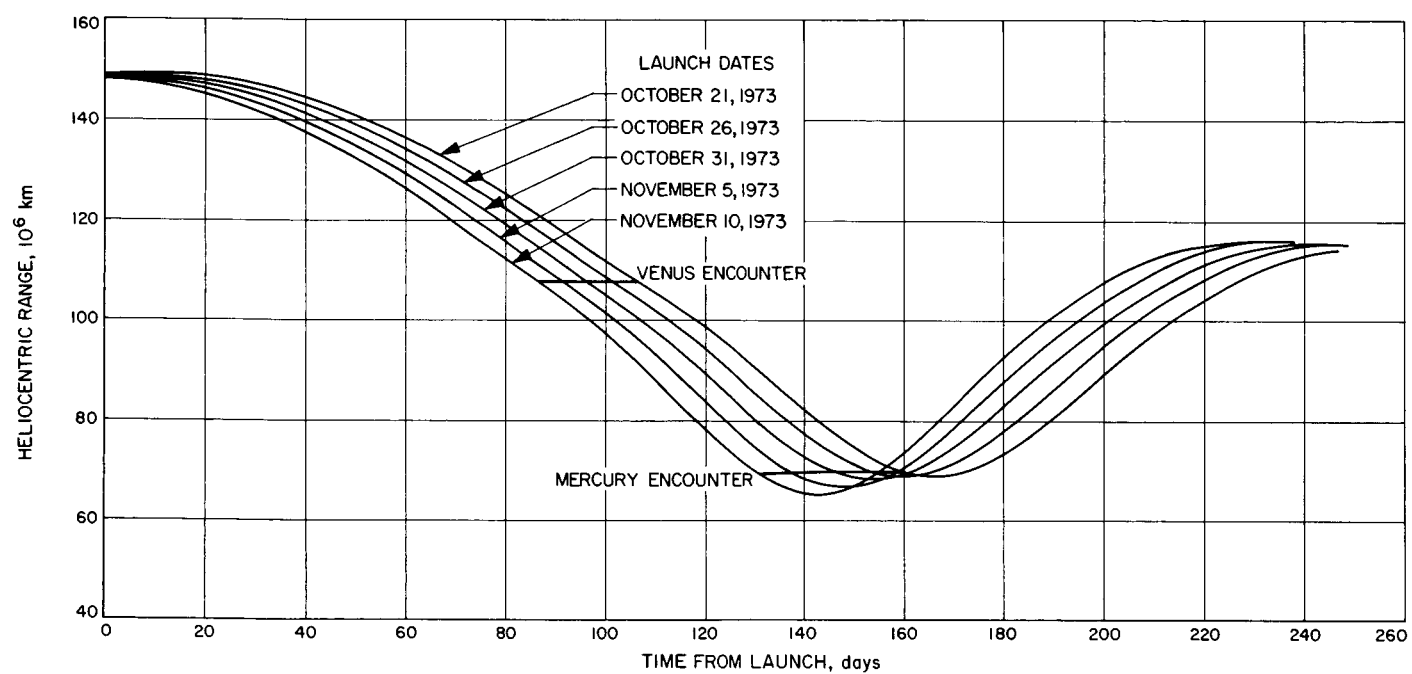


Fig. 49. Heliocentric range vs time from launch for five launch dates

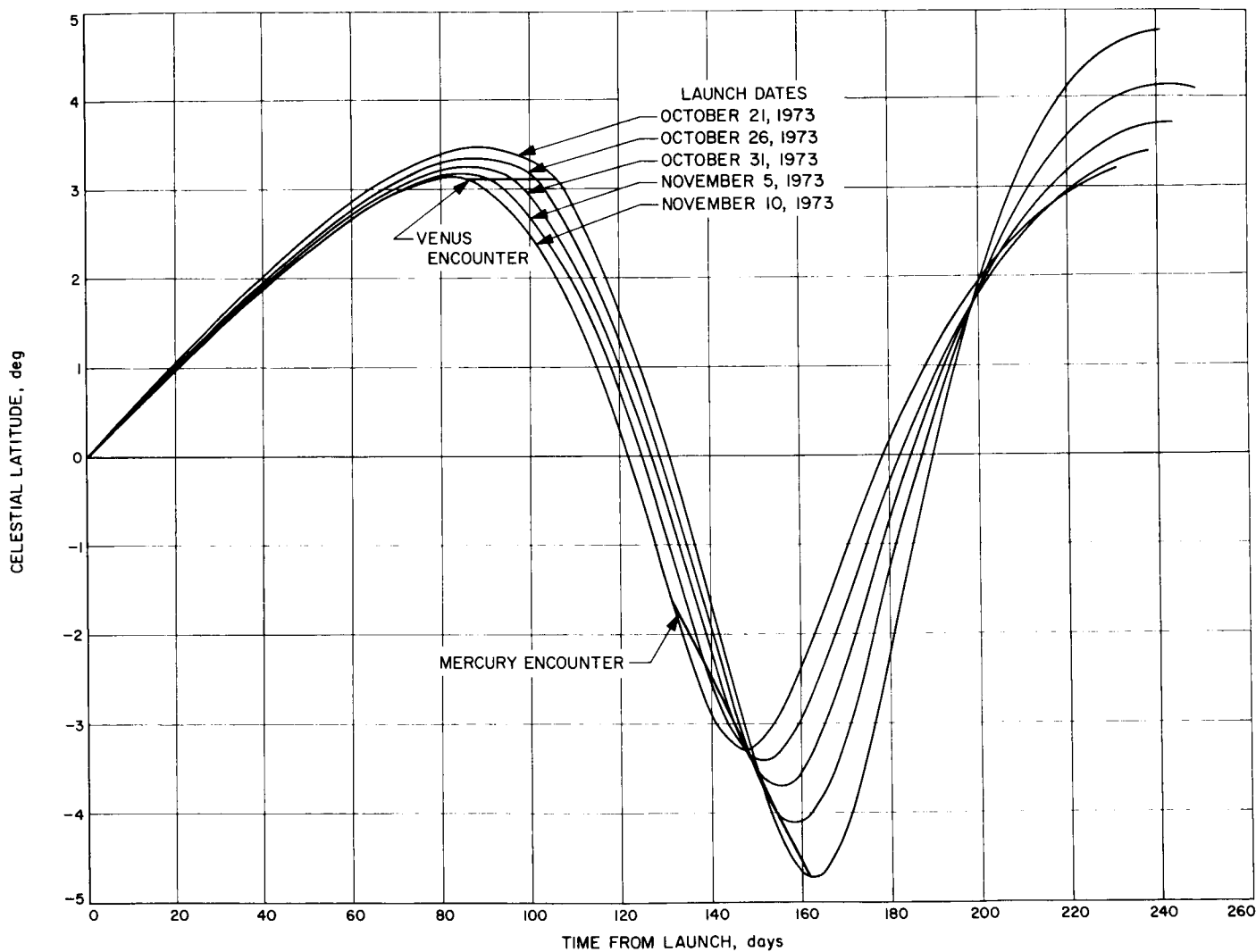


Fig. 50. Celestial latitude vs time from launch for five launch dates

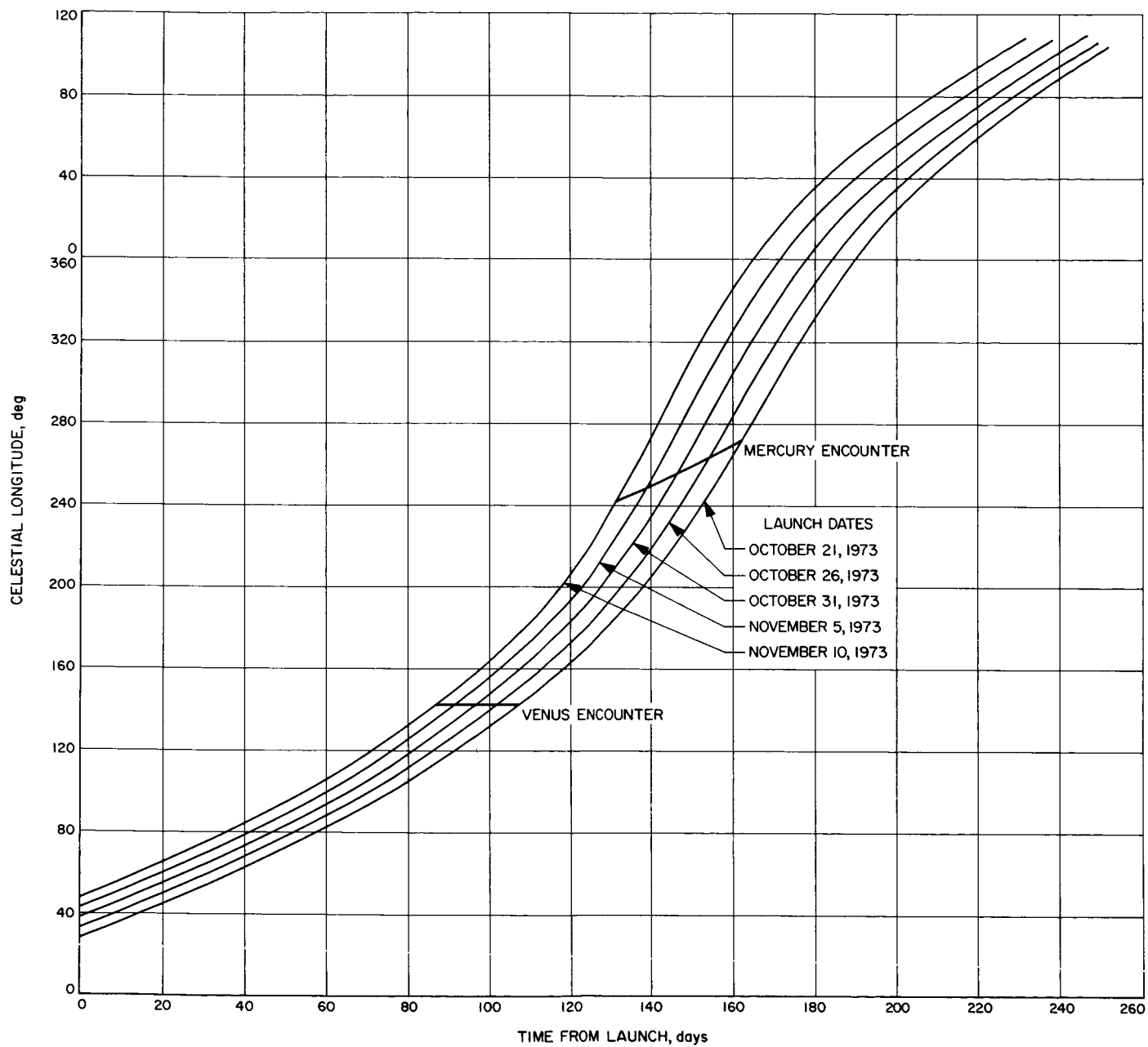


Fig. 51. Celestial longitude vs time from launch for five launch dates

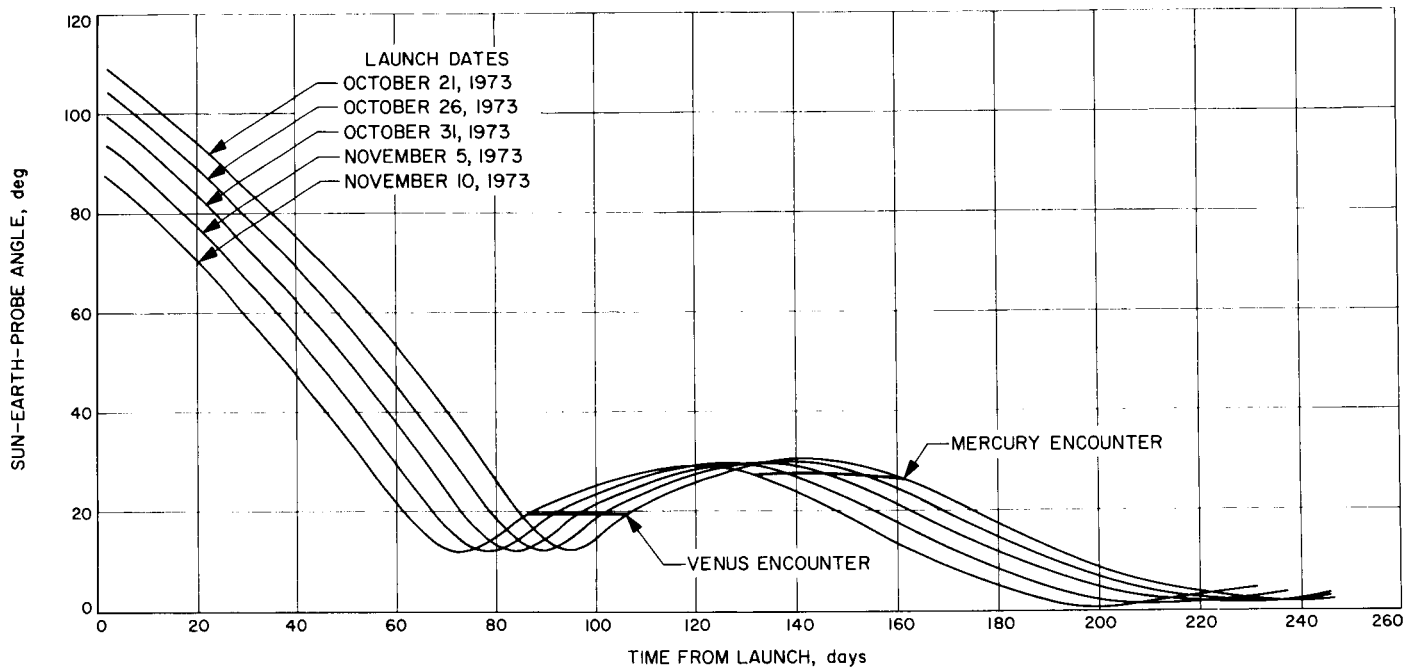


Fig. 52. Sun-Earth-probe angle vs time from launch for five launch dates

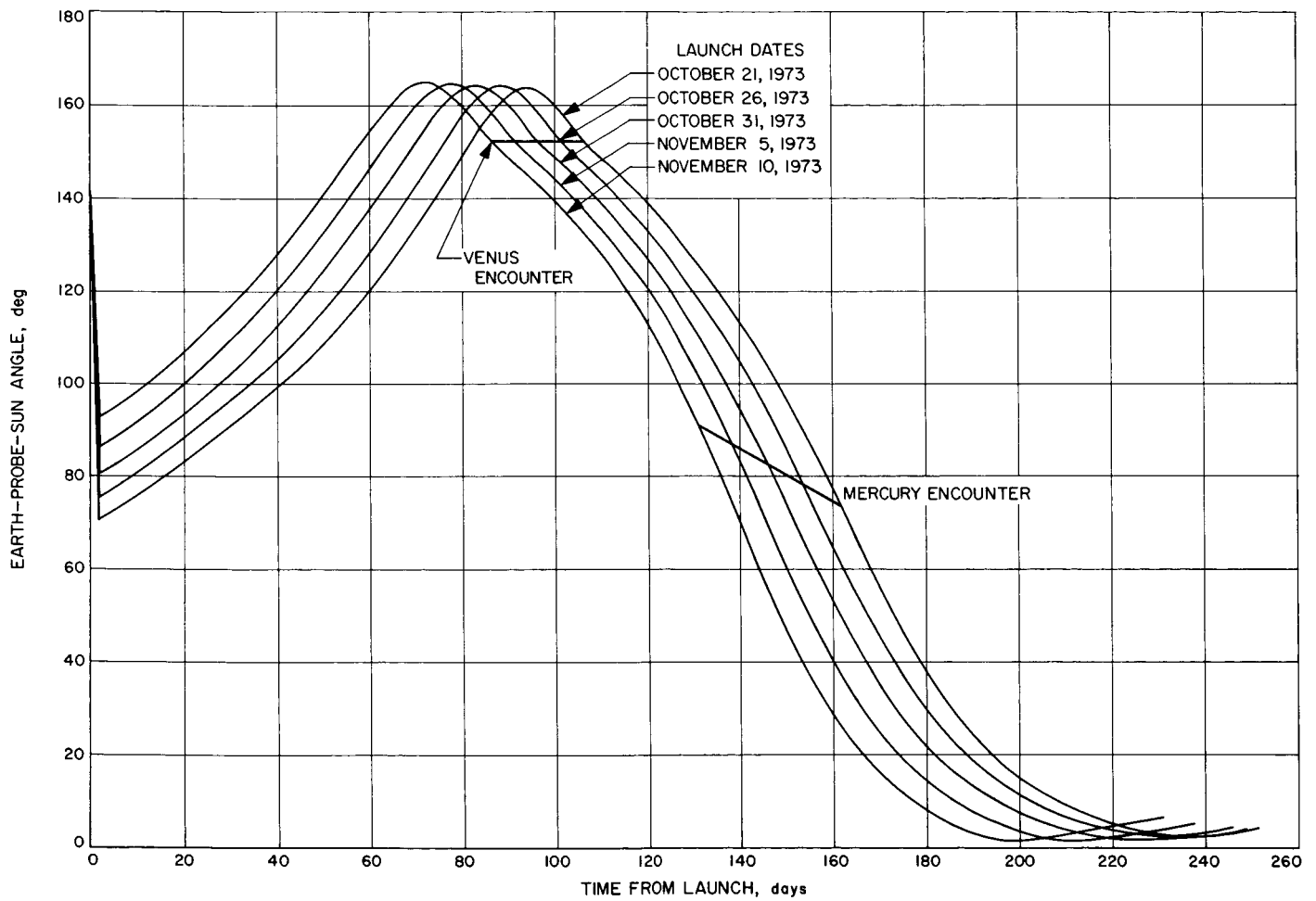


Fig. 53. Earth-probe-Sun angle (Earth cone angle) vs time from launch for five launch dates

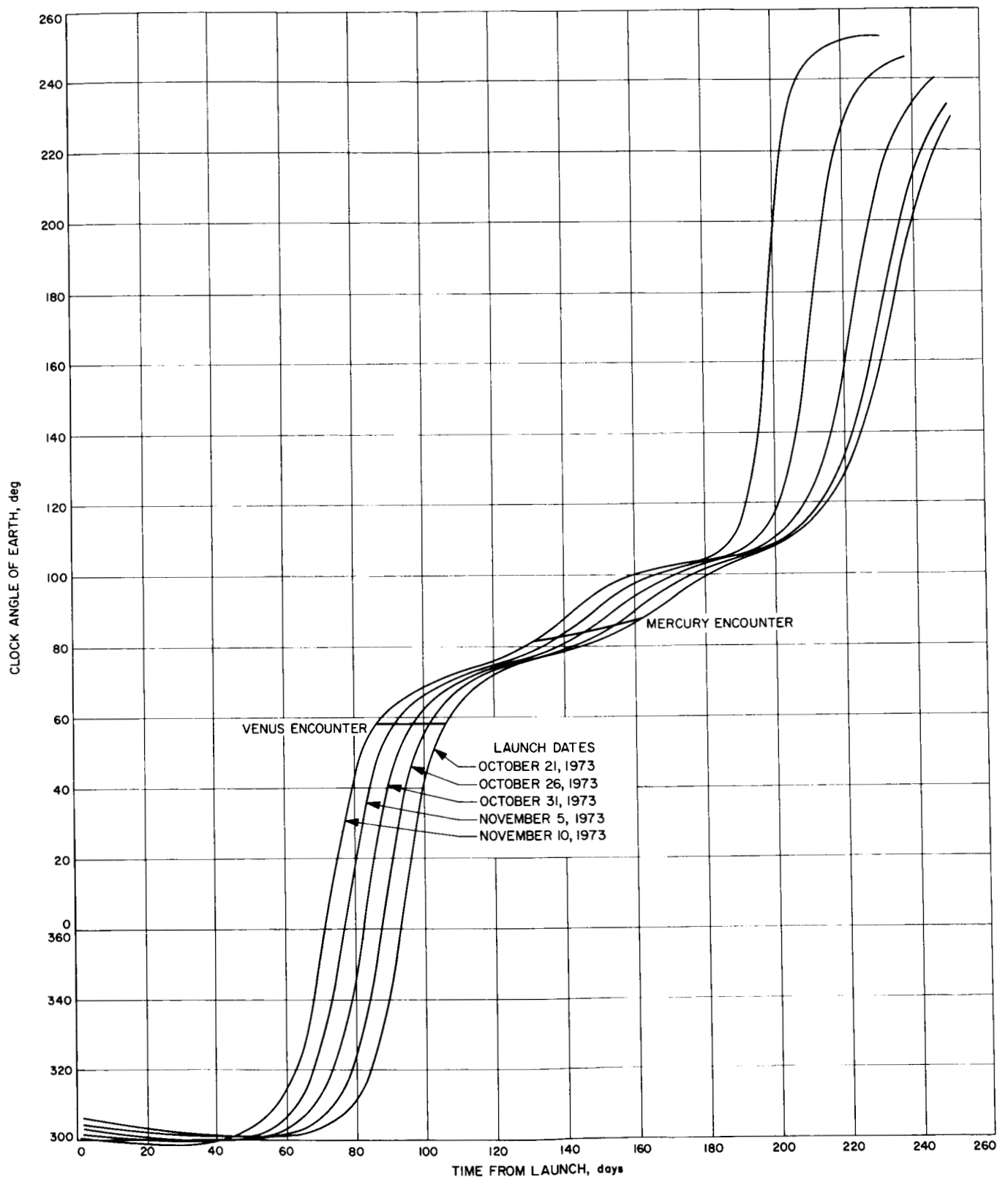


Fig. 54. Clock angle of Earth (with respect to Canopus) vs time from launch for five launch dates

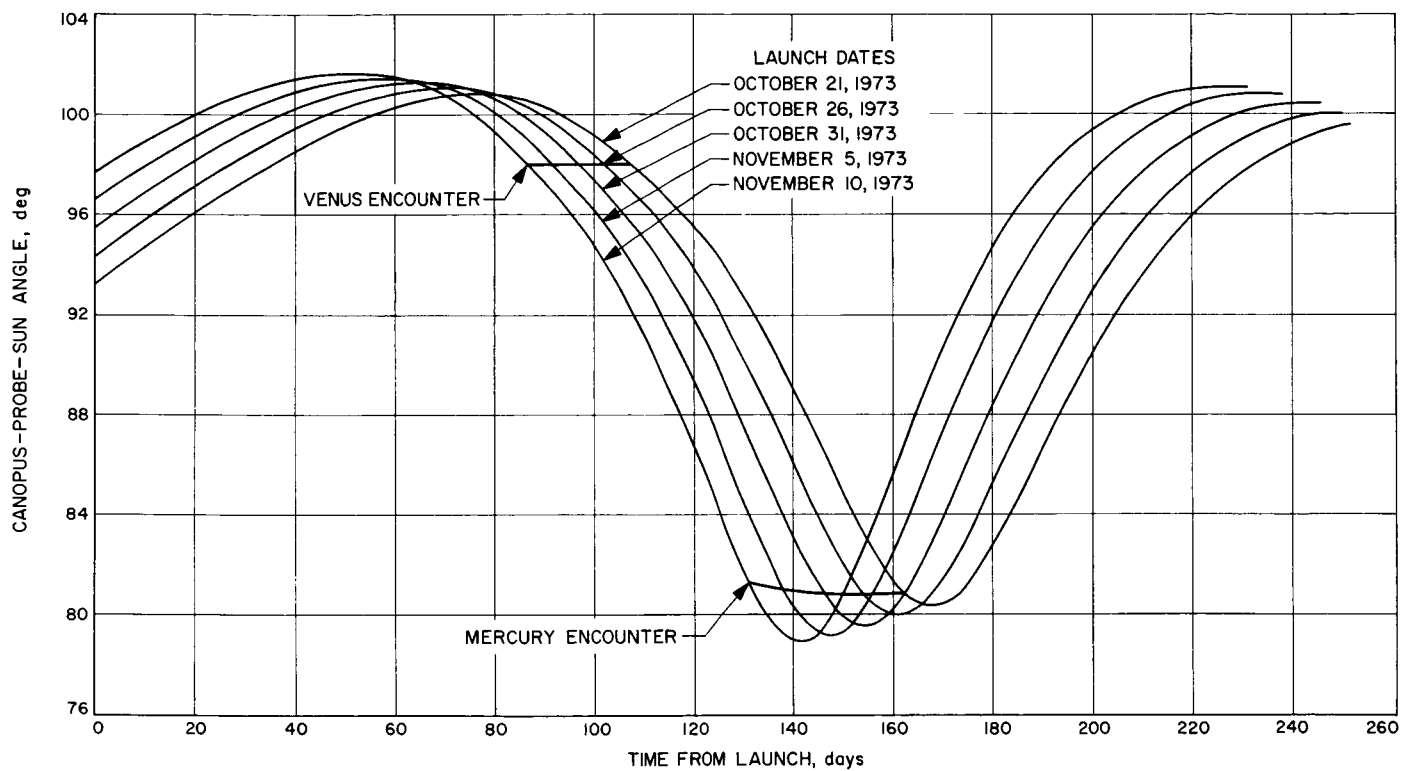


Fig. 55. Canopus-probe-Sun angle (Canopus cone angle) vs time from launch for five launch dates

The spacecraft would probably be attitude stabilized with a Canopus tracker. The Canopus cone angle, shown in Fig. 55, gives the limits over which the sensor must be able to track.

IV. Near-Planet Geometry

In this section, more detailed and more pictorial information is presented concerning the near-planet geometry for the 1973 Venus-Mercury mission. In Figs. 56 to 61, the following information is shown for each of five launch dates for Venus encounter:

- (1) Cone angle of planet (Venus or Mercury).
- (2) Clock angle of planet.
- (3) Planet-spacecraft radius.
- (4) Velocity with respect to planet.
- (5) Percent of planet illuminated.
- (6) Angular semi-diameter of planet.

These data were taken from runs on the conic program MARCAM.¹ Each parameter is plotted vs time from 3 hr

¹MARCAM is a program developed by N. Haynes of the Systems Analysis Section to provide flyby information for the *Mariner-Mars* 1964 project.

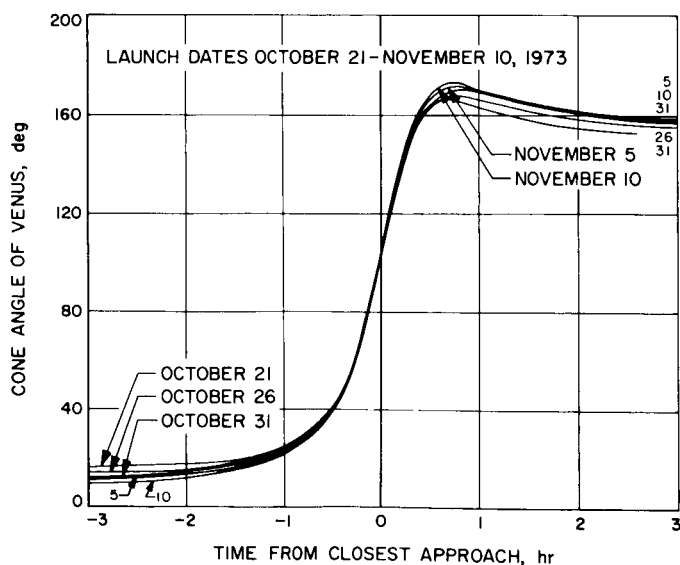


Fig. 56. Cone angle of Venus vs time from closest approach for five launch dates

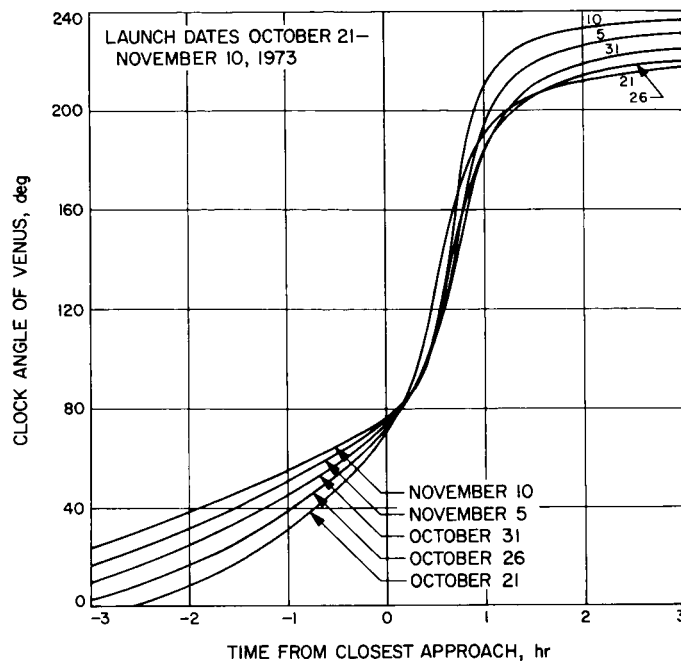


Fig. 57. Clock angle of Venus vs time from closest approach for five launch dates

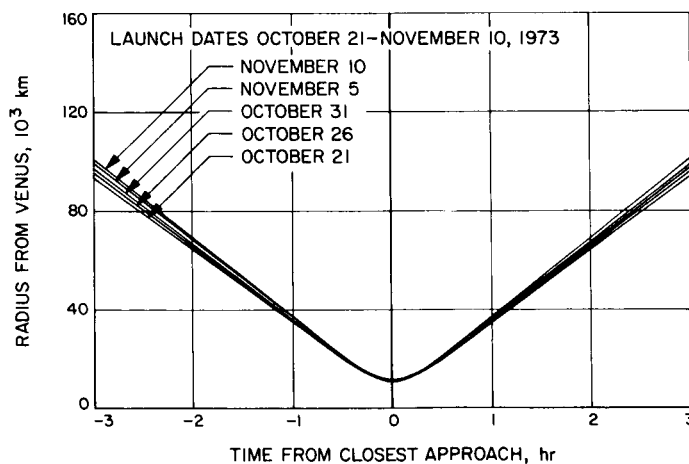


Fig. 58. Radius from Venus vs time from closest approach for five launch dates

before to 3 hr after closest approach. Cone and clock angles of Earth, Sun, and Canopus are fairly constant during encounter and can be obtained from Figs. 53 to 55.

In addition, Figs. 62 to 66 show pictorial views of the near-Venus geometry, plotted in the trajectory plane. At the left of each illustration is a view of the planet as seen along the incoming asymptote. In the center is a view of the planet looking down on the trajectory plane

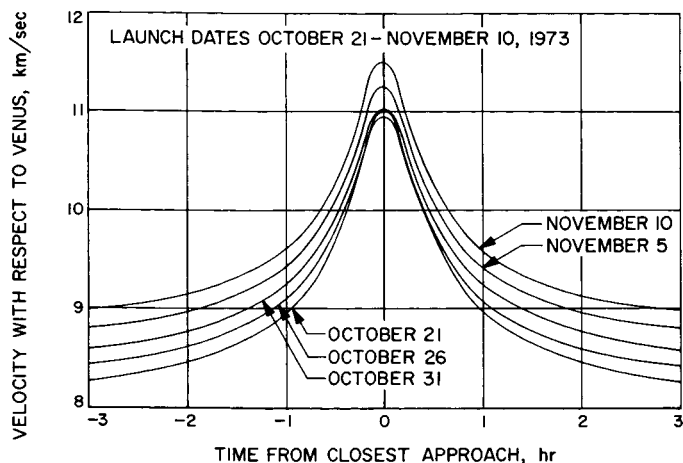


Fig. 59. Velocity with respect to Venus vs time from closest approach for five launch dates

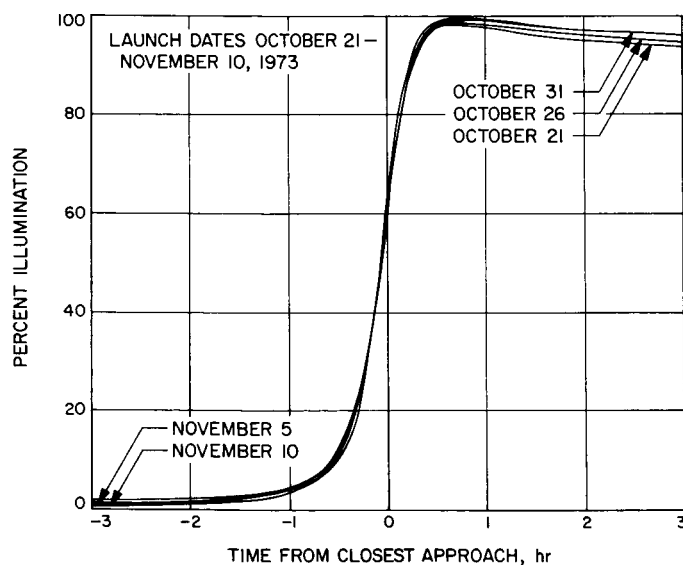


Fig. 60. Percent illumination vs time from closest approach for five launch dates

from the north. Time points are shown along the trajectory—in particular, the times of closest approach, enter and exit occultation, and terminator crossing. The dashed lines are the intersection of the Earth-shadow (occultation region) with the trajectory plane. Figures 67 to 77 show similar plots for Mercury. The Mercury plots are for trajectories targeted to pass through the center of the Earth-occultation region.

Additional graphs (Figs. 78 to 81) are presented for a Sun-side flyby of Mercury. The aiming point is chosen such that the trajectory passes over the subsolar point.

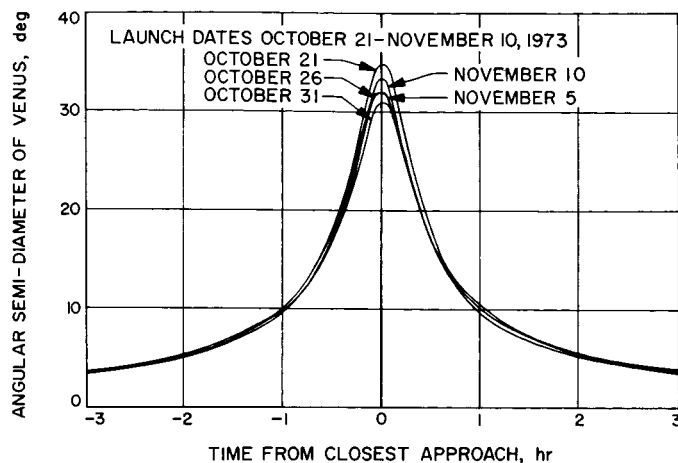


Fig. 61. Angular semi-diameter of Venus vs time from closest approach for five launch dates

The near-Venus geometry is essentially unchanged by a change in aiming point at Mercury. Also the radius, velocity, and angular semi-diameter at Mercury, which are functions of impact parameter and approach speed, only, are the same for a Sun-side flyby at 10,000 km as for an occultation flyby at the same distance.

V. Guidance Analysis

The feasibility of multiple, planetary trajectories is often questioned on the basis that extremely accurate guidance may be required. The trajectory must be bent an appreciable amount by passing very close to the intermediate planet. Thus, a very small error in periapsis can cause an appreciable error in the direction of the outgoing asymptote. Even worse, the probe could impact the intermediate planet. It was shown in Ref. 2 that guidance for the Earth-Venus-Mercury mission is, indeed, more difficult than current planetary missions. However, it is not beyond the capabilities of the current state of the art.

The guidance scheme adopted for the 1973 mission is the same as that proposed for the 1970 mission (Ref. 2); it is based on three midcourse corrections at the following times:

- (1) Earth injection plus 6 days.
- (2) Venus encounter minus 6 days.
- (3) Venus encounter plus 8 days.

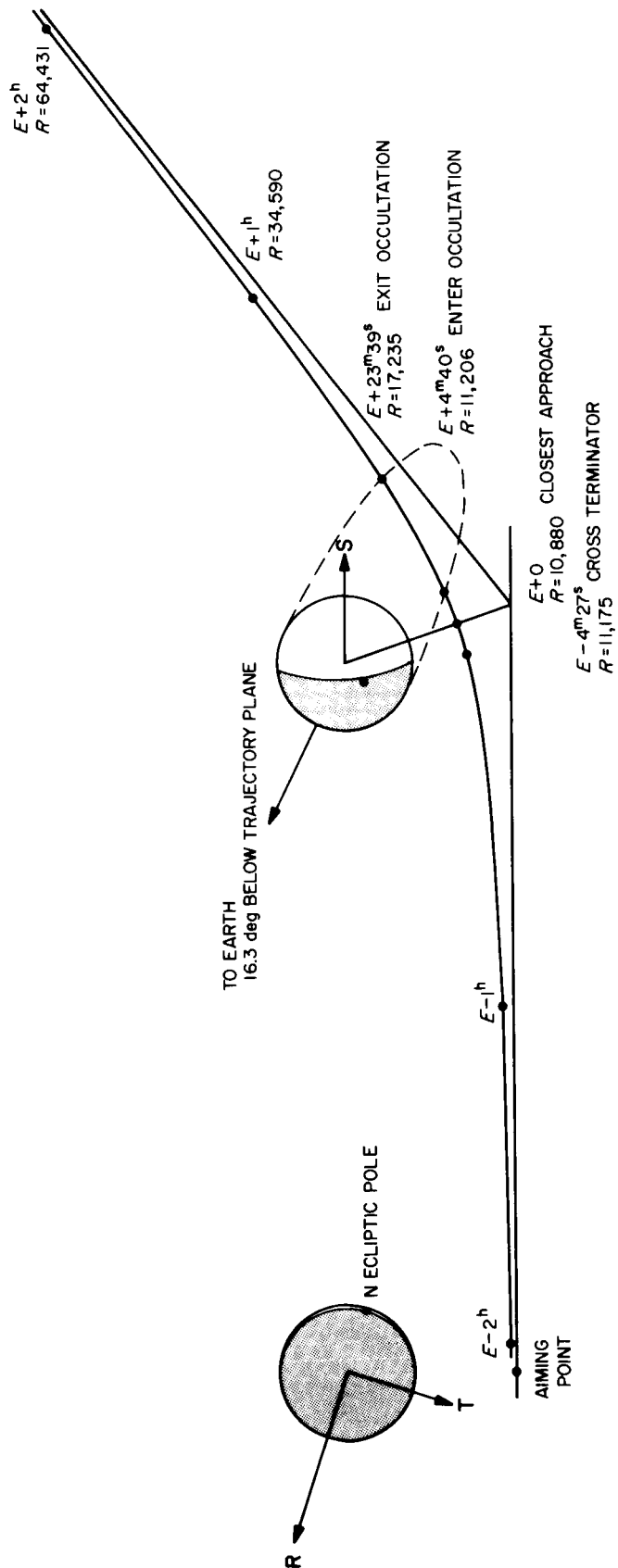


Fig. 62. Near-Venus geometry for October 21, 1973 launch

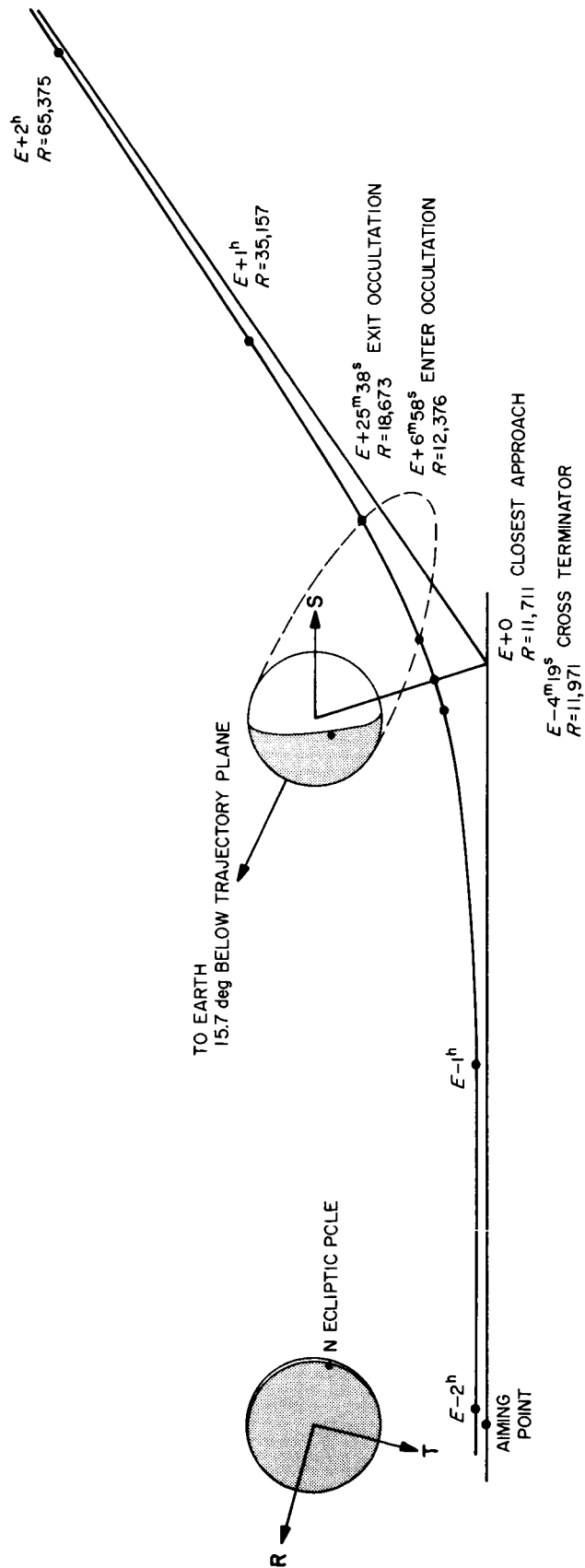


Fig. 63. Near-Venus geometry for October 26, 1973 launch

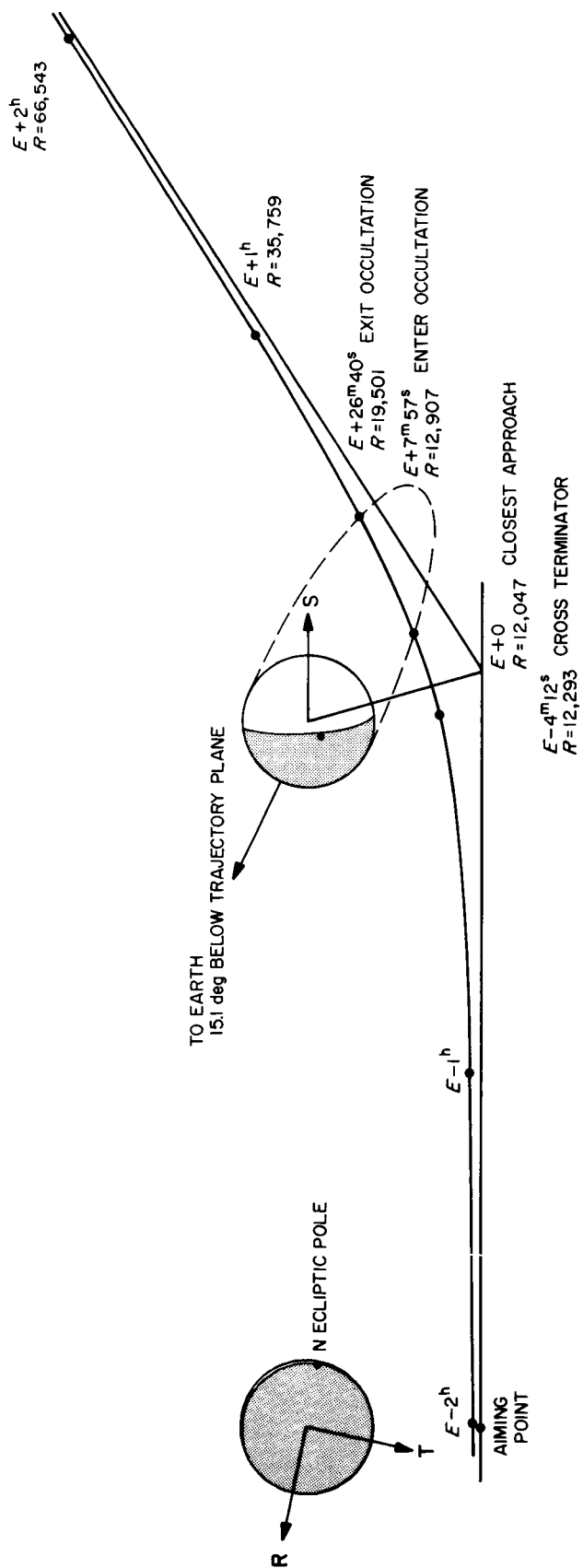


Fig. 64. Near-Venus geometry for October 31, 1973 launch

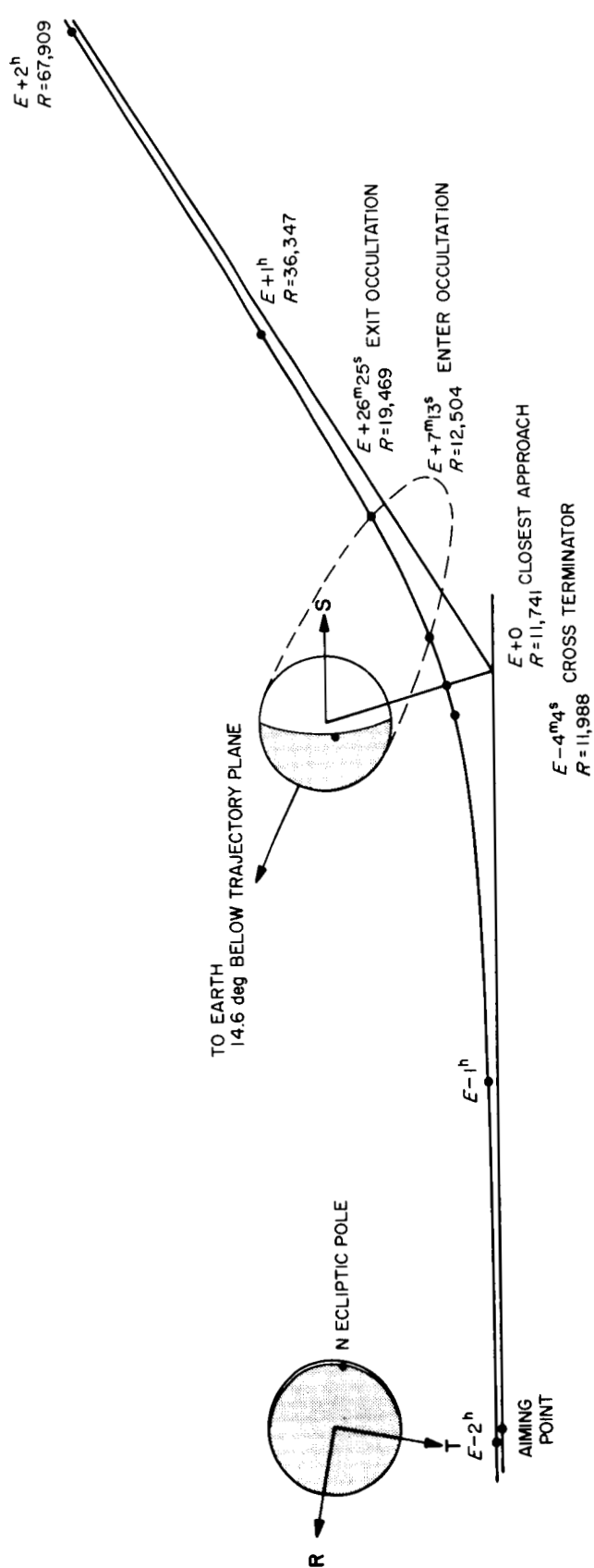


Fig. 65. Near-Venus geometry for November 5, 1973 launch

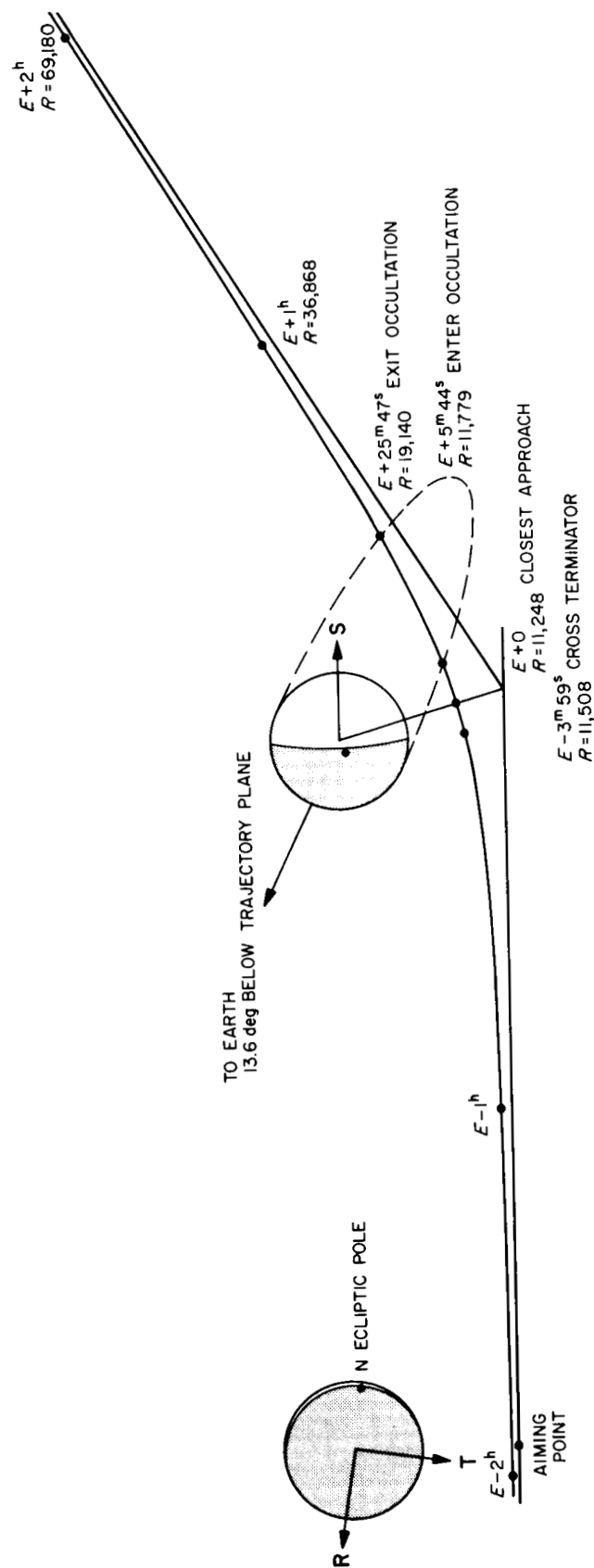


Fig. 66. Near-Venus geometry for November 10, 1973 launch

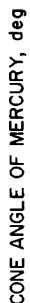


Fig. 67. Cone angle of Mercury vs time from closest approach for five launch dates for occultation flyby

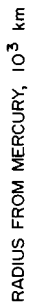


Fig. 69. Radius from Mercury vs time from closest approach for five launch dates for occultation flyby

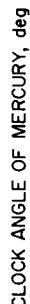


Fig. 68. Clock angle of Mercury vs time from closest approach for five launch dates for occultation flyby

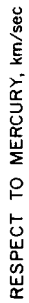


Fig. 70. Velocity with respect to Mercury vs time from closest approach for five launch dates for occultation flyby

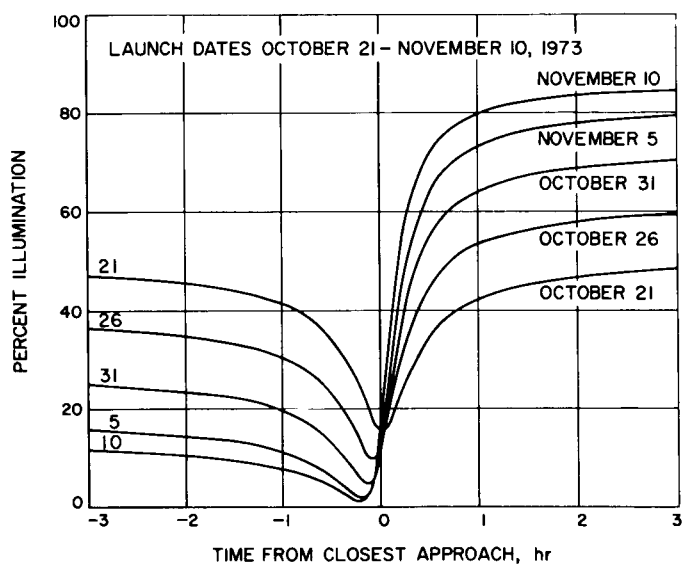


Fig. 71. Percent illumination vs time from closest approach for five launch dates for occultation flyby

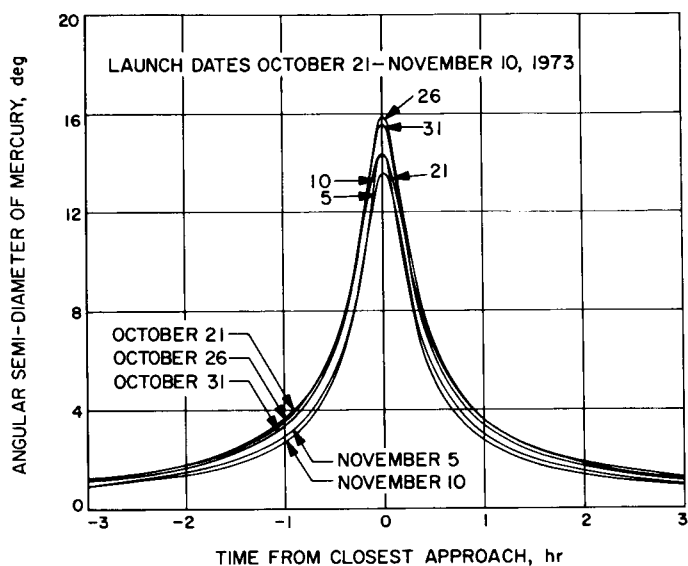


Fig. 72. Angular semi-diameter of Mercury vs time from closest approach for five launch dates for occultation flyby

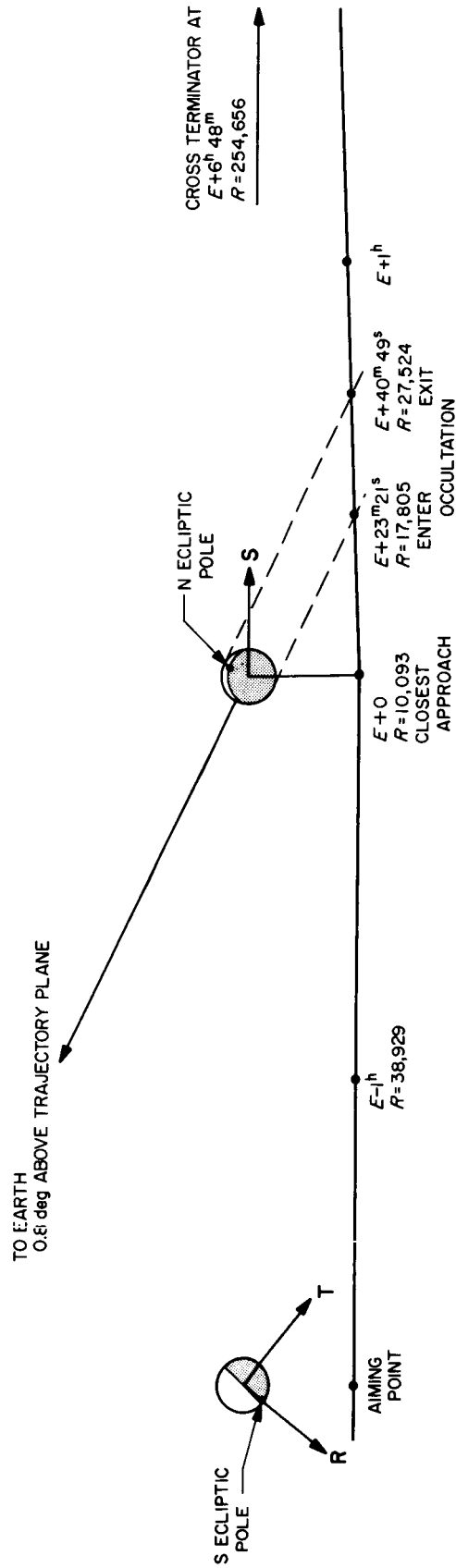


Fig. 73. Near-Mercury geometry for October 21, 1973 launch

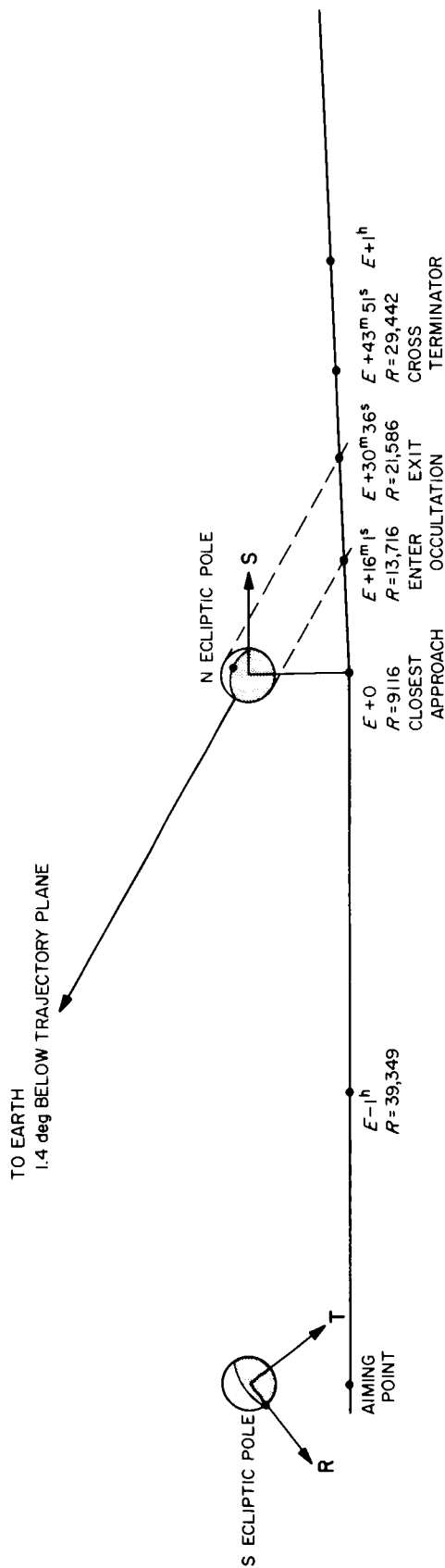


Fig. 74. Near-Mercury geometry for October 26, 1973 launch

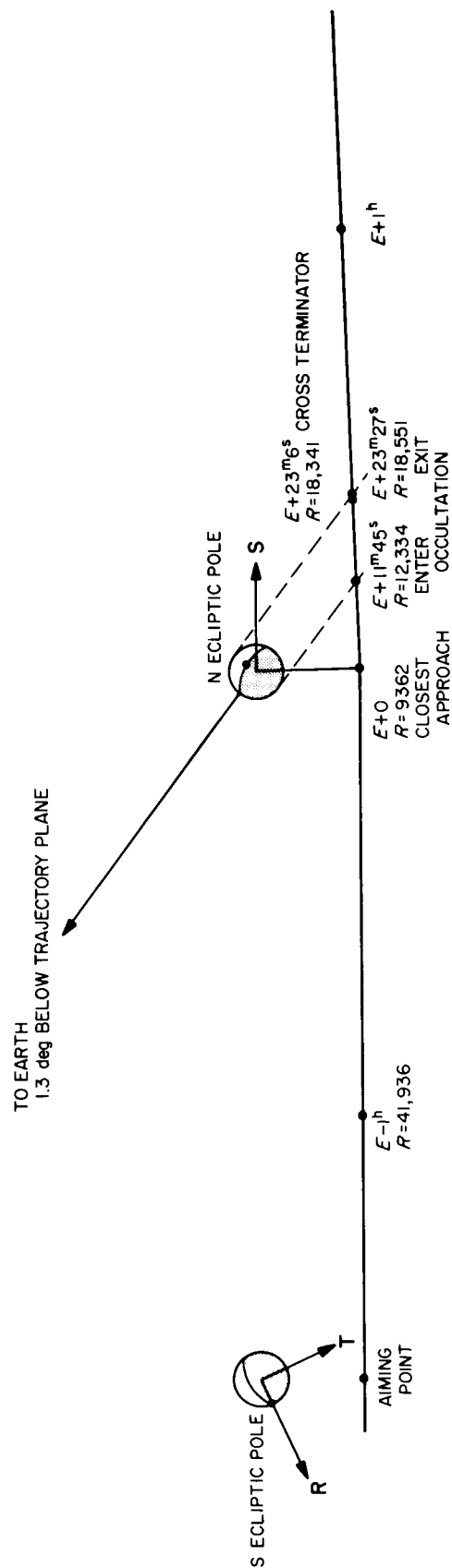


Fig. 75. Near-Mercury geometry for October 31, 1973 launch

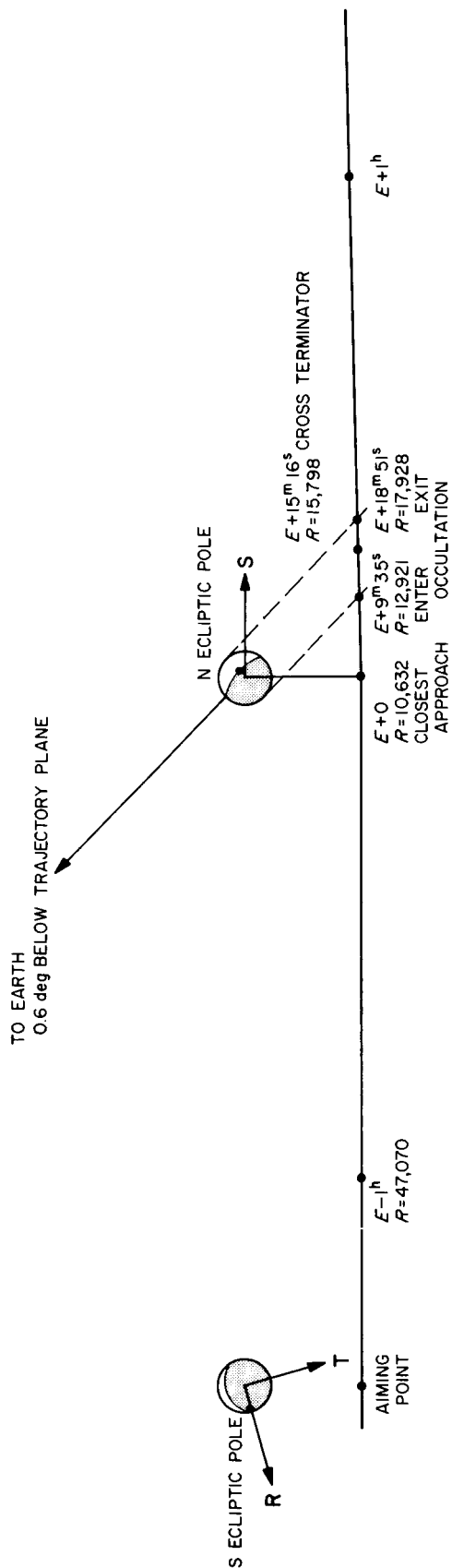


Fig. 76. Near-Mercury geometry for November 5, 1973 launch

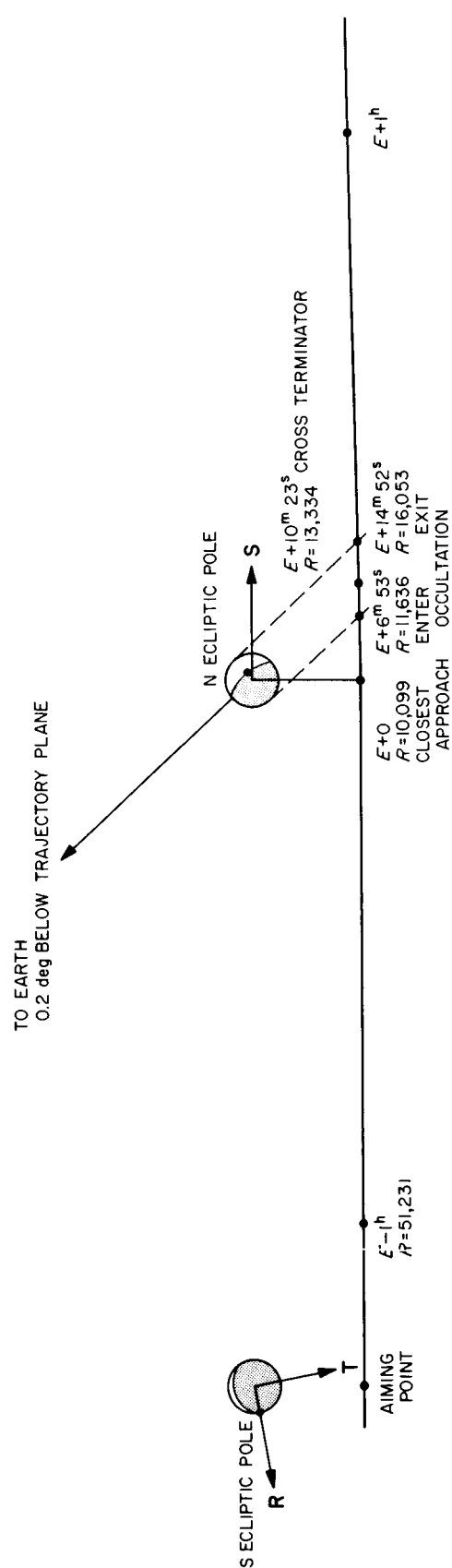


Fig. 77. Near-Mercury geometry for November 10, 1973 launch

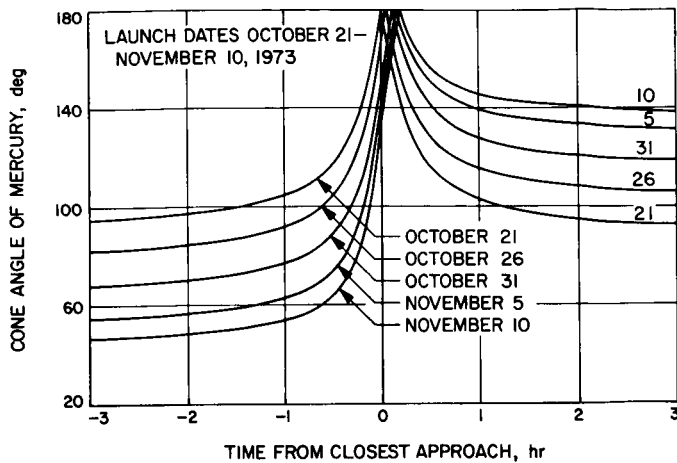


Fig. 78. Cone angle of Mercury vs time from closest approach for five launch dates for Sun-side flyby

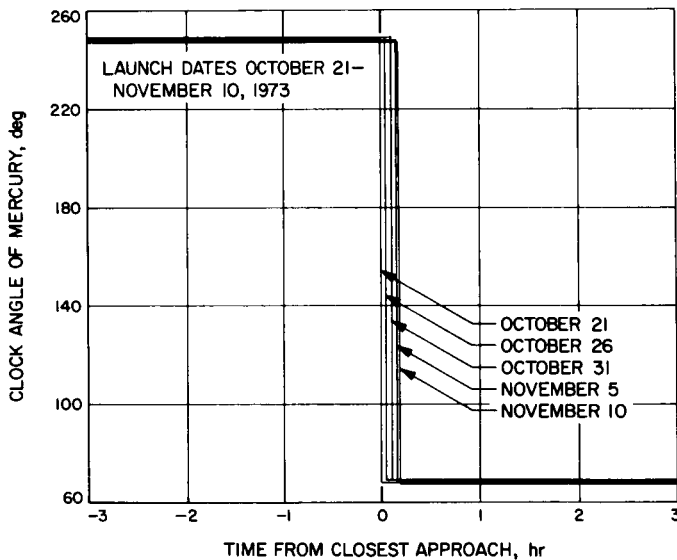


Fig. 79. Clock angle of Mercury vs time from closest approach for five launch dates for Sun-side flyby

The corrections are based on knowledge of the orbit from Earth-based radio tracking. Results are obtained for each of the five launch dates for which integrated trajectories were obtained.

A. Mapping Equations

Starting with a given covariance matrix of booster-injection errors, the errors are propagated along the trajectory, and the covariance matrices of the three midcourse corrections are obtained by the following sequence of equations. For a more complete description, see Refs. 2 and 9.

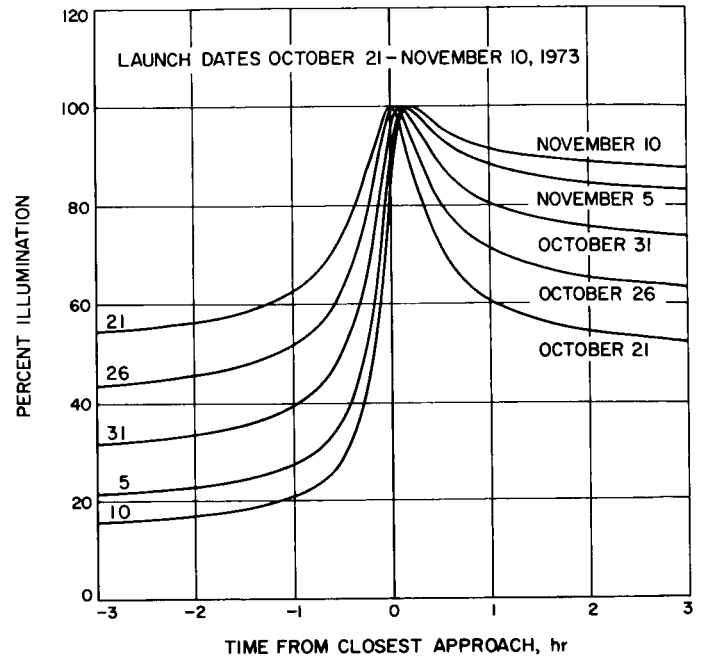


Fig. 80. Percent of illumination vs time from closest approach for five launch dates for Sun-side flyby

The 6×6 covariance matrix of injection errors Λ_{x_0} , is mapped to errors in the Venus-miss parameters by

$$\Lambda_{m_0} = \left(\frac{\partial \mathbf{m}}{\partial \mathbf{x}_0} \right) \Lambda_{x_0} \left(\frac{\partial \mathbf{m}}{\partial \mathbf{x}_0} \right)^T \quad (1)$$

where Λ_{m_0} and all subsequent matrices are 3×3 .

Then, for the first midcourse correction,

$$\Lambda_{v_1} = \left(\frac{\partial \mathbf{m}}{\partial \mathbf{v}_1} \right)^{-1} \Lambda_{m_0} \left(\frac{\partial \mathbf{m}}{\partial \mathbf{v}_1} \right)^{-1T} \quad (2)$$

For the execution errors in the first correction (Ref. 10),

$$\Lambda_{\delta v_1} = \sigma_\epsilon^2 \bar{\mathbf{v}}_1^2 \mathbf{I} \quad (3)$$

which result in errors at Venus given by

$$\Lambda_{m_1} = \left(\frac{\partial \mathbf{m}}{\partial \mathbf{v}_1} \right) \Lambda_{\delta v_1} \left(\frac{\partial \mathbf{m}}{\partial \mathbf{v}_1} \right)^T \quad (4)$$

Next, for the second midcourse correction,

$$\Lambda_{v_2} = \left(\frac{\partial \mathbf{m}}{\partial \mathbf{v}_2} \right)^{-1} \Lambda_{m_1} \left(\frac{\partial \mathbf{m}}{\partial \mathbf{v}_2} \right)^{-1T} \quad (5)$$

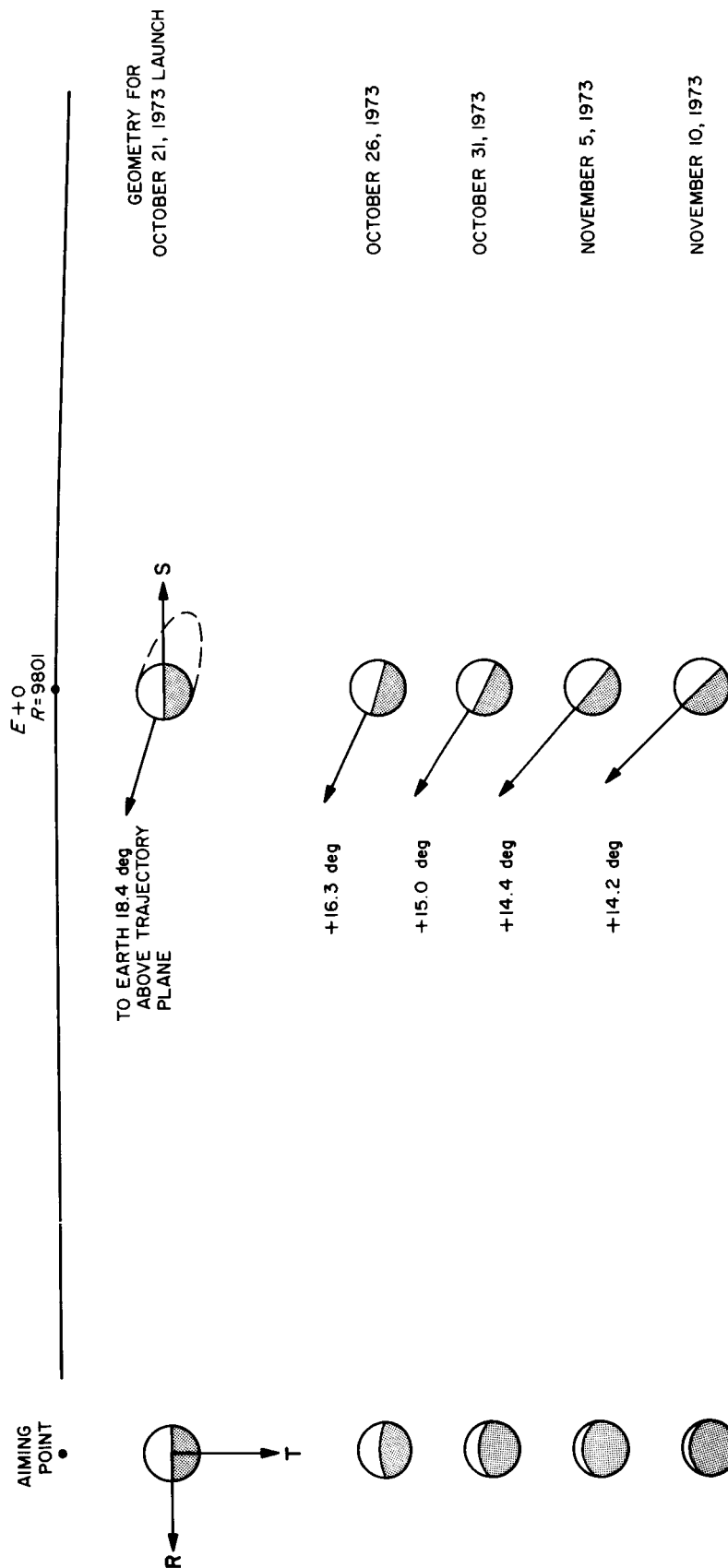


Fig. 81. Near-Mercury geometry for five launch dates for Sun-side flyby

The dominant error after the second correction is the orbit-determination error at the time of the second correction, which results in errors at Venus described by Λ_{m_2} .

These errors are then mapped to Mercury by

$$\Lambda_{m_3} = \left(\frac{\partial \mathbf{m}}{\partial \mathbf{m}_2} \right) \Lambda_{m_2} \left(\frac{\partial \mathbf{m}}{\partial \mathbf{m}_2} \right)^T \quad (6)$$

For the third midcourse correction,

$$\Lambda_{r_3} = \left(\frac{\partial \mathbf{m}}{\partial \mathbf{v}_3} \right)^{-1} \Lambda_{m_3} \left(\frac{\partial \mathbf{m}}{\partial \mathbf{v}_3} \right)^{-1^T} \quad (7)$$

For the execution errors in the third correction,

$$\Lambda_{\delta r_3} = \sigma_\epsilon^2 \overline{\mathbf{v}_3^2} \mathbf{I} \quad (8)$$

which result in final errors at Mercury

$$\Lambda_{m_4} = \left(\frac{\partial \mathbf{m}}{\partial \mathbf{v}_3} \right) \Lambda_{\delta r_3} \left(\frac{\partial \mathbf{m}}{\partial \mathbf{v}_3} \right)^T \quad (9)$$

Equations (1) to (9) have been evaluated for the October 26, 1973, launch date, using partial derivatives obtained from differenced integrated runs. This is also done for Eqs. (1) to (5), (8), and (9) for the other four launch dates. However, because of the difficulty and computer time necessary to obtain $\partial \mathbf{m} / \partial \mathbf{m}_2$, conic error analyses are substituted for Eqs. (6) and (7) to obtain Λ_{r_3} and the upper-left 2×2 part of Λ_{m_3} . The details of

the evaluation of the mapping equations are given in the next three sections.

B. Injection Covariance Matrix

A likely boost vehicle for the Earth-Venus-Mercury mission is the *Atlas-Centaur*. A typical covariance matrix of injection errors for *Atlas-Centaur* with parking orbit was obtained from JPL *Surveyor* personnel.² The elements of the injection are: down-range distance along surface of Earth, radius, velocity, flight-path angle, out-of-plane distance, out-of-plane velocity. The first step is to convert the original matrix to a similar form used at JPL, which has different assumptions as to which parameters are held constant as others are varied about the nominal. This was done by E. Cutting for the 1970 study. This matrix may then be input to a 1620 program, along with the injection-state vector in Earth-equatorial cartesian coordinates. The output of this program is the injection covariance matrix of errors in cartesian components, Λ_{r_0} . This has been done for each of the five launch dates. The result for the October 26, 1973 launch date is given in Table 5.

C. Obtaining Mapping Matrices

Printouts are obtained in the integrated-trajectory fine prints at injection and the three midcourse-correction epochs. State vectors obtained at these points are then used to make runs under the 7094 program SEARCH

²JPL internal communication, T. H. Thornton, Jr., to T. F. Gautschi, et al., "Centaur Injection Covariance Matrices," June 22, 1964.

Table 5. Injection covariance matrix for October 26, 1973 launch date

	x	y	z	\dot{x}	\dot{y}	\dot{z}	
$\Lambda_{x_0} =$	0.289708(2)	-0.323140(2)	-0.516967(1)	0.767474(-1)	-0.280644(-1)	0.212342(-1)	x
		0.555751(2)	0.389871(0)	-0.101130(0)	0.416530(-1)	-0.304633(-1)	y
			0.112288(2)	-0.490645(-2)	0.110385(-2)	0.226089(-2)	z
				0.218080(-3)	-0.831351(-4)	0.636603(-4)	\dot{x}
					0.333874(-4)	-0.245999(-4)	\dot{y}
						0.202658(-4)	\dot{z}
	symmetrical						

rms position error = 9.786 km

rms velocity error = 0.01648 km/sec

Units are km, sec.

Numbers in parentheses are decimal exponents.

Coordinates are Earth-equatorial, true-of-date.

(Ref. 7) to obtain the mapping matrices: $\partial \mathbf{m} / \partial x_0$, $\partial \mathbf{m} / \partial v_1$, $\partial \mathbf{m} / \partial v_2$, $\partial \mathbf{m} / \partial v_3$, and their inverses. SEARCH automatically increments the initial position and velocity components, differences the target miss parameters, constructs the partial derivative matrix, and obtains the inverse. No attempt was made to check for nonlinearity by using both positive and negative increments, since these matrices are generally quite linear. These matrices were obtained for all five launch dates.

The matrix $\partial \mathbf{m} / \partial \mathbf{m}_2$ was somewhat more difficult to compute, so it was obtained for the October 26 launch, only. The Venus target parameters $\mathbf{B} \cdot \mathbf{T}$, $\mathbf{B} \cdot \mathbf{R}$, and LTF were incremented one at a time; a new Earth-Venus leg was searched in, and the converged trajectory run out to Mercury. However, since the new Earth-Venus searches do not exactly preserve the original values of the unperturbed parameters, a simple difference quotient does not give an accurate partial. The system of nine simultaneous difference equations was solved by matrix algebra to yield $\partial \mathbf{m} / \partial \mathbf{m}_2$. Two solutions were obtained for positive and negative increments, and the results were averaged to account for nonlinearity.

The partials of the form $\partial \mathbf{m} / \partial \mathbf{m}_2$ obtained in the automatic targeting procedure could not be used for two reasons:

- (1) They were 2×2 instead of 3×3 (no flight-time partials).
- (2) They were not as accurate as desired because they were constructed from difference quotients.

A complete set of mapping matrices for the October 26 launch date is shown in Table 6.

The orbit determination covariance matrix, Λ_{m_2} , was not reevaluated for the 1973 mission. The values obtained for the 1970 mission (Ref. 2) represent state of the art for Earth-Venus tracking and should be equally applicable to the 1973 mission. Hence,

$$\Lambda_{m_2} = \begin{bmatrix} 10000 & 0 & 0 \\ 0 & 10000 & 0 \\ 0 & 0 & 100 \end{bmatrix} \begin{matrix} \mathbf{B} \cdot \mathbf{T}_2 \\ \mathbf{B} \cdot \mathbf{R}_2 \\ LTF_2 \end{matrix}$$

(See notes on Table 6.)

Table 6. Mapping matrices for the October 26, 1973 launch date

$\frac{\partial \mathbf{m}}{\partial x_0} =$	$\begin{bmatrix} -0.248990(5) & -0.667994(4) & -0.132257(5) \\ 0.799569(4) & 0.210483(3) & 0.509658(4) \\ 0.411186(4) & 0.694372(3) & 0.175207(4) \end{bmatrix}$	$\begin{bmatrix} -0.693427(7) & -0.303833(8) & -0.127188(8) \\ 0.470870(6) & 0.112214(8) & 0.303629(7) \\ 0.487925(6) & 0.505124(7) & 0.197172(7) \end{bmatrix}$	$\begin{matrix} \mathbf{B} \cdot \mathbf{T}_2 \\ \mathbf{B} \cdot \mathbf{R}_2 \\ LTF_2 \end{matrix}$
$\frac{\partial \mathbf{m}}{\partial v_1} =$	$\begin{bmatrix} -0.513580(7) & -0.112741(8) & -0.530534(7) \\ -0.627039(6) & 0.403544(7) & -0.232923(7) \\ -0.260112(6) & 0.150849(7) & 0.854313(6) \end{bmatrix}$	$\begin{matrix} \mathbf{B} \cdot \mathbf{T}_2 \\ \mathbf{B} \cdot \mathbf{R}_2 \\ LTF_2 \end{matrix}$	
$\frac{\partial \mathbf{m}}{\partial v_2} =$	$\begin{bmatrix} -0.357486(6) & -0.345474(6) & -0.149722(6) \\ -0.944454(5) & 0.283071(6) & -0.425701(6) \\ -0.450611(5) & 0.332232(5) & 0.316077(5) \end{bmatrix}$	$\begin{matrix} \mathbf{B} \cdot \mathbf{T}_2 \\ \mathbf{B} \cdot \mathbf{R}_2 \\ LTF_2 \end{matrix}$	
$\frac{\partial \mathbf{m}}{\partial \mathbf{m}_2} =$	$\begin{bmatrix} 0.984043(3) & -0.572418(3) & -0.159935(1) \\ -0.246877(3) & -0.199044(3) & -0.126023(2) \\ 0.376830(2) & -0.114532(3) & 0.329272(1) \end{bmatrix}$	$\begin{matrix} \mathbf{B} \cdot \mathbf{T}_4 \\ \mathbf{B} \cdot \mathbf{R}_4 \\ LTF_4 \end{matrix}$	
$\frac{\partial \mathbf{m}}{\partial v_3} =$	$\begin{bmatrix} -0.219600(7) & -0.316924(7) & -0.145342(7) \\ 0.181235(7) & 0.112568(7) & -0.160880(7) \\ -0.638148(6) & -0.124770(6) & -0.115814(6) \end{bmatrix}$	$\begin{matrix} \mathbf{B} \cdot \mathbf{T}_4 \\ \mathbf{B} \cdot \mathbf{R}_4 \\ LTF_4 \end{matrix}$	

Notes: Numbers in parentheses are decimal exponents.
Units are km, sec.
 $x, y, z, \dot{x}, \dot{y}, \dot{z}$ are geocentric equatorial equinox-of-date coordinates.
 $\mathbf{B} \cdot \mathbf{T}$ and $\mathbf{B} \cdot \mathbf{R}$ are miss components referenced to ecliptic at Venus (sub 2) and Mercury (sub 4).
 LTF is linearized time of flight.

The results of evaluating Eqs. (1) to (9) for the October 26 launch are given in Tables 7 and 8. Table 7 shows the covariance matrices of target errors, Λ_{m_i} ($i = 0, 1, 3, 4$), and Table 8 shows the covariance matrices of the midcourse-correction components, Λ_{v_j} ($j = 1, 2, 3$). Also shown in Table 8 are the execution-error matrices $\Lambda_{\delta v_1}$ and $\Lambda_{\delta v_3}$. The value of σ for proportional pointing and shutoff errors was taken as 0.01.

D. Conic Error Analysis

For each of the five launch dates, Eqs. (6) and (7) are evaluated by an alternate conic analysis, which is described in detail in Refs. 2 and 11.

In the conic analysis, the covariance matrices of Eq. (6) are reduced to 2×2 , and the mapping matrix, $\partial \mathbf{m} / \partial \mathbf{m}_2$, is constructed from partials mapping errors from incoming to outgoing asymptotes at Venus (**B** matrix of Refs. 2 and 11) and partials from the conic program HECON (Ref. 12), which map errors from departure asymptote to target. The computations have been programmed on the 1620.

The covariance matrix of velocity components for the third midcourse correction is obtained by mapping the 2×2 Λ_{m_2} into errors in outgoing asymptote. The third correction is assumed to be that which removes these errors. Equations (8) and (9) are then evaluated

Table 7. Covariance matrices of target errors for October 26, 1973 launch date

	B • T	B • R	LTF	
$\Lambda_{m_0} =$	$\begin{bmatrix} 0.106903(+11) \\ -0.153217(+10) \\ -0.116212(+10) \end{bmatrix}$	$\begin{bmatrix} -0.153217(+10) \\ 0.566840(+09) \\ 0.253706(+09) \end{bmatrix}$	$\begin{bmatrix} -0.116212(+10) \\ 0.253706(+09) \\ 0.151782(+09) \end{bmatrix}$	B • T B • R LTF
$\Lambda_{m_1} =$	$\begin{bmatrix} 0.184046(+07) \\ -0.303165(+06) \\ -0.204723(+06) \end{bmatrix}$	$\begin{bmatrix} -0.303165(+06) \\ 0.223975(+06) \\ 0.431734(+05) \end{bmatrix}$	$\begin{bmatrix} -0.204723(+06) \\ 0.431734(+05) \\ 0.311396(+05) \end{bmatrix}$	B • T B • R LTF
$\Lambda_{m_3} =$	$\begin{bmatrix} 0.129600(+11) \\ -0.129001(+10) \\ 0.102642(+10) \end{bmatrix}$	$\begin{bmatrix} -0.129001(+10) \\ 0.100568(+10) \\ 0.134934(+09) \end{bmatrix}$	$\begin{bmatrix} 0.102642(+10) \\ 0.134934(+09) \\ 0.145377(+09) \end{bmatrix}$	B • T B • R LTF
$\Lambda_{m_4} =$	$\begin{bmatrix} 0.297954(+07) \\ -0.914137(+06) \\ 0.344849(+06) \end{bmatrix}$	$\begin{bmatrix} -0.914137(+06) \\ 0.125296(+07) \\ -0.194907(+06) \end{bmatrix}$	$\begin{bmatrix} 0.344849(+06) \\ -0.194907(+06) \\ 0.765488(+05) \end{bmatrix}$	B • T B • R LTF

Table 8. Covariance matrices of midcourse corrections for October 26, 1973 launch date

	\dot{x}	\dot{y}	\dot{z}	
$\Lambda_{v_1} =$	$\begin{bmatrix} 0.404587(-4) \\ 0.376788(-5) \\ 0.161673(-4) \end{bmatrix}$	$\begin{bmatrix} 0.376787(-5) \\ 0.465156(-4) \\ 0.166290(-4) \end{bmatrix}$	$\begin{bmatrix} 0.161673(-4) \\ 0.166290(-4) \\ 0.143567(-4) \end{bmatrix}$	\dot{x} \dot{y} \dot{z}
$\Lambda_{\delta v_1} =$	$\begin{bmatrix} 0.101331(-7) \\ 0 \\ 0 \end{bmatrix}$	$\begin{bmatrix} 0 \\ 0.101331(-7) \\ 0 \end{bmatrix}$	$\begin{bmatrix} 0 \\ 0 \\ 0.101331(-7) \end{bmatrix}$	\dot{x} \dot{y} \dot{z}
$\Lambda_{v_2} =$	$\begin{bmatrix} 0.109503(-5) \\ -0.664978(-6) \\ -0.345247(-6) \end{bmatrix}$	$\begin{bmatrix} -0.664978(-6) \\ 0.108970(-4) \\ 0.512987(-5) \end{bmatrix}$	$\begin{bmatrix} -0.345247(-6) \\ 0.512987(-5) \\ 0.314300(-5) \end{bmatrix}$	\dot{x} \dot{y} \dot{z}
$\Lambda_{v_3} =$	$\begin{bmatrix} 0.194912(-3) \\ -0.670248(-4) \\ 0.355483(-3) \end{bmatrix}$	$\begin{bmatrix} -0.670248(-4) \\ 0.878703(-3) \\ 0.454792(-4) \end{bmatrix}$	$\begin{bmatrix} 0.355483(-3) \\ 0.454792(-4) \\ 0.681232(-3) \end{bmatrix}$	\dot{x} \dot{y} \dot{z}
$\Lambda_{\delta v_3} =$	$\begin{bmatrix} 0.175485(-6) \\ 0 \\ 0 \end{bmatrix}$	$\begin{bmatrix} 0 \\ 0.175485(-6) \\ 0 \end{bmatrix}$	$\begin{bmatrix} 0 \\ 0 \\ 0.175485(-6) \end{bmatrix}$	\dot{x} \dot{y} \dot{z}

Table 9. Summary of target errors

Statistical parameters		Oct. 21	Oct. 26	Integrated results, Oct. 26	Oct. 31	Nov. 5	Nov. 10
Miss at Venus due to injection errors Δ_{m_0}	σ_T , km	114200.	103400.	---	93400.	83900.	75000.
	σ_R , km	27100.	23800.	---	21100.	18900.	17200.
	rms, km	117300.	106100.	---	95700.	86000.	76900.
	σ_F , sec	13600.	12300.	---	11100.	9820.	8670.
	ρ_{TR}	-0.70	-0.62	---	-0.54	-0.45	-0.34
	σ_1 , km	115800.	104500.	---	94100.	84300.	75200.
	σ_2 , km	19100.	18400.	---	17700.	16800.	16100.
	θ , deg	170.	172.	---	173.	174.	175.
Miss at Venus due to 1st M/C execution errors Δ_{m_1}	σ_T , km	1491.	1357.	---	1227.	1101.	986.
	σ_R , km	499.	473.	---	457.	445.	438.
	rms, km	1572.	1437.	---	1309.	1188.	1078.
	σ_F , sec	194.	176.	---	159.	143.	128.
	ρ_{TR}	-0.56	-0.47	---	-0.38	-0.30	-0.23
	σ_1 , km	1519.	1377.	---	1241.	1111.	992.
	σ_2 , km	405.	411.	---	417.	421.	423.
	θ , deg	169.	170.	---	171.	172.	173.
Miss at Venus due to 2nd M/C orbit determination errors Δ_{m_2}	σ_T , km	100.	100.	---	100.	100.	100.
	σ_R , km	100.	100.	---	100.	100.	100.
	rms, km	141.	141.	---	141.	141.	141.
	σ_F , sec	10.	10.	---	10.	10.	10.
Miss at Mercury due to 2nd M/C orbit determination errors Δ_{m_3} (from conic analysis, except as noted for Oct. 26 launch)	σ_T , km	169200.	115600.	113800.	90400.	78200.	75300.
	σ_R , km	19400.	32600.	31700.	41300.	48800.	56800.
	rms, km	170300.	120100.	118200.	99400.	92200.	94400.
	σ_F , sec	---	---	12100.	---	---	---
	ρ_{TR}	-0.44	-0.35	-0.36	-0.34	-0.34	-0.31
	σ_1 , km	169400.	116200.	114400.	91800.	80700.	79100.
	σ_2 , km	17500.	30400.	29500.	38200.	44500.	51500.
	θ , deg	177.	174.	174.	169.	163.	156.
Miss at Mercury due to 3rd M/C execution errors Δ_{m_4} (conic 3rd M/C mapped with integrated partials, except as noted for Oct. 26)	σ_T , km	2596.	1687.	1726.	1192.	1000.	1018.
	σ_R , km	1239.	1094.	1119.	1012.	974.	999.
	rms, km	2877.	2010.	2057.	1563.	1396.	1426.
	σ_F , sec	316.	270.	277.	228.	188.	167.
	ρ_{TR}	-0.58	-0.47	-0.47	-0.29	-0.07	+0.02
	σ_1 , km	2708.	1795.	1837.	1274.	1025.	1022.
	σ_2 , km	971.	906.	927.	906.	947.	994.
	θ , deg	162.	157.	157.	150.	145.	24.

with conic results for $\overline{v_3^2}$ and integrated partials for $\partial m/\partial v_3$.

The good agreement of conic error analysis with integrated results indicates that more rapid conic methods can save time and money in preliminary studies.

E. Results

The results of the guidance analysis for each launch date are summarized in Tables 9 and 10. Table 9 shows target errors at Venus and Mercury resulting from injection, execution and orbit determination errors (as applicable). Note that the final rms miss at Mercury is less than half that found for the 1970 mission (4900 km). Also shown are the semi-major and -minor axes and orientation angle of the 1-sigma error ellipse in the *B*-plane. The 3-sigma error ellipse after the first midcourse correction is shown in the Venus *B* plane in Figs. 32 to 36. The final 3-sigma error ellipse after the third midcourse correction is shown in the Mercury *B* plane in Figs. 37 to 41.

Table 10 shows the rms velocity magnitudes for each midcourse correction. Also shown are the mean and 1-sigma values for each correction resulting from an assumed Rayleigh distribution. It was shown in Ref. 9 that this analytical distribution accurately approximates the results obtained by a Monte Carlo analysis. The last entry in Table 10 shows the fuel loading as determined from the mean plus 3-sigma on the total velocity magnitude, which was obtained from the Rayleigh distribution.

The maximum value of total midcourse velocity required is 120 m/sec, for the October 21 launch. Assuming a specific impulse of 230 sec for the midcourse propulsion system, the fraction of gross spacecraft weight for propellant is 0.052. Since the *Atlas-Centaur* will deliver about 1000 lb on the 1973 mission, about 52 lb of propellant would be required. The total propulsion subsystem weight would be about 100 lb, leaving 900 lb for remaining spacecraft subsystems and science payload.

Table 10. Summary of midcourse corrections

Statistical parameter ^a		Correction, m/sec					
		Oct. 21	Oct. 26	Integrated results, Oct. 26	Oct. 31	Nov. 5	Nov. 10
1st midcourse correction velocity	rms_1	10.0	10.1	—	10.1	10.2	10.2
	μ_{v_1}	8.9	9.0	—	9.0	9.0	9.0
	σ_{v_1}	4.6	4.7	—	4.7	4.7	4.7
2nd midcourse correction velocity	rms_2	4.2	3.9	—	3.6	3.3	3.0
	μ_{v_2}	3.7	3.5	—	3.2	2.9	2.7
	σ_{v_2}	1.9	1.8	—	1.7	1.5	1.4
3rd midcourse correction velocity	rms_3	45.7	40.9	41.9	39.6	40.4	43.0
	μ_{v_3}	40.5	36.2	37.1	35.1	35.8	38.1
	σ_{v_3}	21.2	18.9	19.4	18.4	18.7	19.9
Total midcourse correction velocity	rms_T	57.6	52.7	53.6	51.1	51.6	54.0
	μ_{v_T}	53.1	48.7	49.5	47.2	47.7	49.8
	σ_{v_T}	22.2	20.0	20.5	19.4	19.7	20.8
	$\mu_{v_T} + 3\sigma_{v_T}$	119.7	108.7	111.0	105.4	106.8	112.2
^a μ and σ from Rayleigh approximation.							
Total values assume unit correlation between v_1 and v_2 .							

Nomenclature

$\begin{bmatrix} \mathbf{B} \cdot \mathbf{R} \\ \mathbf{B} \cdot \mathbf{T} \end{bmatrix}$ = B -plane miss vector components

C_3 = launch energy

h_{ca} = altitude of closest approach

\mathbf{I} = identity matrix

LTF = linearized time of flight

$\mathbf{m} = [\mathbf{B} \cdot \mathbf{T}, \mathbf{B} \cdot \mathbf{R}, LTF]^T$ = target miss vector

$rms = (\sigma_T^2 + \sigma_R^2)^{1/2}$ = rms miss in B plane

rms_i = rms velocity magnitude for i^{th} correction

t_{inj} = injection time

T_F = time of flight

\mathbf{v}_i = i^{th} midcourse correction velocity

V_h = velocity on hyperbolic asymptote

V_{inj} = injection velocity

$\mathbf{x}_0 = [x_0, y_0, z_0, \dot{x}_0, \dot{y}_0, \dot{z}_0]^T$ = injection state vector

$\begin{bmatrix} x \\ y \\ z \end{bmatrix}$ = Earth-equatorial, true-equinox-of-date, cartesian coordinates

β = celestial latitude of asymptote

γ_{inj} = injection flight path angle

δv_i = i^{th} midcourse execution error

θ = angle of semi-major axis from \mathbf{T} -axis

Θ = right ascension of asymptote

λ = celestial longitude of asymptote

$\mathbf{\Lambda}$ = covariance matrix of subscripted vector

μ_{v_i} = mean velocity magnitude for i^{th} correction

ρ_{TR} = correlation coefficient for σ_T and σ_R

σ_F = one-sigma error in LTF

σ_R = one-sigma error in $\mathbf{B} \cdot \mathbf{R}$

σ_T = one-sigma error in $\mathbf{B} \cdot \mathbf{T}$

σ_{v_i} = standard deviation on i^{th} velocity magnitude

σ_ε = standard deviation of proportional pointing and shutoff error

σ_1 = semi-major axis of 1-sigma error ellipse in B -plane

σ_2 = semi-minor axis of 1-sigma error ellipse in B -plane

ϕ = declination of asymptote

Subscripts 1 to 4 refer to Earth departure, Venus arrival, Venus departure, and Mercury arrival, respectively, except where noted in the above definitions.

References

1. Minovitch, M. A., *The Determination and Characteristics of Ballistic Interplanetary Trajectories Under the Influence of Multiple Planetary Attractions*, Technical Report No. 32-464, Jet Propulsion Laboratory, Pasadena, California, October 31, 1963.
2. Sturms, F. M., Jr., and Cutting, E., "Trajectory Analysis of a 1970 Mission to Mercury Via a Close Encounter with Venus," (Paper 65-90) 2nd AIAA Aerospace Sciences Meeting, New York, January 25-27, 1965.
3. Sturms, F. M., Jr., "Earth-Venus-Mercury Mission Opportunities in the 1970's," *Space Programs Summary No. 37-39, Vol. IV*, Jet Propulsion Laboratory, Pasadena, California, June 30, 1966, pp. 1-5.
4. Joseph, A. E., and Richard, R. J., "Space Research Conic Program," Engineering Planning Document 406, Jet Propulsion Laboratory, Pasadena, California, July 1966.
5. Clarke, V. C., Jr., et al., *Design Parameters for Ballistic Interplanetary Trajectories, Part I. One-Way Transfers to Mars and Venus*, Technical Report No. 32-77, Jet Propulsion Laboratory, Pasadena, California, January 16, 1963.
6. Kizner, W., *A Method of Describing Miss Distances for Lunar and Interplanetary Trajectories*, External Publication No. 674, Jet Propulsion Laboratory, Pasadena, California, August 1, 1959.
7. Newhall, N. S., *A Users' Guide for SEARCH and ITER*, Technical Memorandum No. 33-203, Jet Propulsion Laboratory, Pasadena, California, April 15, 1965.
8. White, R. J., et al., *SPACE - Single Precision Cowell Trajectory Program*, Technical Memorandum No. 33-198, Jet Propulsion Laboratory, Pasadena, California, January 15, 1965.
9. Sturms, F. M., Jr., "Statistical Analysis of Three Midcourse Corrections on an Earth-Venus-Mercury Trajectory," *Space Programs Summary No. 37-37, Vol. IV*, Jet Propulsion Laboratory, Pasadena, California, February 28, 1966, pp. 1-11.
10. Gates, C. R., *A Simplified Model of Midcourse Execution Errors*, Technical Report No. 32-504, Jet Propulsion Laboratory, Pasadena, California, October 15, 1963.
11. Sturms, F. M., Jr., "Error Analysis of Multiple Planet Trajectories," *Space Programs Summary No. 37-27, Vol. IV*, Jet Propulsion Laboratory, Pasadena, California, June 30, 1964, pp. 6-13.
12. Clarke, V. C., Jr., et al., *Earth-Venus Trajectories 1970*, Volume 5, Parts A and B, Technical Memorandum No. 33-99, Jet Propulsion Laboratory, Pasadena, California, September 16, 1964.